Effects of road surface characteristics and geometries on Safer Users Behaviour

Murad Shoman

Effects of Road Surface Characteristics and Geometries on Safer User Behavior

Thèse de doctorat de l'Université Gustave Eiffel

École doctorale n° 632, Mathématiques Et Des Sciences Et Technologies De L'information Et De La Communication (MSTIC)

Spécialité de doctorat : Signal, Image, et Automatique (CNU 27, 61)
Unité de recherche : COSYS- PICS-L

Thèse présentée et soutenue à l'Université Gustave Eiffel, le 06/07/2022, par

Murad SHOMAN

Composition du Jury

Hichem ARIOUI Professeur, Université d'Évry Val d'Essonne	Président
Francesca DE CRESCENZIO Professeure, University of Bologna	Rapporteur
Michel BASSET Professeur, Université de Haute-Alsace	Rapporteur
Patricia DELHOMME Directeur derecherche, Université Gustave Eiffel	Examinatrice
Hocine IMINE Directeur derecherche, Université Gustave Eiffel	Directeur de thèse

DEDICATION

I dedicate my dissertation work to my family and many friends. A special feeling of gratitude to my loving parents, Mohammad and Sa'ida whose words of encouragement and push for tenacity ring in my ears. My sisters Suhad, Sanaa', Iman and Hasnaa' and my brothers Ibrahim and Yamin have never left my side and are very special.

ACKNOWLEDGEMENTS

First and foremost I am extremely grateful to my supervisor, Dr. Hocine Imine for his invaluable advice, continuous support, and patience during my PhD study. His immense knowledge and plentiful experience have encouraged me in all the time of my academic research and daily life. I would like to warmly thank Mrs. Francesca DE Crescenzio, Professor at University of Bologna and Mr. Michel Basset, Professor at Université de Haute-Alsace for the interest they brought to my work by accepting to be reviewers (rapporteurs) of my thesis. I would like to thank Mr. Hichem Arioui, Professor at Université d'Évry Val d'Essonne and Mrs. Patricia Delhomme, Research Director at Université Gustave Eiffel for accepting to examine my work. I would like also to thank the following people for helping with this research project: Dr. Stephane Caro and Thomas Surand and all the colleagues in SimTeam in Gustave Eifeel University; Dr. Kenth Johannson and Dr. Viveca Wallqvist from The Research Institues of Sweden (RISE); Eng. Chirag Savant from Integrated Transport Research Lab (ITRL) in KTH Royal Institute of Technology; Jose Luis Borau Jordán from Fundacion ONCE; Eng. Célia Meghough from Toulouse University 3, Prof. Andrea Simone, Dr. Piergiorg Tataranni and Eng. Claudia Brasile from University of Bologna besides all the volunteers who participated in the experiments of this research. My appreciation also goes out to my family and friends for their encouragement and support all through my studies.

This work is fully funded by Horizon 2020 Model Grant Agreement for Marie Skłodowska-Curie Actions-Innovative Training Networks (H2020 MGA MSCA-ITN) within the SAFERUP project under grant agreement number 765057.

ABSTRACT

This doctoral thesis presents the improvements conducted on PICS-L bicycle simulator and the instrumentation of a city bicycle in order to provide objective measures to evaluate cycling safety based on cyclist's behavior and the interaction with the road infrastructure and other road-users.

The related research activities were implemented on the bicycle simulator developed by the Perceptions, Interactions, Behaviors and Simulations Lab for road and street users (PICS-L) at Gustave Eiffel University in Paris, and in collaboration with the Research Institute of Sweden (RISE), Stockholm and ONCE Foundation, Madrid under SAFERUP European funded project. The activities are divided into two main parts; the cycling simulation conducted in Gustave Eiffel University and on-road experiments using an instrumented bicycle in Stockholm.

The first part of the research is focused on improving the simulator platform and the underlying dynamic model. Three actuators were installed on the platform to render the road vibrations, and an asphalt specimen was fixed under the rear tire to render road adhesion. The bicycle dynamic model was developed using MATLAB-Simulink with 6 degrees of freedom. The physical and subjective validity of the developed model was analyzed through experimentation on the bicycle simulator; the results of the experiments are discussed in case study I and II.

The second part includes the instrumentation of a city bicycle with multiple sensors, such as: tri-accelerometers, IMU, GPS, potentiometer to measure the steering angle, a laser scanner, pedaling power meter, speed and cadence sensors. Beside, the cyclists were asked to wear a mobile eye-tracker to record their gaze and the surrounding environment. After the instrumentation and calibration of the sensors, an experiment was conducted in the city of Stockholm using the instrumented bicycle; case study III aims to evaluate cycling safety and comfort on snowy/icy surface conditions with focus on the effects of road characteristics on cycling behavior. The same experiment was reproduced on PICS-

L bicycle simulator in Paris by building a virtual environment of the experimental route in Stockholm. Case study IV aims to to validate the simulator behaviorally by comparing the results from the on-road and simulator experiments.

Significant attention is given to vulnerable road-users needs when interacting with cyclists. The special needs of disabled and elderly are studied through: distributing an online questionnaire about their perception and interaction with cyclists; and conducting an on-road experiment to test the possibility of sharing cycling infrastructure with wheelchair-users. In case study V, a number of cyclists and wheelchair users were asked to ride their vehicles on a cycling lane in Madrid in order to evaluate wheelchair users' interaction with cyclists and reaction to the infrastructure.

TABLE OF CONTENTS

LIST OF TABLES

LIST OF FIGURES

LIST OF ABBREVIATIONS

B | D | G | I | L | M | N | R | S | T | V | W

B

BMI Body Mass Index.

D

DoF Degrees of Freedom.

G

GPS Geographic Positioning System.

I

IMU Inertial Measurement Unit.

L

LQR Linear–Quadratic Regulator.

M

MAIS Maximum Abbreviated Injury Scale.

N

NGO Non-Governmental Organization.

R

RI Cycling Risk Indicator.

S

SCI Spinal Cord Injury.

T

TLX NASA Task Load Index.

V

VDM Vehicle Dynamics Model.

W

WHO The World Health Organisation.

CHAPTER 1. INTRODUCTION

Cycling, as an active mode of transportation, provides a wide range of advantages compared to motor vehicles, it is quiet and clean, cost-effective, quick means of transportation, healthy as it provides regular physical activity, but at the same time, it takes up limited space and requires minimal infrastructure investment [1, 2, 3]; as a result, it started gaining popularity among transportation stakeholders as one of the most sustainable modes of transportation for short and medium-distances, especially with the appearance of new cycling modes such as E-bikes and Bike-sharing services, for example, in USA, the number of cycling trips increased from 1.7 billion trips in 2004 to 4 billion trips in 2009 [4]. Despite all these benefits, cycling share remains low when compared to other forms of transportation [5, 6]; this could be explained by the obstacles facing cyclists, including: fear of crime/vandalism, bad weather conditions, social pressure, steep slopes, long commuting distances [7, 8, 9, 10, 11], traffic safety and comfort, [12, 13, 14, 15, 16, 17], lack of adequate infrastructure and continuity of the cycling network [7, 10, 18, 19], and exposure to air pollution [20, 21]. The growth of cycling is still limited due to the lack of investment in cycling infrastructure comparing to highways and public transport [22]. [23] found out that improving the infrastructure design promotes cycling, this becomes evident when looking at countries like The Netherlands, Germany, and Denmark where the governments invested to improve safety, convenience, and comfort of cycling facilities [24, 25].

The fear of traffic accidents is one of the most important reasons behind discouraging people from cycling. Despite all the efforts to prevent them, the number of fatalities and injuries remains high, mainly due to the inability to control the human factor in order to mitigate its effect; statistics show that user behaviour is the main cause of accidents (around 90%) [26]. Furthermore, the continuous increase in car usage has resulted in serious traffic and environmental issues, particularly in large cities. It is no longer feasible

to construct new roadways due to a lack of space. Hence, encouraging and designing sustainable, safer and green transportation alternatives is critical.

The reliability of the road-vehicle-drivers' system is determined by numerous and complex factors, generally, there are three main components that control the safety of any transport network: the first is related to the infrastructure geometric design and control system and maintenance, the second is described by the vehicle condition and the third by the regulations of road users [27, 28]. Figuring out the relationship among all three factors leads to a better understanding of the mechanisms that trigger the occurrence of accidents, which in turns helps to take efficient actions to reduce accident risk.

1.1 Accident Data Analysis

Road traffic crashes represent the eighth leading cause of death worldwide, with more than 1.35 million fatalities each year and up to 50 million injuries [29]. More than half of all road traffic deaths are among vulnerable road users (pedestrians, cyclists and motorcyclists); in fact, several countries reported an increased number of fatalities among cyclists in recent years, probably reflecting the increased popularity of this mode of travel [30]; cycling fatalities represents 4% of traffic fatalities with more than 50 000 deaths per year [31]. A study by [32] shows that the risk for a cyclist to be killed in traffic accident is 3 times higher than for a car driver when considering the time spent in transportation. Cycling also poses a risk to other road users, In 2016, three pedestrians were killed in crashes with cyclists in the United Kingdom, out of 1792 road fatalities reported [33].

In the European Union more than 2000 cyclists are killed annually, which represents 6% of all traffic fatalities [34]. In Sweden, 17 cyclists were killed in 2019 (8% of all traffic fatalities), in 2018, 921 persons suffered Maximum Abbreviated Injury Scale (MAIS), 40% of them were cyclists, with a slight increase comparing to 2017 [35]. In Norway, the risk of injury, expressed as fatalities per kilometer, for cyclists is about 7.5 times higher than for car drivers [36, 37]. In the Netherlands about 5.5 times more fatal injuries are recorded per kilometer travelled by bicycle than by car [38]. A study in

Portland (US) [39] reported that nearly one in five cyclists experienced an event leading to injury, regardless of gender, age, Body Mass Index (BMI), or cycling skill level; injuries were mainly caused by 'slipping' (35%) or 'collision with a car' (19%). In 2015, in Japan, among 4117 traffic fatalities 572 (13.9%) cyclists were killed [40] where the most frequent cause of death was head injuries [41]. In France, despite the fact that cycling represents 2.7% of all commuting trips, cyclists represent 5% of accidents' mortality; in 2017, 173 cyclists were killed in road accidents (which represents an increase by 6.8% compared to 2016), 68 % of them were over 50 years old and 44% were over 65 years [42]; this value has never been reached since 2006 (181 were killed). 93% of people killed or hospitalized in accidents involving a cyclist were cyclists; 12% of them were killed or hospitalized during self accidents and 3% in accidents with another cyclist. According to a survey in 2005, only 14.5% of cyclists in France wear helmets, despite the fact that helmets can help to reduce the severity of accidents [43].

Looking at the causes behind cycling accidents, 'Imprudence' of the cyclist was the cause of accident in 26% of reported cases, 'Distraction' was responsible for 11% of accidents [44]. In Belgium, a study showed that men have more accidents than women as they cycle more frequently for a longer time and distances. 83% of the investigated accidents occurred during a trip to or from work, 53% of the accidents took place during the morning peak hours and 17% during the evening peak hours [44]; the morning peak hours are the most dangerous moment of the day to cycle to work [45], this could be explained by the aggressive behavior of both motorists and cyclists during the busy morning commute which increase the likelihood of having an accident [45]. Another study shows that a typical collision involves cyclists being hit by turning motorised vehicles, occurred due to the cyclist presence in the blind spot of the driver [46]. Cycling accidents may also occur due to the combined effect of low visibility near intersections and the cyclists' behavior in terms of their velocity [47]. The safest areas tend to be where people cycle the most and where cycling infrastructure is most developed[38]; this is known as "safety in numbers" effect, and applies to both cyclists and pedestrians: the greater the number

of cyclists, the more they are expected and observed, and so the risk decreases [47].

1.2 Bicycle Modeling and Simulators' Contribution to Cycling Safety

Bicycles display interesting dynamic behavior, as they are statically unstable except under certain conditions when they are well controlled and balanced in forward motion; this stability depends also on the forces between the wheels and the ground: acceleration and braking require longitudinal forces; whereas balancing and turning depend on lateral forces [48].

There are two main approaches to construct a Vehicle Dynamics Model (VDM): the first one depends on theoretical physics and attempts to produce an exact model of the vehicle, for example by using Lagrange or Newton-Euler methods, even-though the computing-time is high [48, 49]. For example, the researchers in [50] developed the motion equations based on the Lagrange's equation where they applied the Runge–Kutta method to conduct the numerical simulation; the second approach attempts to model the vehicle as simply as possible with lower computing-time [51]. For example, the researchers in [52] used the detailed nonlinear Whipple scientific description to develop 2 DOF bicycle mathematical model in which the control law is solved by Linear–Quadratic Regulator (LQR) algorithm.

The use of simulators seems to be an interesting alternative for responding to several challenges such as: dynamic modeling, learning to drive or cycle, awareness of risks, road safety, and road-user's behavior. Many simulators have been developed over the past three decades for different types of vehicles; for example, flight simulators have been widely used as references and inspiration in the field of driving simulation and two-wheelers. Generally, there are two categories of simulators: motionless simulators and mobile-based simulators [53]. Motionless simulators are built around a screen providing visual feedback, while mobile-based simulators provide, in addition to visual information, indices of movements consistent with those of a real vehicle. It has been recognized that often, a mobile platform if well controlled, can significantly improve the realism of

the simulator of conduct. The researchers in [54, 55] developed a bicycle simulator (so-called KAIST) in order to simulate the dynamics of the bicycle, the simulator consists of a motion generation system of 6 linear actuators and upper and lower platforms and provided by an electric Stewart platform to provide 6-DoF. In [56] the researchers developed a bicycle simulator with profile moving platform with 2 DoF in order to run the simulation of the bicycle dynamic system more accurately.

The literature shows that bicycle simulators are also used to study cyclists' behavior and their reaction to different feature of the road and interaction with other road users; in [57] a bicycle simulator was used to explore the visual behavior and the effect of cycling speed on steering and gaze behavior, which was recorded using a head-mounted eye-tracking device. In [58] the researchers conducted an experiment to investigate the underlying mechanisms that affect the participants' behavior and the main cues for perceiving self-speed in a bicycle simulator. Another study focused on studying the impact of social interaction on children's riding behavior especially while road-crossing by studying peer influence [59].

1.3 The Use of Instrumented Bicycles

Bicycle instrumentation could be used for different purposes and contexts such as: determine the trajectory classes for cyclists, collect naturalistic cycling date, study the bicycle's dynamics, and study cyclists' behaviors. For example, a bicycle was instrumented with gyroscope, accelerometer, absolute encoder and hall effect sensors to determine the trajectory of cyclists in London [60]. In [61, 62] the researchers used an instrumented bicycle to validate a multibody model. The bicycle was equipped with five sensors including: Inertial Measurement Unit (IMU), an inclinometer, and incremental rotary encoders. In [63] the researchers used a bicycle equipped with Geographic Positioning System (GPS), video camera, accelerometer, compass, and gyroscope to discover and characterize conflict points between cyclists and other road users.

In Gothenburg, Sweden, a bicycle was equipped to collect naturalistic cycling data,

the instrumentation consists of two cameras (one facing forward and the other facing the cyclist's face), a GPS, two IMU, two pressure brake sensors, a speed sensor, and a push button, to allow the cyclist to report any risks [64]. The findings reveal that cycling near crossings increases the danger, particularly when there is sight blockage (e.g., buildings and hedges), whereas poor maintenance and road surface condition raised the risk by ten times[65, 66]. In [67, 68] the researchers studied the effect of appearance of cyclists on drivers' overtaking proximity, it was found that overtaking distance decreases when vehicles pass a male cyclist, a cyclist wearing a helmet, or a cyclist cycling away from the road's edge; whereas in [69] the results show that the passing distance decreased when motorcycles overtake a cyclist compared to cars and small trucks. Cyclists appeared unstable when a bus (where the passing time is longer) overtook them. Another study by [10] shows that vehicle drivers do not provide a comfortable passing distance to cyclists in the adjacent cycling lane.

1.4 Disability and it Impact on Mobility

The World Health Organisation (WHO) defines disability as 'The interaction between individuals with a health condition (e.g., cerebral palsy, Down syndrome and depression) and personal and environmental factors (e.g., negative attitudes, inaccessible transportation and public buildings, and limited social supports)' [70]. Globally, the numbers of people who are currently experience disability are over 1 billion, which represents about 15% of the global population. In fact, almost everyone will experience some kind of disability during their life time (movement difficulties that accompanies ageing) [71, 72, 73]. At least 430 million suffer hearing impairment that requires assistance [74], around 253 million people are visually impaired, out of which 36 million are blind [75].

250 000 to 500 000 people suffer a Spinal Cord Injury (SCI) around the world every year; caused by trauma (e.g. a car crash) or from disease or degeneration (e.g. cancer), around 90% of these cases are due to traumatic causes. SCI symptoms may include partial or complete loss of sensory function or motor control of arms, legs and/or body [76],

which leads to reduced or complete loss of walking and ,accordingly, using a wheelchair to mobilize. WHO defines the wheelchair-user as 'The person who is not able to walk at all or has difficulty in walking/moving around and, therefore, uses a wheelchair for personal mobility' [77].

The different types of disability, cognitive or physical, leads to problems in mobility which can be caused by disease, trauma or ageing [78, 79, 80, 81]. A lot of challenges face urban roads accessibility, such as: narrowing in sidewalks (urban furniture, trees), inadequate paving, lack of recess in the crossings and elements that limit the free height of step [82]. According to a survey conducted by a Non-Governmental Organization (NGO), 98% of blind people experienced accidents while traveling [83, 84]. These mobility difficulties limited the inclusion of people with disabilities in social activities [85, 86, 87].

1.5 Thesis Contribution

This research aims to study the different factors that impact cycling safety, with focus on the interaction between cyclists and road infrastructure in order to establish recommendations to improve cyclist behavior and the interaction with the infrastructure and other road users. The main focus will be on bicycles; the goal is to consider both the bicycle and the cyclist as one control system in order to better understand his behavior and increase the quality of bicycle and simulator modeling. Analyzing the cyclist as the center of this modeling will provide important data on how to improve the quality of modeling, as well as, understanding the cyclist's behaviour. On basis of this data, it is possible to provide solutions that enhance safety and stability of bicycles especially in bad weather conditions.

The major tasks of the research are: developing new models for PICS-L bicycle simulator, taking into account road characteristics; knowledge transfer from human factor studies in order to simulate the cyclists's perception/action loop in control tasks; testing on simulator and model validation (scenario programming, Base and 3D objects imple-

mentation... etc.); analyzing road characteristics and their influence on the safety; defining cyclists and trajectories classes and conducting real tests with an instrumented bicycle and compare it with simulation.

1.6 Thesis outline

The thesis is structured in six chapters. Chapter 1 is an introduction to the thesis. chapter 2 is dedicated to present the bicycle dynamic model, the improvements on PICS-L bicycle simulator platform, and presents two original case studies on the physical and subjective validity of the simulator. Chapter 3 is focused on equipping a city bicycle with different sensors, signals analysis, then, in case study III, the experimentation using the instrumented bicycle and the evaluation of cycling safety and comfort in Stockholm city are presented. In chapter 4, a comparative study between PICS-L bicycle simulator and the instrumented bicycle is presented in order to verify the reliability of the simulator, another case study on the bicycle simulator is conducted with the goal to validate cyclists' behavior by comparing the simulation results with the on-road experiment. Chapter 5 is focused on studying the special needs of disabled and wheelchair users when interacting with cyclists. An online questionnaire targeting different groups of people with disabilities was distributed in order to ask them about their perception and interaction with cyclists in urban areas. In case study V, wheelchair users were asked to use the cycling infrastructure, their behavior was then studied and the wheelchair speed profile was compared to the bicycle's one. Finally, in Chapter 6, the conclusion presents the main findings of the thesis and recommendations to improve cycling safety.

CHAPTER 2. SIMULATOR PLATFORM AND MATHEMATICAL MODEL IMPROVEMENT

2.1 Introduction

Experimentation in real environment is not always the appropriate mean to evaluate cycling safety, due to its costs, bias related to uncontrolled variables and risks facing cyclists. On the contrary, simulators allow to detect the behavior of cyclists and other road users in various riding situations, while controlling the variables at play and avoiding the risks associated with a real environment. Bicycle simulator is used, as other simulators of conduct, for different purposes, such as: learning how to cycle, sport, road safety studies, and dynamic modeling. Modeling and analyzing the framework and interactions between the cyclist, bicycle and infrastructure is an essential tool for the development of systems aiming to enhance the safety of road users. However, simulator studies are valid insofar as they are: providing results that can be generalized to real-world situations; and minimizing the occurrence of unwanted symptoms that may result from motion or exposure to the virtual environment (i.e. simulator sickness).

This chapter is structured as follows: the first part is devoted to describe the simulator architecture; the second part describes the the bicycle mathematical model; the third part describes the developed 3 DoF model and the first case study; the forth part describes the 6 DoF model, the physical improvements on the bicycle simulator platform, and discuss the results of the second case study in terms of physical and subjective validity of the simulator; and finally the conclusion.

2.2 Simulator architecture

PICS-L bicycle simulator, which was developed by The French Institute of Science and Technology for Transport, Development and Networks (IFSTTAR), was built by placing a real bicycle on a platform, it has one Degrees of Freedom (DOF), which is the steering angle. The simulator is equipped with two force feedback devices: one providing haptic feedback to the handlebar and the other dedicated to the rear wheel. The speed of the rear wheel and the angular position of the handlebar are measured and logged. Force feedback is applied to the rear wheel using a motor attached to a cylinder in contact with the wheel. In order to provide more realistic circumstances, the simulator consists of several components as shown in Fig. 2.1 and detailed below:

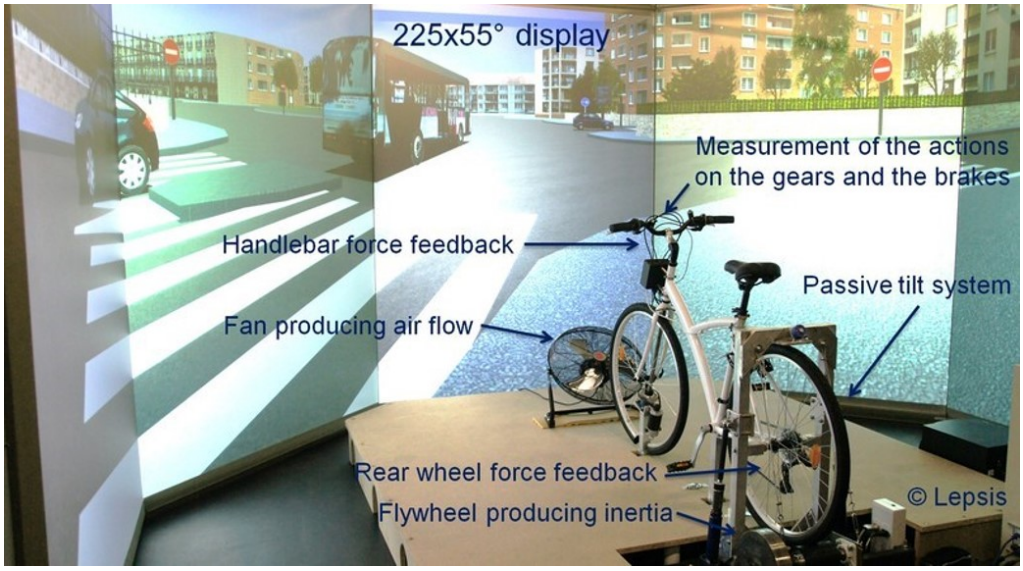

Figure 2.1. PICSL-L bicycle simulator, features explained under the experimental setup section.

1. A fan, placed in front of the bicycle, reproduces the airflow felt by cyclists in real situations. The fan speed is proportional to the rear wheel's speed.

2. An incremental encoder, attached to the fork, allows the rider to interact with the virtual environment and provides realistic haptic force feedback to the handlebar and measures the steering angle and velocity.

3. A passive mechanical lateral suspension system allows participants to slightly tilt the bicycle when turning left or right.

4. A flywheel, attached to the rear wheel, simulates an inertia equal to 60 kg mass in actual cycling. The simulator is also equipped with a motor with the ability to increase the inertia up to 85 kg as in actual cycling.

5. An incremental encoder attached to the rear wheel, with the purpose to calculate the speed of the bicycle to use it as an input for the virtual reality to define the cyclist position and trajectory.

6. Five visual displays installed in front and sides of the bicycle forming a cave virtual environment that provides simulated conditions similar to real-life environment. The visual displays provide a visual angle of 225 degrees horizontally and 55 degrees vertically in order to improve the immersion in the virtual reality. A supplementary display device is placed behind the left shoulder of the cyclist for the rear visualisation of the road.

2.3 Bicycle Dynamic Model

In PICS-L bicycle simulator, the single-track model was used to produce more convenient and accurate model in order to study the following environmental determinants of cyclists' behavior [58, 88, 89]:

1. The environmental elements to which cyclists adapt their behavior (i.e. speed, safety gap, steering, etc.);

2. How cyclists adjust their riding practices as they interact with other road users;

3. How cyclists anticipate risks in hazardous riding situations, and what strategies, equipment or behaviours they employ to cope with those risks.

The mathematical model that runs the simulator was developed by the engineers of the simulators' team (SimTeam) in PICS-L laboratory in Gustave Eiffel University (SimTeam is a group of engineers and technicians in Gustave Eiffel University who are responsible of operating, maintenance and development of the simulators of conduct in the university) [90]. The aim of this model was to run the simulator efficiently in coordination with the virtual environment, without focusing on the dynamical parameters of the bicycle. The bicycle dynamic model, which was created using MATLAB-Simulink, shows the relations between the different parts of the bicycle model in a graphical format. This allows to graphically trace the various inputs and visualize their relation in MATLAB script format. The model has different sub-layers showing the relative outputs of the different parts, the different blocks of the model are shown in Fig.2.2 and explained below.

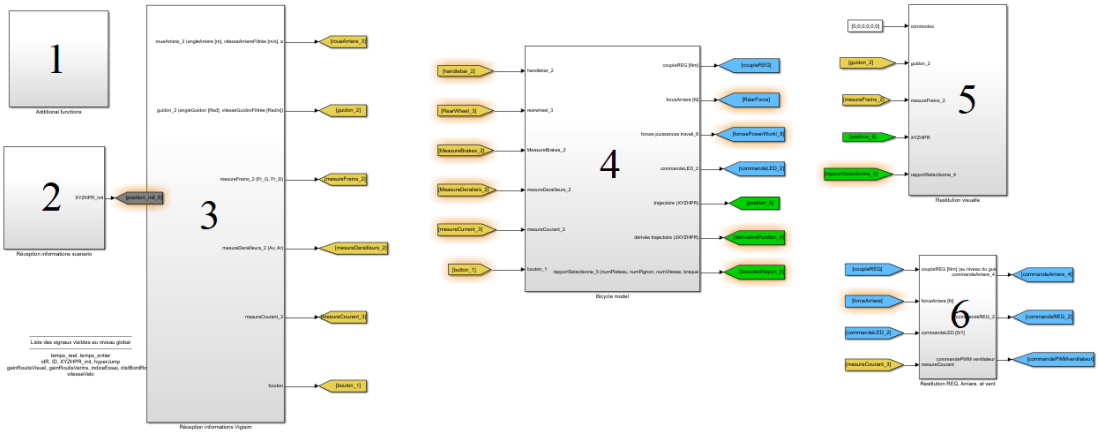

Figure 2.2. SimTeam simulink model, including bicycle model, input, outputs, washout, etc.

1. The first block is the simulation Time manager: the aim is adjusting the time step and the real time in the simulation.

2. The function of the second block is to receive information of the bicycle coordinates (XYZ) on the scenario (visual), which is used to calculate the trajectory of

the bicycle simulator in the virtual reality environment.

3. The function of the third block is to receive signals from the control cabin (e.g. steering angle) and store it in order to be used as inputs for the bicycle model.

4. The forth block represents the Bicycle Dynamic Model: it receive inputs from the cabin running the simulator including information from the incremental encoders attached to the rear wheel and the handlebar, gear and brakes and use these inputs to compute the return effort torque, rear wheel friction force and speed, and yaw rate. For example, the friction force of the rear wheel was estimated using (2.1):

$$m.a = F_f + F_a + F_c + F_b + F_g \tag{2.1}$$

where m is the total mass of the bicycle-rider system in kg, a is the longitudinal acceleration in m/s^2 (the speed was measured using an incremental encoder attached to the rear wheel of the bicycle, F_f is the friction force to be calculated, F_c is the force applied by the cyclist on the pedals which is measured using a pedal power meter, F_b is the breaking force and F_g is the gravity force caused by the slopes, F_a is the aerodynamic resistance calculated on the basis of the following equation:

$$F_a = 0.5 C_{ax} \rho S V_x^2 \tag{2.2}$$

with C_{ax}, the coefficient of aerodynamic resistance given by the bicycle manufacturer,ρ the air density in kg/m^3, S the frontal surface of the bicycle and the rider body in m^2 and V_x the longitudinal velocity of the bicycle.

The yaw rate was calculated using (2.3):

$$\dot{\psi} = \frac{V_x}{R_c} \tag{2.3}$$

where V_x is the bicycle velocity and R_c is the radius of curvature calculated using (2.4):

$$R_c = \frac{l_f + l_r}{sin\ \delta_s} \tag{2.4}$$

where l_F and l_R are distances from COG to front and rear axles and δ_s is the steering angle.

5. The fifth block was used for the visual projection, but it is no longer used, because the visual is on the 5 fixed projector and there is no need to correct the position of the visual based on the longitudinal movement.

6. The sixth block is for the restitution of couple, rear force feedback, and fan speed.

2.4 Three DoF Dynamic Model

This model was built and improved based on the SimTeam one. The model under investigation in this section was developed to have 3 DoF (longitudinal, lateral, vertical) adding the following features to the previous dynamic model:

- The vertical model was developed considering the road profile, the vertical displacement of the wheels' centre of gravity, the static normal force and the normal force according to the vertical stiffness of the bicycle.
- The road adhesion was considered when building the longitudinal model of the bicycle wheels.
- The lateral model considers the effect of the side slip angle and the lateral stiffness of the bicycle wheels.

2.4.1 Vertical modeling

The tires of the front and rear wheels are modelled by springs with k_F and k_R coefficients respectively. The front and rear wheel masses are given respectively by m_F and m_R. At

the tire road contact, the road profile, the skid resistance, and the radius of curvature are considered inputs of the system. The pitch angle of the bicycle is neglected. Fig. 2.3 shows the vertical model of the bicycle.

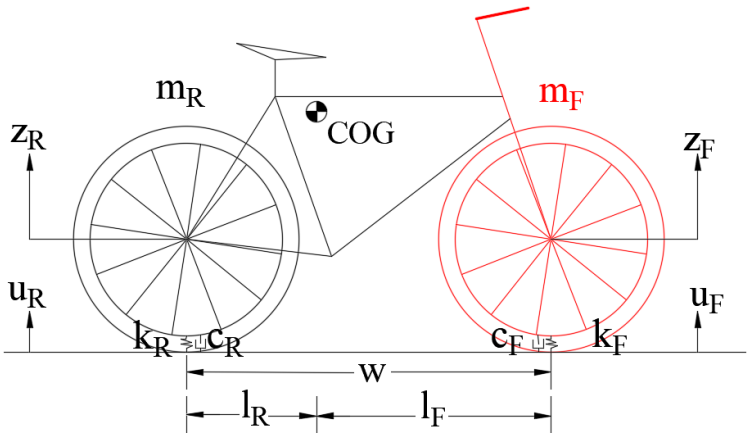

Figure 2.3. Side view of the bicycle model shows the geometrical and dynamic parameters of the bicycle used in the mathematical model. The model is divide into two parts: the front part (red) and the rear part (black).

The vertical acceleration values of the wheels are obtained using (2.5):

$$\begin{cases} \ddot{z}_F = \dfrac{k_F(u_F - z_F)}{m_F} \\ \ddot{z}_R = \dfrac{k_R(u_R - z_R)}{m_R} \end{cases} \tag{2.5}$$

Where m_F and m_R are the masses of the front and rear parts of the bicycle including cyclist's body mass, k_F and k_R are the front and rear tires vertical stiffness, z_F and z_R are the vertical displacement of the COG of the front and rear wheel respectively, u_F and u_R are respectively the front and rear value of road profile. To obtain the vertical displacement z_R we integrate twice this acceleration. The normal forces F_{nF} and F_{nR} acting on the wheels are calculated as in (2.6). The force generated by damping effects is neglected.

$$\begin{cases} F_{nF} = F_{cF} + k_F(u_F - z_F) \\ F_{nR} = F_{cR} + k_R(u_R - z_R) \end{cases} \tag{2.6}$$

Where F_{cF} and F_{cR} are respectively the static rear and front force due to the static mass of the vehicle.

2.4.2 Lateral modeling

In order to calculate the wheel forces, it is necessary to know wheel slip, tire side slip angle and friction coefficients, as these are inputs for the force equations. For the tire side slip angle calculation, the wheel caster has to be considered and the radius of curvature of the individual wheels, see equations (2.7).

$$\begin{cases} \alpha_F = -\dot{\beta} + \delta_w - \dfrac{l_F\,\dot{\psi}}{v_{COG}} \\ \alpha_R = -\dot{\beta} + \dfrac{l_R\,\dot{\psi}}{v_{COG}} \end{cases} \tag{2.7}$$

where α_F and α_R are the side slip angles for the front and rear tires respectively, $\dot{\beta}$ is the velocity of the side slip angle at the COG, δ_w is the steering angle of the handlebar, l_F and l_R are distances from COG to front and rear axles, v_{COG} is the COG velocity, $\dot{\psi}$ is the yaw rate calculated using (2.3) in section 2.3:

After the calculation of the different parameters, it is possible to calculate the lateral force for both the front and rear wheel using (2.8).

$$\begin{cases} F_{yF} = \alpha_F\, C_y \\ F_{yR} = \alpha_R\, C_y \end{cases} \tag{2.8}$$

where F_{yF} and F_{yR} are the lateral forces of the front and rear wheel respectively, C_y is the tire lateral stiffness.

2.4.3 Longitudinal modeling

The coefficient μ is a function of the slip λ and the vehicle speed v. It characterizes the grip of tire contact with the road. We say that the grip is maximal when this coefficient is equal to 1. Adherence is zero when μ tends to 0. According to the Burckhardt model [51, 91], μ is given by:

$$\mu_i = C_1 \left(1 - e^{-C_2 \lambda_i}\right) - C_3 \lambda_i, \quad i = 1, 2 \tag{2.9}$$

Where C_1, C_2 and C_3 define the characteristics of the tire (level, quality, deterioration, inflation pressure, temperature) , C4 defines the condition of the road grip. These parameters can be determined by experimental measurements, where: C_1: The maximal value of the friction curve. C_2: corresponds to the shape of the friction curve. C_3: the difference between the maximal value of the friction and 1. C_4: is known and it depends on the maximal velocity of the wheel. C_5: determines the influence of the vertical load on the wheel. By changing the values of the C parameters, many different road conditions may be modeled. For the current model the following values were chosen: C_1=1.2801, C_2=23.99, C_3=0.52, C_4=0, C_5=0.

The longitudinal slip rate λ_i for wheel i can be obtained using the following equation taken from [92] :

$$\lambda_i = \begin{cases} \dfrac{r_e\, w_i}{v_i} - 1, & \text{if } v_i > r_e\, w_i \;\; (braking) \\ 1 - \dfrac{r_e\, w_i}{v_i}, & \text{if } v_i < r_e\, w_i \;\; (acceleration) \end{cases} \tag{2.10}$$

Where: w_i is the angular velocity of the center of i-th wheel, v_i is the speed of the center of i-th wheel and r_e is the effective radius of the wheel, when a vertical force is applied on the tire. For the model under discussion, the calculation of mu is not possible as v_i input is missing, because the lack of a sensor to measure it for the simulator as it is stationary.

In the case of excessive drift angles, the definition of the behavior of the tire is often described by the empirical formula proposed by Bakker and Pacejka [93, 94]. This model, which takes into account many parameters identified on the basis of measurements, makes it possible to best approach the longitudinal and lateral behavior of the tire in the nonlinear case. However, Pacejka model was not developed in this study as it was

not possible to get all the required bicycle parameters.

The Longitudinal frictional forces of the front and rear wheels can be calculated depending on the adhesion co-efficient using (2.11). This provides the frictional forces in the direction of the wheel ground contact velocity.

$$\begin{cases} F_{xF} = \mu \, F_{zF} \, cos\alpha_F \\ F_{xR} = \mu \, F_{zR} \, cos\alpha_R \end{cases} \tag{2.11}$$

where F_{xF} and F_{xR} are the longitudinal forces for the front and rear wheel respectively, μ is the adhesion coefficient and F_{zF} and F_{zR} are the vertical forces applied on the front and rear wheels.

2.5 Case Study I

Several tests and scenarios have been realized at various speeds with the bicycle simulator. Selected results of the vertical displacement and forces, side slip angle, lateral forces and longitudinal forces are presented in this section. The dynamic parameters and the static vertical forces are stated from the literature [95, 96, 97]. The values of the static front and rear vertical forces (which were calculated according to the combined mass of the bicycle and rider by applying the equilibrium equations with known COG) are 230 and 630 N, respectively.

2.5.1 Vertical displacement and force

The longitudinal road profile, which was measured in a previous experiment conducted by IFSTTAR) is used as an input signal for the Simulink model (see Fig.2.4). A close up on the time interval of [10, 15] s is given on the right side of the figure. The vertical displacement with a close up on the time interval of [10, 15] s to the right shown in Fig. 2.5 was estimated using equation (2.5). Despite the double filtering effect caused by integrating two times, the two signals indicate the effect of road profile on vertical displacement of the wheels.

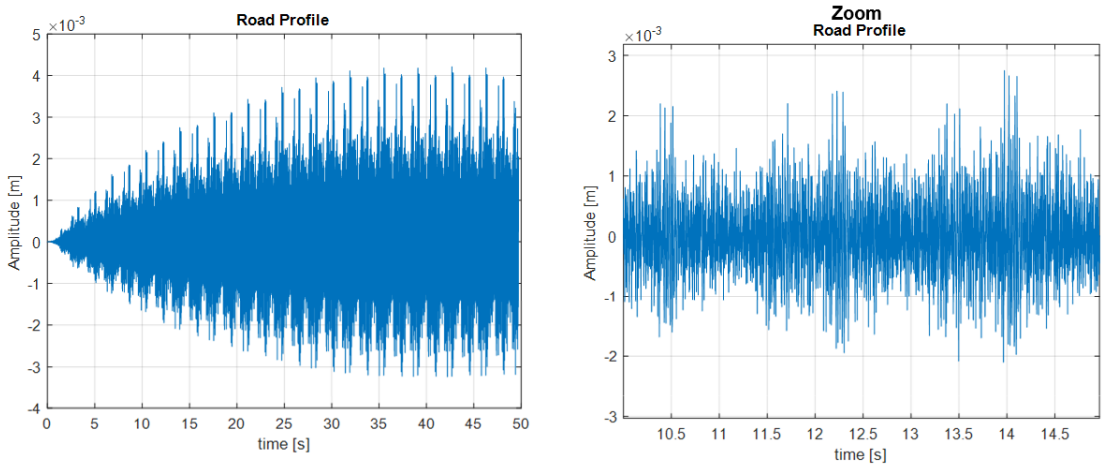

Figure 2.4. Road profile input.

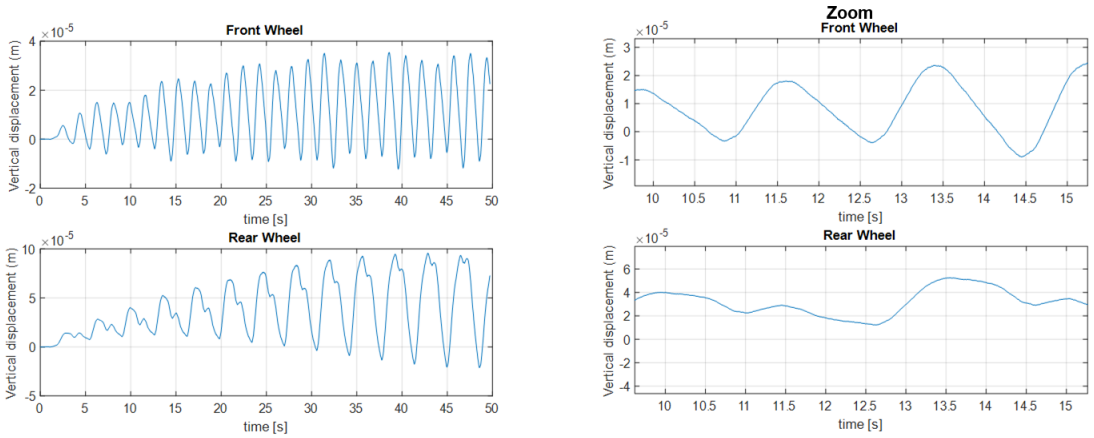

Figure 2.5. Vertical displacement for the front and rear wheel.

In Fig. 2.6, the vertical forces of the front and rear wheels are presented. The close up on the time interval of [10, 15] s is displayed on the right side of this figure. It can be noticed that at the 10.5th, 12.3th, and 14th second, the vertical force increases following the amplitude of the road profile at this time.

2.5.2 Side slip angle and lateral force

The steering angle of the bicycle handlebar during the test (shown in Fig.2.7) was measured using the incremental encoder connected to the handlebar of the bicycle simulator. The side slip angle shown in Fig. 2.8 noticeably reflects the angular movement of the handlebar.

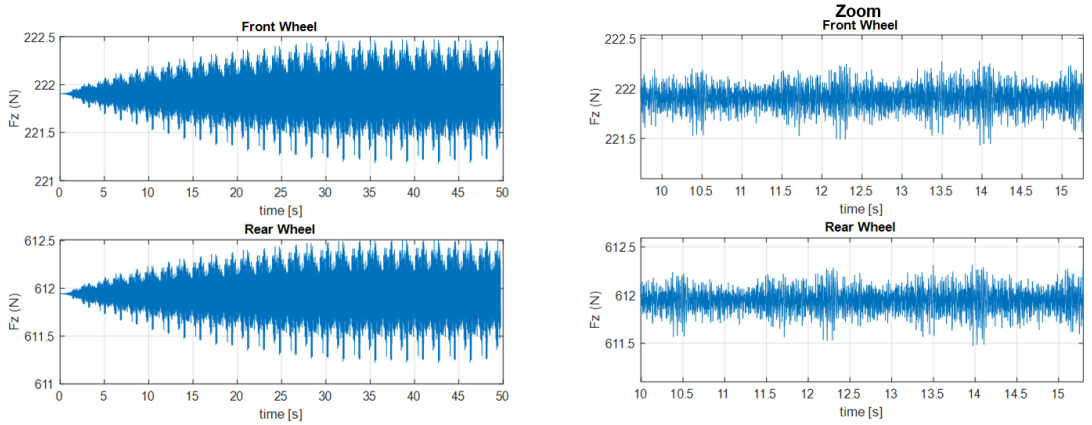

Figure 2.6. Vertical force for the front and rear wheel.

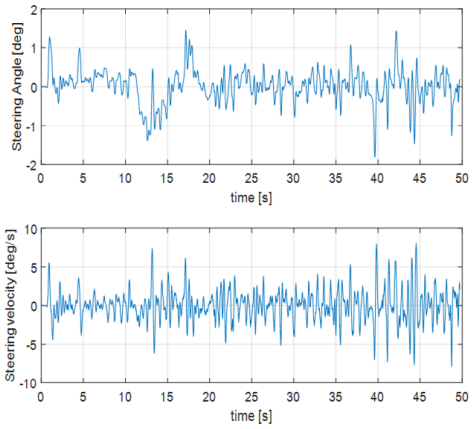

Figure 2.7. Steering velocity and angle extracted from the incremental encoder.

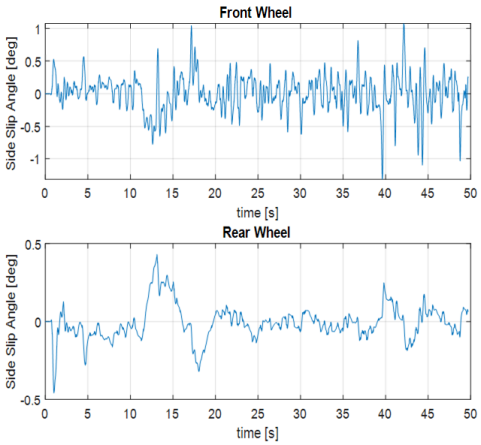

Figure 2.8. Side slip angle for the front and rear wheel.

The lateral trajectory of the bicycle as shown in Fig. 2.9 is perceived to be affected by the steering angle. With a closer look at the span between [10,15] s, the effect of high steering angle on the trajectory can be observed.

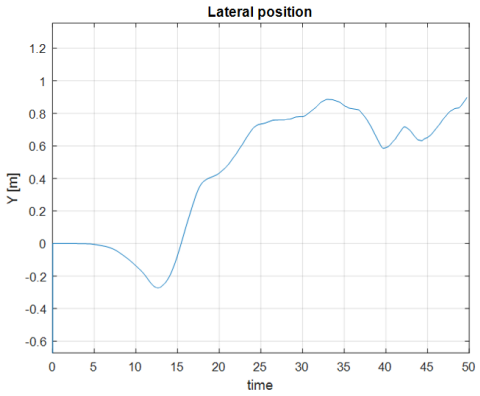

Figure 2.9. Lateral position calculated using SimTeam model.

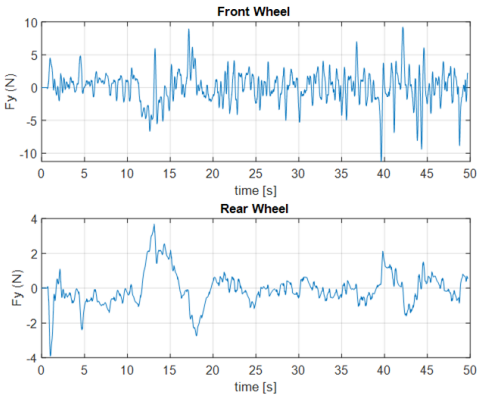

Figure 2.10. The calculated lateral force for the front and rear wheel.

Fig. 2.10 illustrates the lateral force of the front and rear wheels. The graphs show that the increase of the sides slip angle causes an increase in the lateral force, this becomes obvious at 40th and 45th second.

2.5.3 Longitudinal force

In the simulation several adhesion coefficient representing different surface condition (due to different weather conditions) came to use. The longitudinal force shown in Fig. 2.12, which was calculated based on the adhesion coefficient (Fig. 2.11), illustrates the impact of different adhesion coefficient. While the road surface is dry (μ=0.8) the longitudinal friction force in high whereas a wet surface (μ=0.2) results in a low longitudinal friction force.

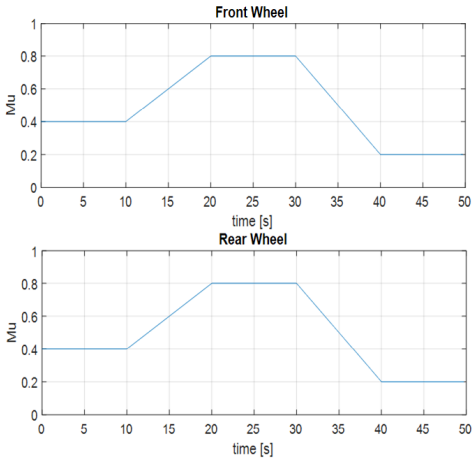

Figure 2.11. Road adhesion input for the front and rear wheel.

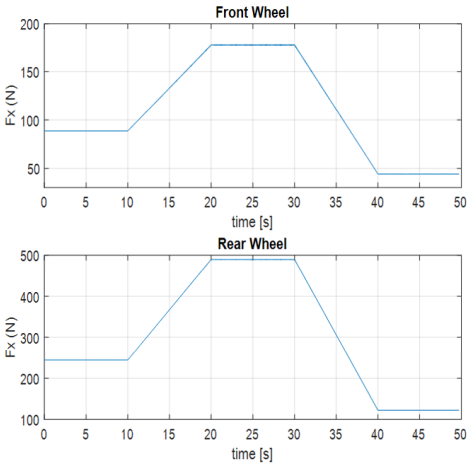

Figure 2.12. The calculated longitudinal force for the front and rear wheel.

2.5.4 Experimental scenario

The experiment took place in a simulated urban environment. The route was straight (no curves) and consists of two sections: the first is a bicycle-bus shared lane, the latter with a separated bicycle lane. The participants took a pre-ride for 2 minutes in order to familiarize themselves with the simulator. After the end of the familiarization, the participants rode the bicycle for around 10 minutes. The traffic was generated at the same and opposite directions of the cyclist and buses were passing beside the cyclist from time to time. The participants were asked to maneuver with the simulator using the different features such as: handlebar, pedals, gear and brakes. Ten subjects (6 male; mean age=28.17, SD=3.76 and 4 females; mean age=25.25, SD=2.06) participated in this experiment. All had normal or corrected-to-normal vision. The mean cycling experience of the participants was 12.9 years. The average number of cycling kilometers per month was 62. None of them rode a bicycle simulator before.

2.5.5 Experiment's subjective results

At the end of the experiment, the participants completed 3 questionnaires: the first one regarding their cycling experience and the impact of the bicycle simulator on their personal

Table 2.1 Analysis of the The Simulator Sickness Questionnaire (SSQ)

Participant number	Total severity	Oculomotor	Nausea	Disorientation
mean	32.538	22.896	24.256	43.152
SD	36.80	35.18	23.92	62.75
Min	0	0	0	0
Max	115.94	114.48	68.22	194.88

status; the second one consists of the NASA Task Load Index (TLX) form [98] which is used to assess the work load, and the thirs one is Simulator Sickness Questionnaire (SSQ) developed by [99] to evaluate the different symptoms of the bicycle simulator. The results of the first questionnaire show that the average evaluation of the similarity to cycling in real environment ranges between 4 and 8 on scale of 10 (mean= 6.1, SD= 1,6). Assessing the realism of the simulator, the participants mentioned as the most realistic aspects of the simulator: the good design of the virtual road, the effort of pedaling, traffic and other sensory cues, such as the wind and the sound of the passing traffic. As suggestions for improvement, most participants agreed they expect higher speed compared to the cycling effort.

Simulator Sickness

The analysis of the simulator sickness questionnaire listed in Table 2.1 shows that the average total severity of all participants is around 32.5. These results may be interpreted by comparing this number to the possible scores listed in Table 2.2, we could see that the total severity of the simulator is slight (less than 78.5). It is also noticed that participants wearing lenses experienced the highest total severity (participant 6 no. has 115.9 and participant no. 10 has 71). The affected participants showed high disorientation symptoms.

The results also show that one participant suffered from simulator sickness, as he had severe symptoms of eye strain, difficulty focusing, sweating, nausea and dizziness with eyes open. Accordingly the participant was immediately asked to stop the experiment.

Table 2.2 Possible score results of The Simulator Sickness Questionnaire (SSQ) and their interpretation.

	Nausea	Oculomotor	Disorientation	Total Severity
none	0	0	0	0
slight	66.8	53.1	97.4	78.5
moderate	133.6	106.1	194.9	157.1
severe	200.3	159.2	292.3	235.6

On the other hand, 30% of the participants felt a slight general discomfort and 30% experienced a slight sweating increase.

The average exposition to different symptoms during and after riding the bicycle simulator are reported in the radar chart view in Fig. 2.13.

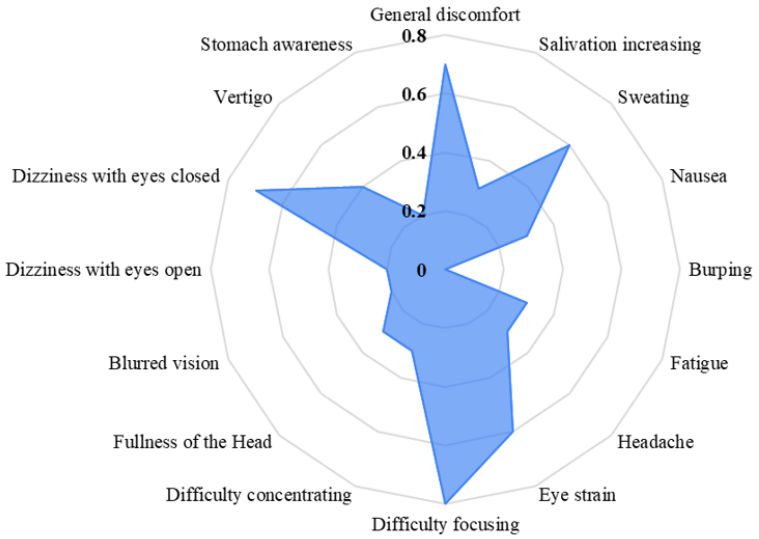

Figure 2.13. Mean scores observed in each item of the exposure of simulator sickness questionnaire.

NASA Task Load Index

The Nasa Task Load index is used to collect subjective workload assessments for different simulators [98]. Table 2.3 shows the weighted ratings of the NASA TLX. The first column shows the scales under assessment, the second represents the average weight of each scale according to the personal opinion of the participant. The scorer chooses different factors on an evaluation cards according to its importance, while the weight of each

factor is the number of times it was circled. The third column is the average raw rating taken from the TLX questionnaire, where the participants evaluated each factor on a scale of 100. The last column represents the adjusted weighting, which is the multiplication of the weight and raw rating of each factor. It is noticed that the physical demand was highly weighted affecting the overall work load (87.4 on a scale of 100), while the raw rating shows a moderate overall workload. The analysis of NASA Task Load Index (TLX) for the 10 participants shows that the simulator requires a medium physical demand. This is explained by the effort the participants required to do when riding any bicycle since it is an active transport mode.

Table 2.3 Weighted rating of NASA Task Load Index (TLX).

Scale title	Weight	Raw Rating	Adjusted rating
Mental Demand	3	27.78	83.33
Physical Demand	4	47.78	191.11
Temporal Demand	2	31.11	62.22
Performance	1	42.22	42.22
Effort	3	34.44	103.33
Frustration	2	21.11	42.22
Overall workload		34.07	87.41

Fig. 2.14 shows the weighted average of each work load factor; the width of each column represents the weight of each factor. We notice the performance was weighted the least, this could be explained because the required task was simple and easy to accomplish, so the participant chose not to give it a high rating.

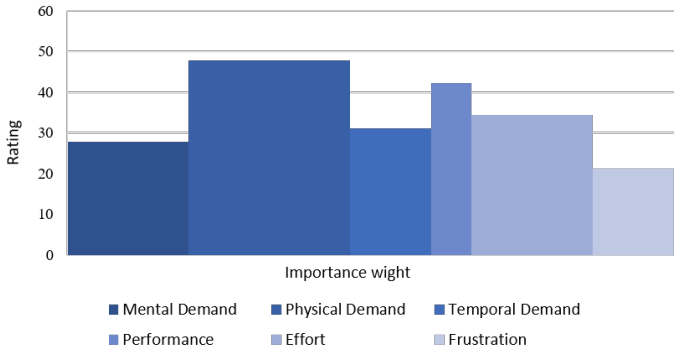

Figure 2.14. Graphic representation of the composition of a weighted workload score.

2.6 The Improvements Conducted on The Simulator Platform

In order to improve the simulator in terms of the tire-surface contact, it is important to consider the unevenness of road surface and road adhesion and study their effect in the model. Two components have been installed on the simulator in addition to the features shown in Fig. 2.15. Each feature is described in details:

1. Three actuators, installed on the platform, simulate the vibrations caused by the unevenness of the road surface. The acceleration is limited to +/- 1 g in order to keep the platform stable, the amplitude is limited to +/- 2.5 mm (up to +/- 5 mm) when the frequency is 10 Hz (up to 20 Hz). [100] found that vibrations input improves the estimation of speed.

2. A cylindrical asphalt specimen in contact with the rear tire (installed recently to replace a plastic cylinder) simulates road adhesion. The specimen is made of hot mixed asphalt concrete. It is 10 cm in diameter and 12 cm in height, the specimen is penetrated in the center to allow a shaft of 2 cm diameter to pass along its axis for fixation (see Fig.2.16).

2.7 Six DoF Bicycle Model

This bicycle dynamic model aims to reproduce the dynamics of a bicycle in simulation or in a real environment, with more accuracy and reasonable computing time. Comparing

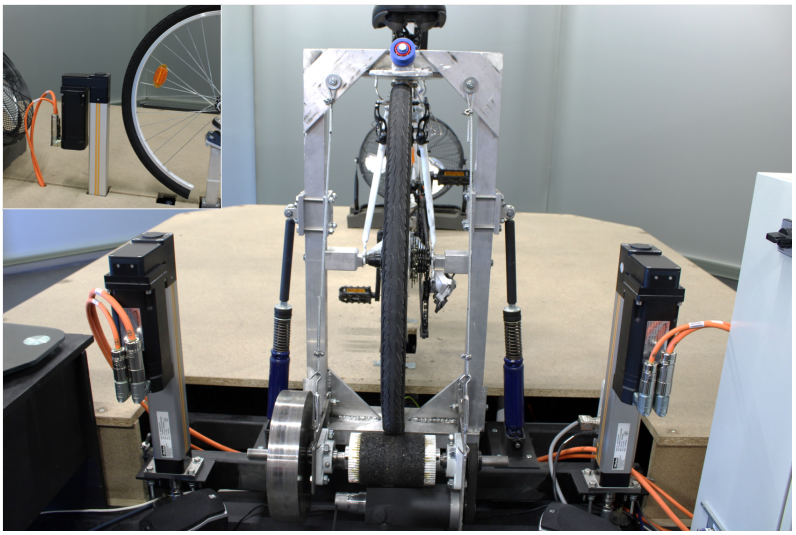

Figure 2.15. The actuators fixed on the simulator platform.

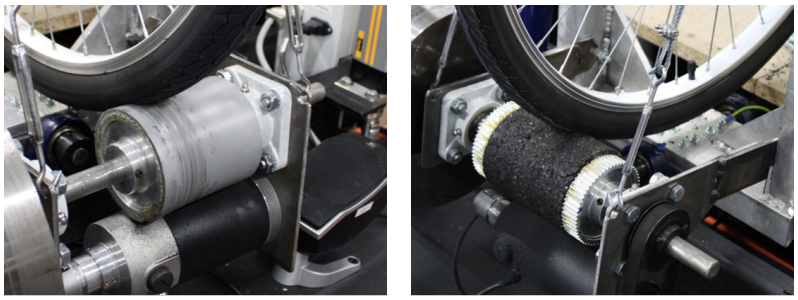

Figure 2.16. Wheel-road surface interaction system (a) before and (b) after the installation of the asphalt specimen.

to the last model described in previous section, the new one has 6 DoF (longitudinal, lateral, vertical, Yaw, Pitch and Roll), the damping coefficient of the wheels was included in vertical modeling whereas it was not considered before. The road profile input is taken from a real measurement of road surface, whereas in the previous model it was a sinusoidal signal. Fig. 2.17 shows the operating flow of the bicycle simulator and the interaction between its different parts.

2.7.1 Vertical Modeling

The same geometrical and mass parameters of 3 DoF model of the bicycle were used as illustrated in the schematic in Fig. 2.3 and divided as follows: the front part includes the steering axis, the front fork, the front wheel and a fraction of the cyclist mass; and the rear

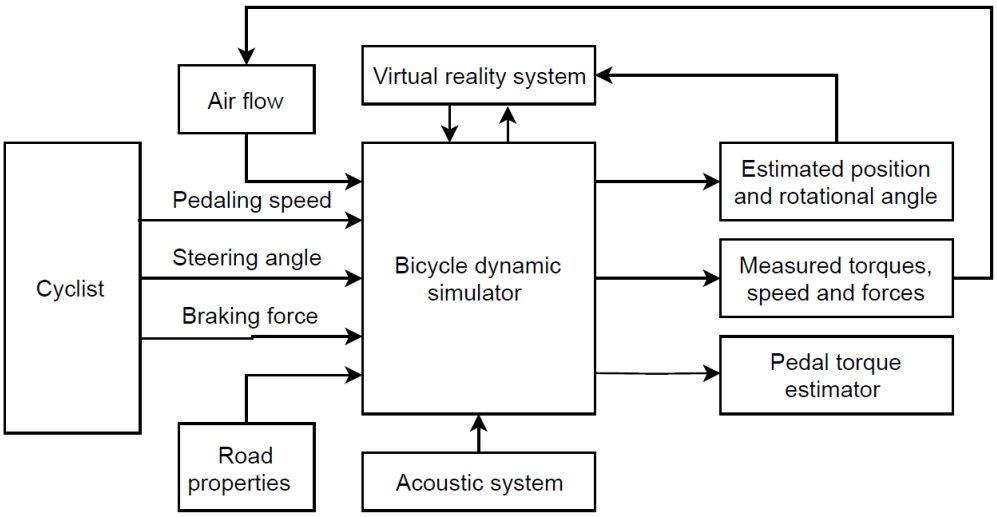

Figure 2.17. Operating flow of the bicycle simulator.

part includes the frame, the rear wheel and the other fraction of the cyclist body mass. The reactions of total mass are modelled by springs representing the tires stiffness (k_F and k_R) and damping coefficients (B_F and B_R). The bicycle has no suspension system. The fractions of the bicycle-rider system mass are m_F and m_R. The tire contact, road profile, road adhesion, and radius of curvature are considered inputs of the system. The pitch angle effect is neglected [101, 102]. Fig. 2.17 shows the main parameters used in the dynamical model and the operating flow of the simulator .

The vertical acceleration values of the wheels ($\ddot{z}$) are obtained using (2.12):

$$\begin{cases} \ddot{z}_F = \dfrac{k_F(u_F - z_F) - B_F\,\dot{z_F} - k_F\,l_R\,sin\phi}{m_F} \\ \ddot{z}_R = \dfrac{k_R(u_R - z_R) - B_R\,\dot{z_R} - k_R\,l_F\,sin\phi}{m_R} \end{cases} \tag{2.12}$$

where m_F and m_R are the masses of the front and rear parts, k_F and k_R are the front and rear tire vertical stiffness, B_F and B_R are the damping coefficients of the front and rear wheel, z_F and z_R are the vertical displacements of the Center of Gravity (COG) of the front and rear parts respectively, u_F and u_R are the front and rear values of road profile. ϕ is the roll angle to be calculated using (2.21).

To obtain the vertical displacements z_F and z_R, the acceleration is integrated twice. The normal forces F_{nF} and F_{nR} acting on the wheels are calculated in (2.13):

$$\begin{cases} F_{nF} = F_{cF} + k_F(u_F - z_F) + B_F(\dot{u_F} - \dot{z_F}) \\ F_{nR} = F_{cR} + k_R(u_R - z_R) + B_R(\dot{u_R} - \dot{z_R}) \end{cases} \tag{2.13}$$

where F_{cF} and F_{cR} are the static forces of the bicycle-rider system applied to the front and rear wheel. They were calculated by applying the equilibrium equation. Assuming the bicycle-rider mass equals 85 kg, F_{cF} and F_{cR} are 230 and 630 N, respectively.

2.7.2 Lateral modeling

Lateral forces of the bicycle depend on different factors, such as: the tire slip, the side slip angle and the road adhesion coefficient. The tire side slip angle for both wheels are calculated using (2.7) of the 3 DoF model in section 2.4.

The lateral forces for both front and rear wheel (considering the lateral slope of the road) are obtained as following:

$$\begin{cases} F_{yF} = \alpha_F \, C_y + m_F \, g \, sin\phi \\ F_{yR} = \alpha_R \, C_y + m_R \, g \, sin\phi \end{cases} \tag{2.14}$$

where F_{yF} and F_{yR} are the lateral forces of the front and rear wheel respectively, C_y is the tire lateral stiffness and ϕ is the roll angle. The lateral acceleration of the bicycle simulator (a_y) is then calculated using the following formula:

$$a_y = \frac{F_{yF} + F_{yR}}{m} \tag{2.15}$$

where m is the total mass of the bicycle-rider system. The double integration of the acceleration gives the lateral displacement.

2.7.3 Longitudinal modeling

The longitudinal frictional forces of front and rear wheels can be calculated from the adhesion coefficient using (2.16). This provides the frictional forces in the direction of the wheel ground contact velocity.

$$\begin{cases} F_{xF} = \mu \, F_{zF} \, cos\alpha_F + F_{sF} + F_{aero} \\ F_{xR} = \mu \, F_{zR} \, cos\alpha_R + F_{sR} + F_{aero} \end{cases} \tag{2.16}$$

where F_{xF} and F_{xR} are the longitudinal forces for the front and rear wheel respectively, μ is the adhesion coefficient and F_{zF} and F_{zR} are the vertical forces applied on the front and rear wheels. F_{sF} and F_{sR} are the forces caused by the longitudinal slope of the road calculated as following:

$$\begin{cases} F_{sF} = m_F \, g \, sin\theta \\ F_{sR} = m_R \, g \, sin\theta \end{cases} \tag{2.17}$$

where θ is the road longitudinal slope. The aerodynamic force resistance (F_{aero}) is calculated as:

$$F_{aero} = 0.5 \, Cax \, \rho \, S \, V_x^2 \tag{2.18}$$

where C_{ax} is the coefficient of aerodynamic resistance given by the bicycle manufacturer, ρ is the air density in kg/m^3, S is the frontal surface area of the bicycle and the rider in m^2 and V_x is the longitudinal velocity in m/s. The longitudinal acceleration of the bicycle simulator (a_x) is then calculated using the following formula:

$$a_x = \frac{F_{xF} + F_{xR}}{m} \tag{2.19}$$

2.7.4 Rotational modeling

Yaw rotation modeling can be obtained by using the lateral forces as described in (2.20) :

$$\ddot{\psi} = \frac{F_{yF} \, l_f - F_{yR} \, l_r}{Izz} \tag{2.20}$$

where $\ddot{\psi}$ is the yaw angle acceleration, F_{yF} and F_{yR} are the lateral forces of the front and rear wheel and I_{zz} is the moment of inertia around z-axis. Yaw rate $\dot{\psi}$ was also

calculated using (2.3). The yaw angle value is calculated by integrating the yaw rate.

The roll angle about the bicycle's x-axis (ϕ) can be calculated using the speed and radius of curvature [103] as in (2.21):

$$\phi = \tan^{-1} \frac{V_x^2}{g\, R_c} \tag{2.21}$$

The roll acceleration ($\ddot{\phi}$) is calculated using the mass and rotation matrices [103] as in (2.22):

$$\ddot{\phi} = \frac{r_{31}\, \phi + r_{32}\, \delta + r_{34}\, v_x\, \dot{\psi} + r_{36}\, v_x \dot{\delta} - (m_{13}\, v_y + m_{23}\, \ddot{\psi} + m_{34}\, \ddot{\delta})}{m_{33}} \tag{2.22}$$

with

$$r_{31} = (m_F\, j + m_R\, h)g \tag{2.23}$$

where j and h are the vertical component of the center of gravity for the front and rear part of the bicycle respectively, and g is the gravitational acceleration.

$$r_{32} = m_F\, e\, g - \eta\, F_{zF} \tag{2.24}$$

where e is the perpendicular distance between the center of gravity of the front part and the fork and η is the bicycle trail.

$$r_{34} = -m_F\, j - m_R\, h - \frac{I_{yRF}}{R_F} - \frac{I_{yRR}}{R_R} \tag{2.25}$$

where I_{yRF} and I_{yRR} are the moments of inertia around the y-axis for the front and rear wheel respectively, R_f and R_r are the radii of front and rear wheel.

$$r_{36} = -\frac{I_{yRF}}{R_F\, cos\epsilon} \tag{2.26}$$

where ϵ is the bicycle caster angle (i.e. the angular displacement of the steering axis from the vertical axis of a steered wheel).

$$m_{13} = m_F\, j + m_R\, h \tag{2.27}$$

$$m_{23} = m_F\, j\, k - C_{xzGR} + (I_{zGF} - I_{xGF})\, sin\epsilon\, cos\epsilon \tag{2.28}$$

$$m_{33} = m_F\, j^2 + m_R\, h^2 + I_{xGR} + I_{xGF}\, cos\epsilon^2 + I_{zGF} sin\epsilon^2 \tag{2.29}$$

$$m_{34} = m_F\, e\, j + I_{zGF}\, sin\epsilon \tag{2.30}$$

The roll rate is calculated by integrating the roll acceleration.

The pitch angle acceleration of the bicycle body $\ddot{\theta}$ can be calculated depending on the stiffness of the tires as in (2.31):

$$\ddot{\theta} = \frac{-k_R\, l_r\, z_R + k_F\, l_f\, z_F + (k_R\, l_r - k_F\, l_f)z - (k_R\, l_r^2 - k_F\, l_f^2)\, sin\theta}{I_{yy}} \tag{2.31}$$

where I_{yy} is the moment of inertia around y-axis. Pitch rate and angle were calculated by integrating pitch acceleration. The numerical values of the parameters are given in Appendix A.

2.8 Case Study II

36 participants (18 male; mean age=28, SD=3.76 and 18 females; mean age=25.25, SD=2.06) participated in this experiment. All declared normal or corrected-to-normal vision. The mean cycling experience of the participants was 14.5 years. The average number of cycling kilometers per month was 20.6 km. Fig. 2.18 shows one of the par-

ticipants during the familiarization phase of the experiment; the bus-bicycle shared lane, and the traffic on both sides.

Figure 2.18. A participant during the familiarization phase of the experiment.

2.8.1 Experiment Scenario

The experiment took place in a simulated urban environment of Vanves (a city situated 7.5 km south-west of Paris). The experiment's itinerary is shown in Fig. 2.19. The road consists of an on-street bicycle lane of 1.5 m in width with no separation between the cyclists and the motorized vehicles. Moderate traffic was generated in the same and opposite directions of the cyclist, and buses passed the cyclist from time to time. The participants were asked to ride the simulator for around 5 minutes to familiarize themselves with it (the virtual environment of the familiarization phase was different from the one used for this experiment). After the familiarization phase, we asked them to perform a simple task consisting of riding the bicycle for a short promenade (620 m) following the directional arrows painted on the bicycle lane until they reached the stop sign. In contrary to the first case study, which only consists of a straight route, the road geometry of the second case study included two curves and three intersections. The cyclists were asked to turn right at the third intersection. The participants had full control over the different features of the simulator such as: handlebar, pedals, gears and brakes.

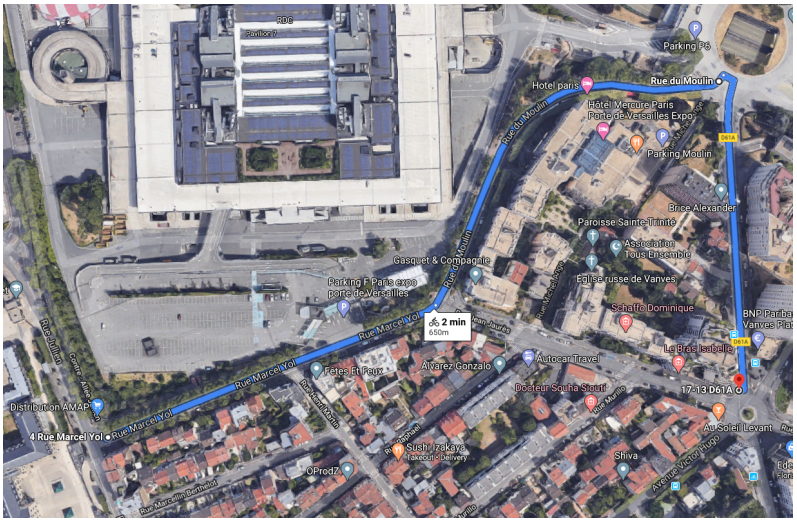

Figure 2.19. The cycling track in the city of Vanves (Source: Google Maps).

The experiment lasted around 10 minutes, a duration which we deemed sufficient to test all the features of the simulator and to collect enough data for the post-analysis without exhausting the participants.

At the end of the experiment, the participants answered three questionnaires: The first one to collect general information about the participants and their cycling experience in real life and using the simulator; the second one was the Simulator Sickness Questionnaire (SSQ) [99]: with 16 questions to evaluate the occurrence of different symptoms during the experiment using a four-level scale (None, Slight, Moderate and Severe); and the third one was the NASA Task Load Index (TLX) [98], to evaluate the overall work-load of the cycling task and the importance of each of the 6 work-load-factors under investigation, the participants evaluated each factor on a scale of 10 (1 for low and 10 for high, except for the performance where 1 for good and 10 for poor), then, it was converted to a 100-scale by multiplying by 10. The questionnaires were available both in English and French, as some participants only speak French. The trajectory, due to the coordinate system of the virtual reality, and the speed profile for one of the participants are shown in Fig. 2.20 and 2.21.

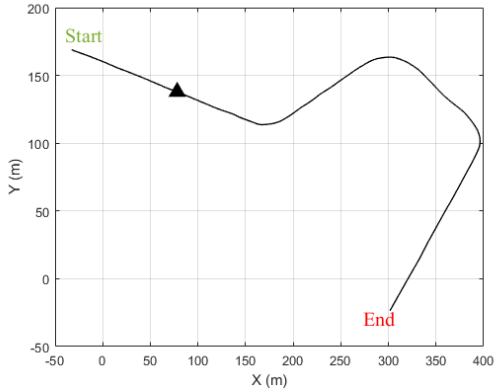

Figure 2.20. Trajectory of a participants.

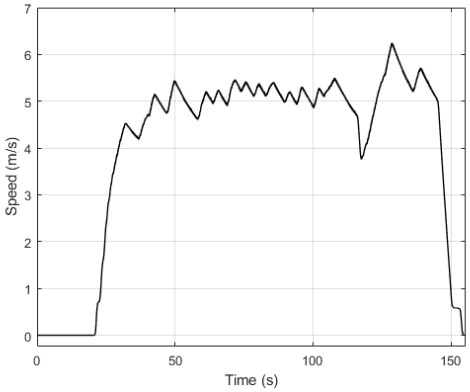

Figure 2.21. Speed profile of a participant.

2.8.2 Physical Validity

Several tests and scenarios were conducted at various speeds with the bicycle simulator. Sample results of the vertical displacement, side slip angle, lateral and longitudinal forces and rotational angles are presented in this section. The parameters of dynamic model of the bicycle were set to values from the literature [95, 96] and the stiffness and damping coefficients were taken from [97].

Vertical displacement and force

The input for the longitudinal road profile was measured along an asphalt driving lane in a previous experiment conducted by IFSTTAR (see Fig. 2.22). The signal had a frequency of 1 kHz and a maximum amplitude of about $\pm$ 2.0 cm. A zoom on the time interval [20, 25] s shows the input signal in details. In order to reproduce the unevenness of the road surface we used a sinusoidal signal with random pulses as an input for the vibration actuators shown in Fig. 2.23.

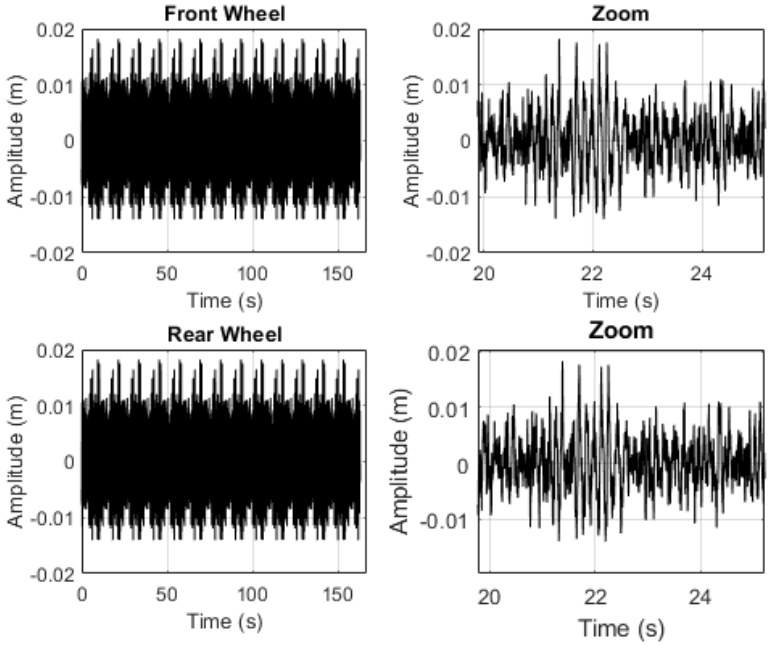

Figure 2.22. The road profile input under the front rear wheels, with zooms between 20 and 25 s.

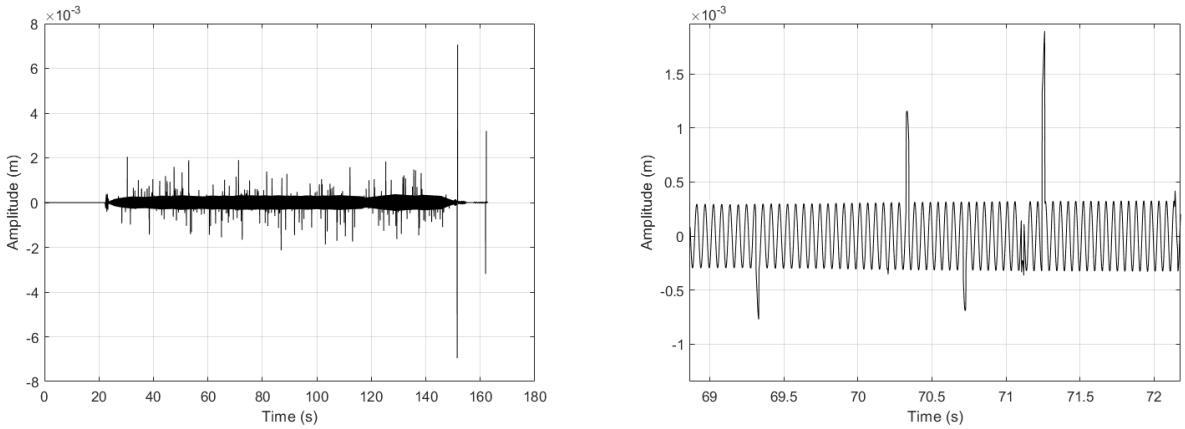

Figure 2.23. Actuators input with zoom between 69 and 72 s.

Fig. 2.24, 2.25 and 2.26 show that the vertical displacement, the vertical acceleration and the vertical force of the front and rear wheels are influenced by the amplitude of the road profile (Fig. 2.22); this becomes clearer at the peaks and lows caused by the unevenness of the road profile between 22 and 23 s. We also notice that the vertical acceleration of the rear wheel is bigger than the front wheel due to the mass distribution (i.e. the rear wheel carries more weight than the front wheel).

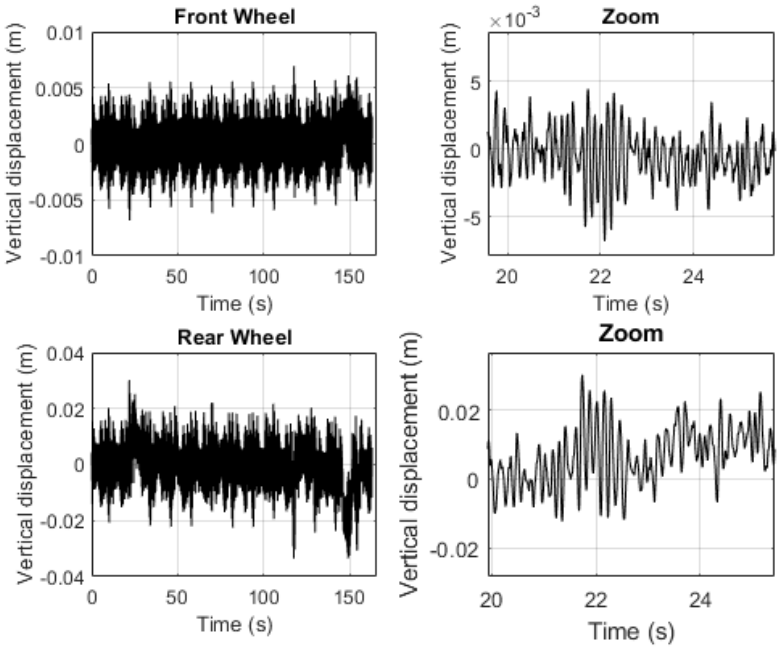

Figure 2.24. Vertical displacement estimation for the front and rear wheels, with zooms between 20 and 26 s.

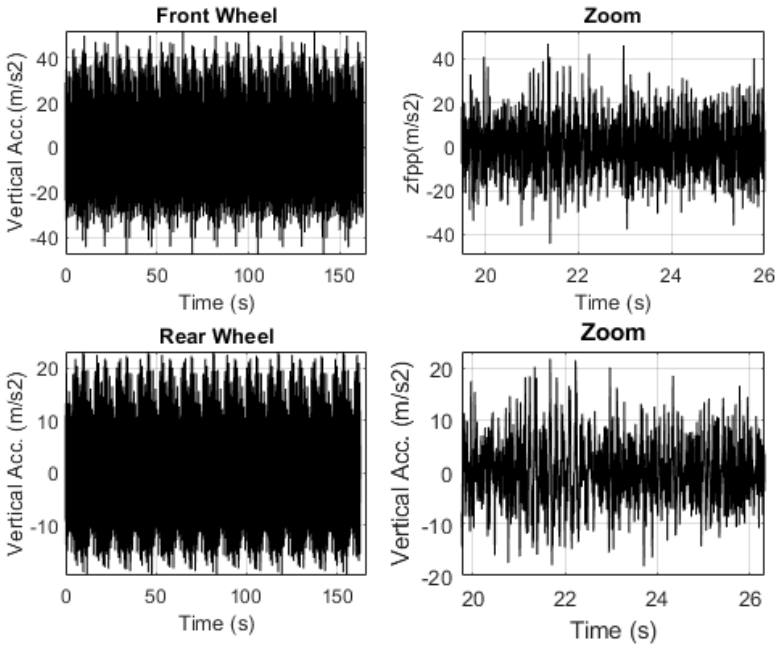

Figure 2.25. Vertical acceleration estimation for the front rear wheels with zoom between 20 and 26 s.

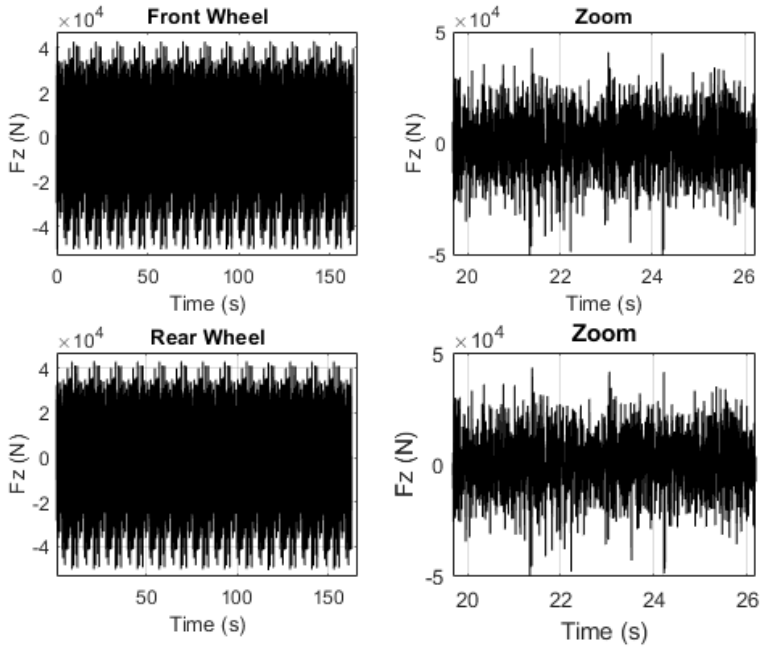

Figure 2.26. Vertical force for the front and rear wheels and zoom between 20 and 26 s.

Side slip angle and lateral force

Fig. 2.27 shows the steering angle and velocity measured and logged during one test using the incremental encoder. Fig. 2.28 shows the side slip angle of the front and rear wheels calculated using (2.28). The simulation results show the direct impact of the steering angle on the calculation of the side slip angle which becomes noticeable at the peak value of 120 s.

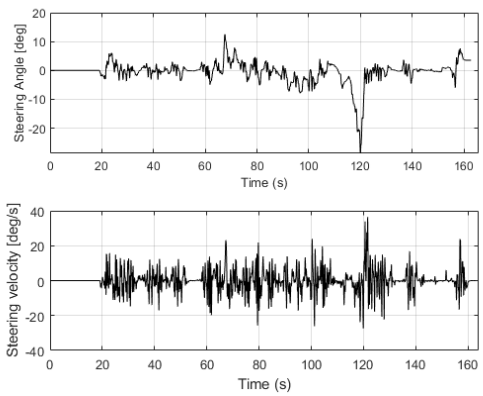

Figure 2.27. Steering angle and velocity of the bicycle simulator handlebar.

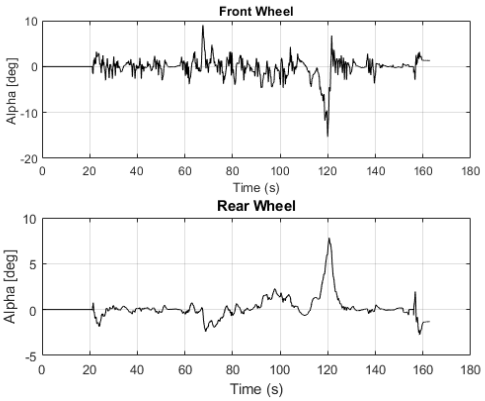

Figure 2.28. Side slip angle for the front and rear wheels.

Fig. 2.29 shows the lateral position estimation of the bicycle simulator. The black line results from the former model where the lateral position was estimated depending on the coordinate system of the virtual reality, whereas the red line results from the new model where the lateral position was calculated using (2.9). The new model shows higher accuracy. This can be observed through the impact of the steering angle and velocity; especially around 70 and 120 s, where high values in steering angle result in substantial changes in the lateral position.

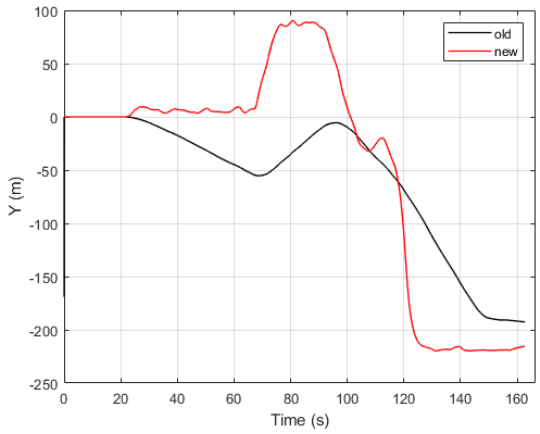

Figure 2.29. Lateral position estimation using SimTeam and 6 DoF model.

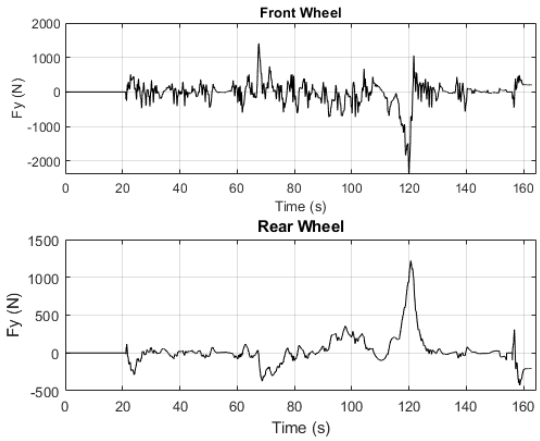

Figure 2.30. Lateral force of the front and rear wheels.

Fig. 2.30 shows the lateral force of the front and rear wheels calculated using (2.14). The graph indicates that the increase of the side slip angle causes an increase in the lateral force, this is particularly noticeable around 70, 100 and 120s.

Longitudinal force

During the simulation we used three different values of road adhesion coefficient to represent different surfaces and weather conditions. The longitudinal force shown in Fig. 2.32, which was calculated based on the adhesion coefficient in Fig. 2.31, shows the influence of different adhesion coefficients. For example, when the road surface is dry ($\mu = 0.8$) the longitudinal friction force peaks, whereas a wet surface ($\mu = 0.2$) causes a low longitudinal friction force.

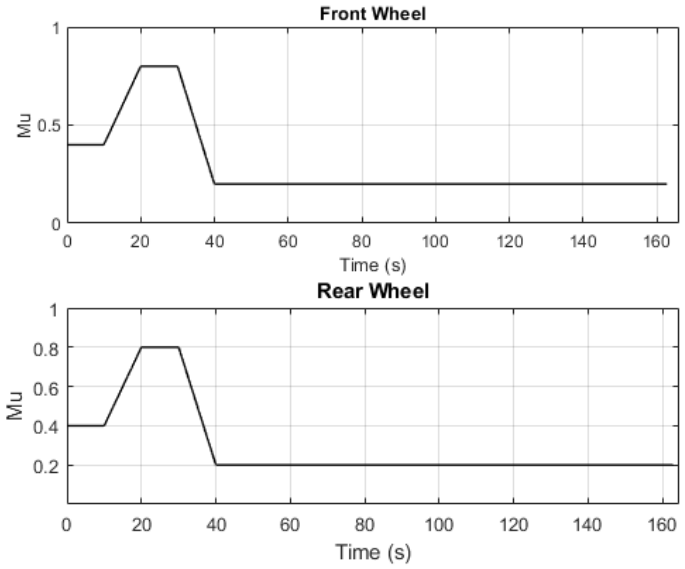

Figure 2.31. Adhesion coefficient input for the front and rear wheels of the bicycle simulator.

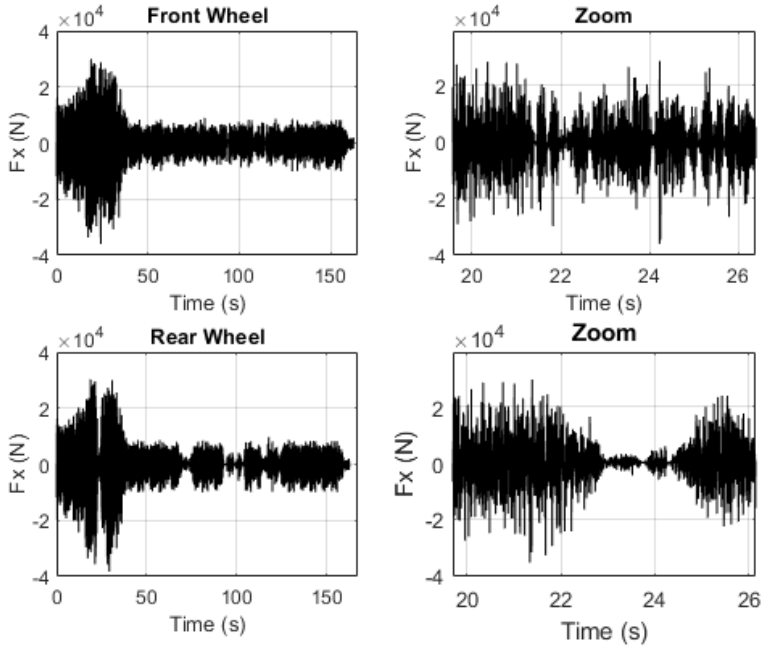

Figure 2.32. Longitudinal Force (N) for the front and rear wheel.

Roll angle

Fig. 2.33 shows the simulation output for the roll angle. As noticed, the roll angle runs similarly to the steering angle as the increase of the steering angle implies a decrease of the radius of curvature. This effect of steering angle and radius of curvature is also

noticed in roll rate and acceleration shown in Fig. 2.34 and 2.35. In the former model, the roll angle acceleration was calculated using the second derivative of the roll angle, whereas the new model calculates the roll angle acceleration using (2.22). Fig. 2.35 compares the outputs of the former and new models, it shows the improvement brought by the new model regarding accuracy and noise removal.

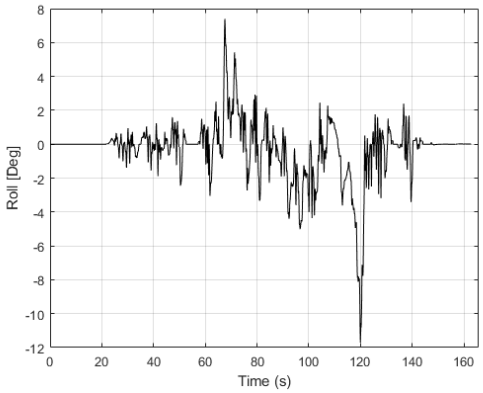

Figure 2.33. Roll angle.

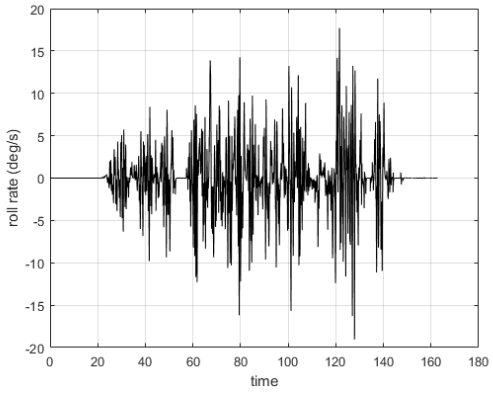

Figure 2.34. Roll rate.

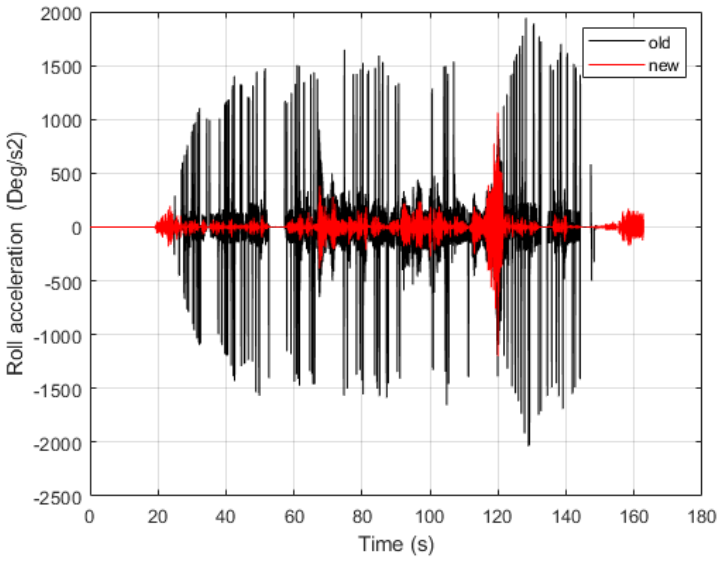

Figure 2.35. Comparison between roll acceleration values for the former and new models.

Yaw angle

Fig. 2.36 shows yaw angle simulation. We notice the direct effect of the lateral position (Fig. 2.29) on this calculation. Yaw rate and acceleration are shown in Fig. 2.37 and 2.38. In the former model, yaw angle acceleration was calculated using the second derivative of the yaw angle, whereas the new model calculates the Yaw acceleration using (2.20). By comparing the results of the old and the new model (Fig. 2.38) we notice the improvement brought by the new model regarding accuracy and noise removal.

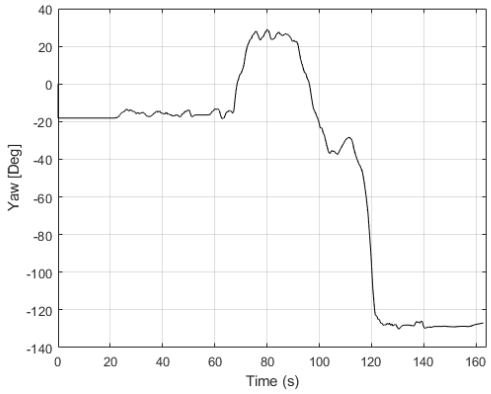

Figure 2.36. Yaw angle.

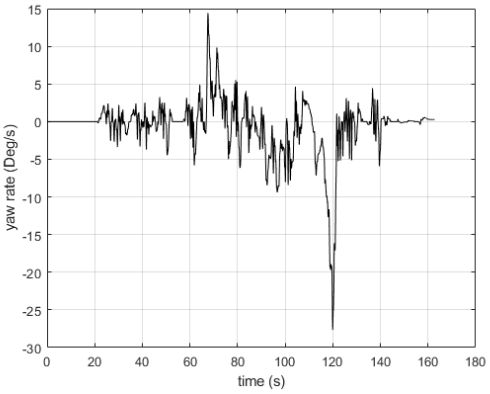

Figure 2.37. Yaw rate.

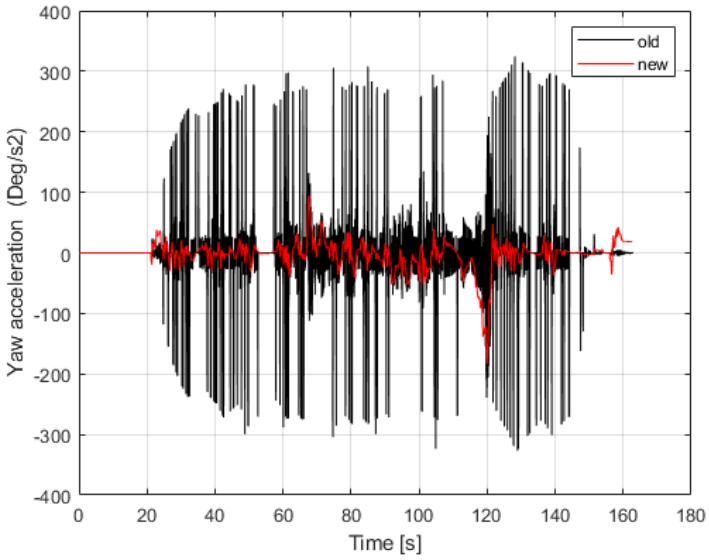

Figure 2.38. Comparison between yaw acceleration values for the former and new models.

Pitch angle

The simulation output of the pitch rotation angle, rate and acceleration are shown in Fig. 2.39, 2.40 and 2.41. The small values could be explained by cycling on a flat surface which has minor impact on the pitch angle. An increase of the pitch angle could be noticed in acceleration and breaking phases. By comparing results between the previous and the new model (Fig. 2.41) we see the advantages of the new model regarding accuracy and noise removal.

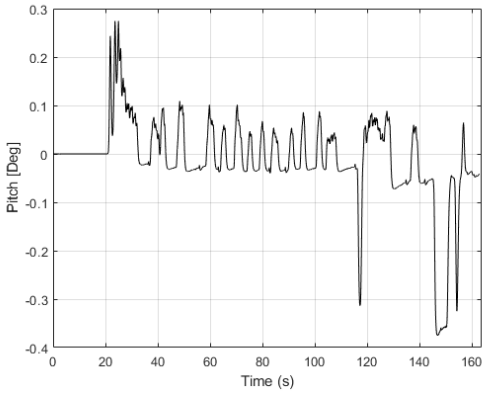

Figure 2.39. Pitch angle.

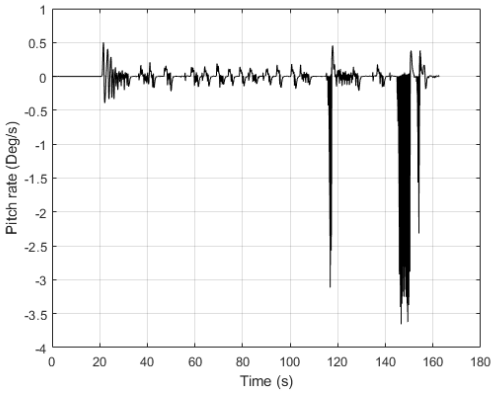

Figure 2.40. Pitch rate.

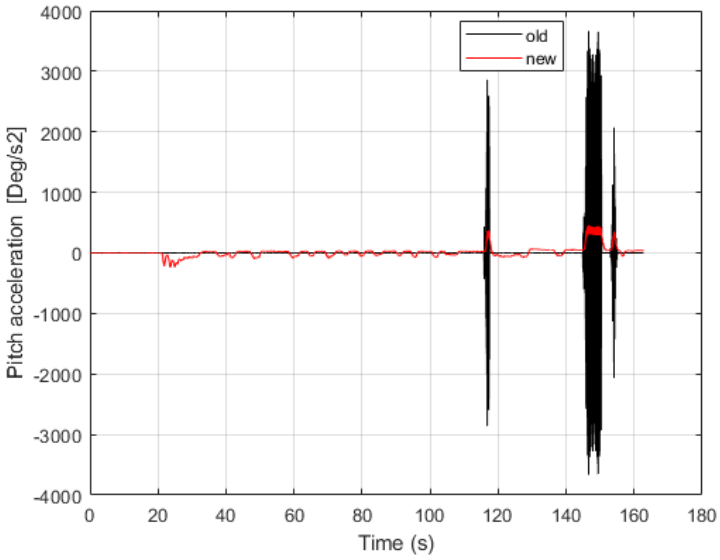

Figure 2.41. Comparison between pitch acceleration values for the former and new models.

2.8.3 Subjective Validity

The analysis of the first questionnaire shows that 7 of the participants had participated in a previous experiment using the same bicycle simulator before the recent improvement [104]. 8 of of all participants declared sensitivity to motion sickness; 5 of them when reading during travelling. On evaluating the realism of the simulator (compared to riding a real bicycle) the participants rating ranges between 3 and 9 on scale of 10 (mean=6.74, SD=1,57) [105]. This shows an improvement of the simulator compared to a previous experiment, where the participants evaluated the simulator with 6.1/10 [106]. The physical feeling of cycling, the design of the virtual road, traffic generation and other sensory cues, such as wind and the sound of the passing traffic were mentioned as the most realistic aspects of the simulator. However, some of the participants mentioned lacking the effect of the body posture when turning. This is because turning in the virtual reality is only affected by the steering angle and the body posture has no effect. The complete answers to the first questionnaire are shown in Appendix B.

Table 2.4 summarizes the results of NASA TLX questionnaire for the 36 participants. The first column shows the scales under assessment, the second column represents the average weight of each scale according to the personal opinion of each participant. This was calculated by answering 15 questions in which the scorer chose between two scales according to their importance. The weight of each scale is the number of times it was chosen. The third column is the average raw rating taken from the TLX questionnaire; and the last column represents the adjusted weighting, which is the multiplication of the weight and raw rating of each factor.

Table 2.4 Weighted rating of TLX questionnaire. The overall workload (OW)= mean of weighted ratings.

Scale title	Weight	Raw Rating	Adjusted rating
Mental Demand	3.13	45.56	142.61
Physical Demand	2.35	45.28	106.30
Temporal Demand	2.26	40.83	92.32
Performance	3.35	22.50	75.33
Effort	2.17	44.44	96.62
Frustration	1.74	24.17	42.03
Overall workload		37.13	92.53

The raw rating results show that the simulator requires intermediate mental/physical/temporal demand and effort. This is explained by the effort and concentration required when riding any bicycle and interacting with traffic since it is an active transport mode.

Fig. 2.42 compares the weighted average of each workload scale. It can be seen that the performance factor received a relatively low rating but a high importance, whereas the frustration factor received an intermediate rating but a low importance (meaning that the task was simple and easy to accomplish), so that both factors contribute in the similar amounts to the overall workload.

The analysis of the simulator sickness questionnaire listed in Table 2.5 shows that the average total severity for all participants is 14.65. By comparing this result to the possible scores listed in Table 2.2, we see that the total severity of the simulator is slight (less than 78.5).

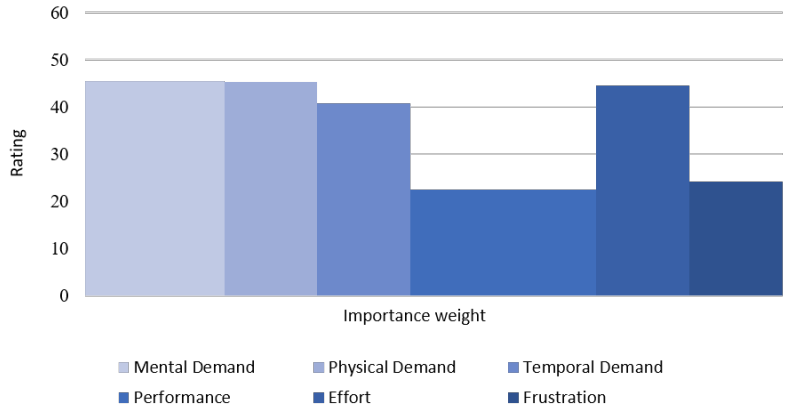

Figure 2.42. Nasa Task Load Index analysis results: Weighted work load score. The width of each column represents the importance weight of each factor.

Table 2.5 Simulator Sickness Questionnaire Results.

	Nausea	Oculomotor	Disorientation	Total Severity
mean	10.86	14.32	12.37	14.65
SD	18.25	14.26	19.2	17.58
min	0	0	0	0
max	57.24	37.9	41.76	52.36

Fig. 2.43 contains the score distribution obtained from the 36 participants. It can be seen that 6 participants (17 %) reported no symptoms from their exposure to the simulator, and the rest reported slight symptoms of simulator sickness (less than 78.5),

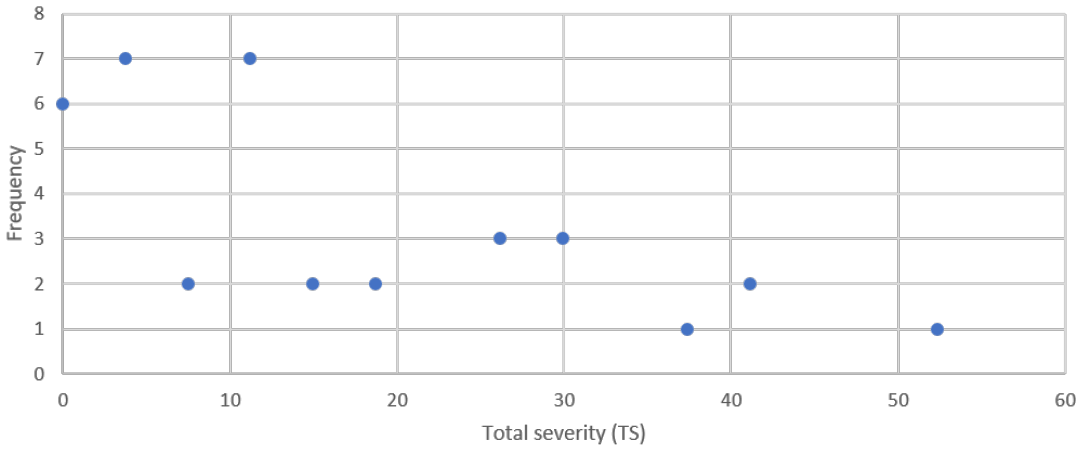

Figure 2.43. Frequency distribution of total sickness scores (N=36).

Fig. 2.44 shows that the average severity of all symptoms is slight (less than 1), with a slight increase in the general discomfort, which could be explained by the exposure to the virtual reality displays.

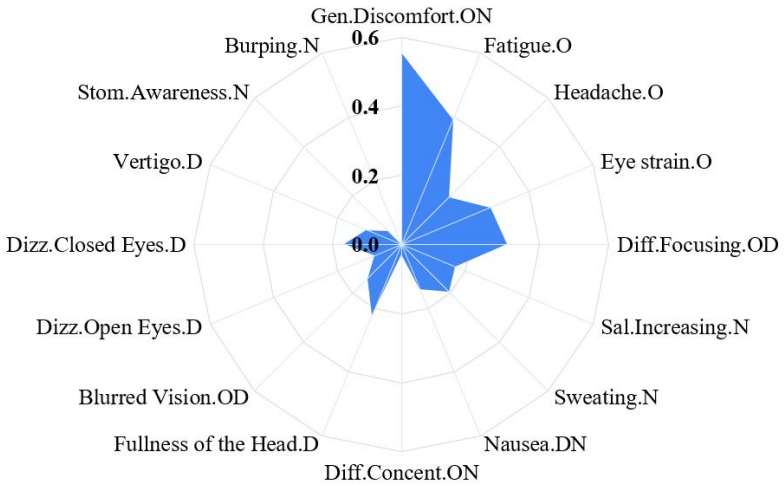

Figure 2.44. Mean scores observed in each item of the exposure of simulator sickness questionnaire. The O, D and N letters following the name of each item indicate in which class(es) of symptoms the corresponding item was involved: O corresponds to Oculomotor discomfort, D to Disorientation and N to Nausea.

Fig. 2.45 shows that males experienced an increase of eye strain, whereas females experienced an increase in difficulty focusing.

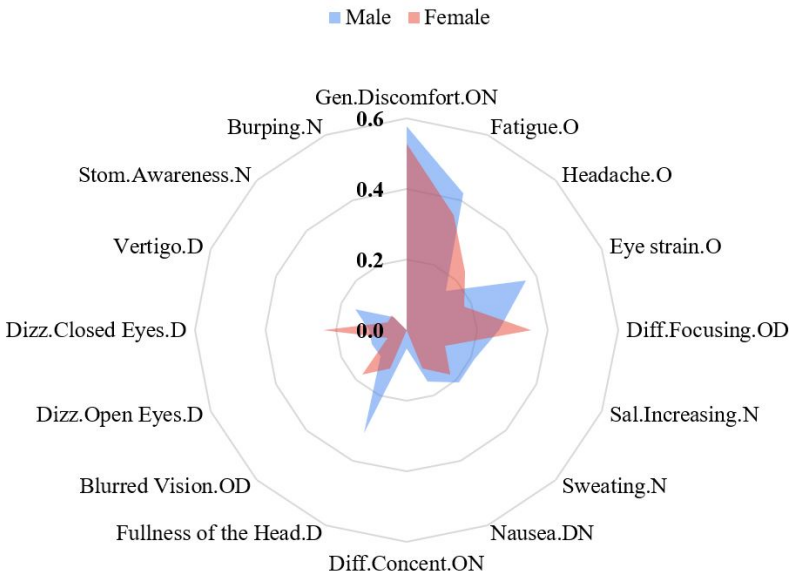

Figure 2.45. Mean scores observed in each item of the simulator sickness questionnaire during the experiment. (a) Men (blue area) and women (red area).

Fig. 2.46 shows that participants with corrected vision experienced higher symptoms in general discomfort and fatigue, whereas normal vision participants experienced more eye strain and difficulty focusing.

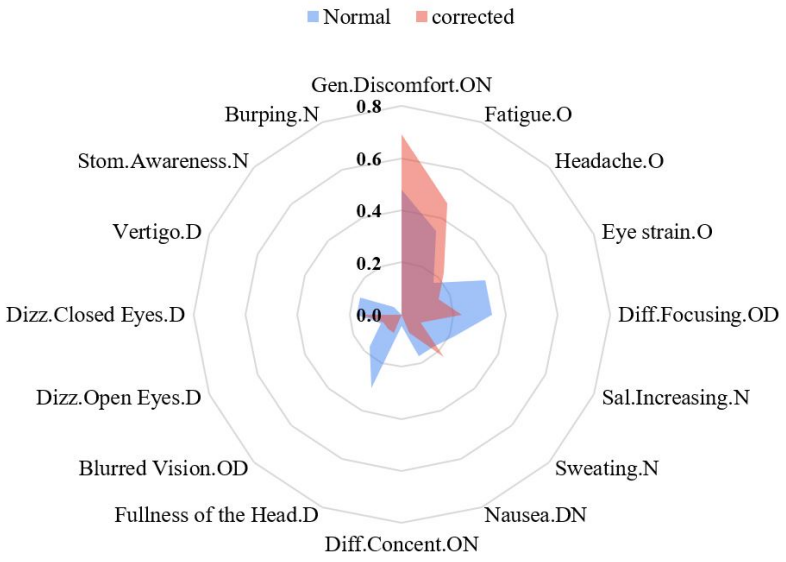

Figure 2.46. Mean scores observed in each item of the simulator sickness questionnaire during the experiment. (a) normal vision (blue area) and corrected-to-normal vision (red area).

2.9 Conclusion

In this chapter, a bicycle dynamic model was developed and experimentally validated on an immersive bicycle simulator at various speeds and different cycling maneuvers. The developed model has 6 degrees of freedom (longitudinal, lateral, vertical, Yaw, Pitch and Roll). The main advantages of the model are its simplicity, compatibility with the bicycle simulator, and its ability to be applied to a real bicycle. By conducting comparative studies between the theoretical and practical aspects, it is possible to verify the reliability of the simulator. Further improvements were applied on the simulator including the development of the virtual environment and the installation of three actuates and asphalt specimen to simulate the interaction between the road surface and the bicycle. The inputs of the model, such as steering angle, pedaling and braking were measured and logged in real time. Their influence on vertical, lateral and longitudinal forces, velocities and displacements were observed. The comparison between the SimTeam model and the 6 DoF developed model shows that the proposed model produces more accurate estimations. Improvements were noticed in the following areas: the compatibility of the lateral position with the trajectory and yaw angle, the noise removal when calculating yaw, pitch and roll accelerations, the impact of the unevenness of the road profile on the vertical displacement and force, the steering angle effect on the side slip angle, lateral displacement and yaw, and the effect of road adhesion on the longitudinal force.

The analysis of the simulator sickness questionnaire in the second case study shows a drop in the severity of the simulator (TS =14.65) compared to the first case study (TS= 32.54). This could be explained by using more realistic virtual reality which affected (alongside the installation of the actuators and the asphalt specimen) the subjective evaluation of the realism of the simulator increased from 6.1 to 6.74/10. The bicycle simulator enables us to put cyclists in a riding situation and accurately measure their effective behavior, while controlling the variables at play and avoiding the risks associated with a real environment. The validity of the bicycle simulator proves it is a safe tool to study

cyclists' behavior in risky situations and analyze their reactions and interactions with different features of the infrastructure such as, radius of curvature, intersections, lateral and longitudinal slopes.

CHAPTER 3. BICYCLE INSTRUMENTATION AND CYCLING SAFETY EVALUATION

3.1 Introduction

Experimentation using the bicycle simulators investigated in chapter 2 allowed us to put cyclists in various riding situations, while recording all the inputs and output of the system at high frequencies and low noise of the signals, however, some important inputs are still missing compared to the real environment, such as: road infrastructure characteristics which includes the vertical and lateral slopes of the road and road adhesion especially on snowy surface; the weather conditions (temperature and the wind speed and direction); and the increased feeling of safety inside the lab compared to on-road experiment, which could impact the behavior due to the absence of real risks during simulation. The absence of all these factors made it very important to conduct on-road experiment in order to include all inputs that affect cyclists' behavior and bicycle dynamics. To make this possible, different sensors and devices were used to instrument a bicycle in order to collect exact data about bicycle dynamics, trajectory, speed, as well as information that allows to study the behavior of the cyclists, their reaction to the different features of the road surface and geometric design during their journey and their interaction with other road users such as: pedestrians, vehicles and other cyclists.

This chapter is structured as follows: the second part is devoted to bicycle instrumentation and processing of the output signals; the third part describes the experimentation conducted using the instrumented bicycle and discusses the results of all participants; the forth part is dedicated to the analysis of the eye-tracker videos and the behavior of cyclists and their interaction with the road infrastructure and other road users; the fifth part shows the analysis of the questionnaire answered by the participants regarding their evaluation of cycling safety and comfort; and finally the conclusion.

3.2 Bicycle Instrumentation Setup

A city bicycle was instrumented with different sensors to detect the corresponding dynamical and kinematical data [107]. The details about the used bicycle and sensors are given below:

Bicycle: The bicycle used in this experiment is called Nova (from Skeppshult, a Swedish manufacturer), tyres: 28" front and rear single-walled aluminum wheels with 36 spokes, the tyre pressure was set to 4 bar (the recommended pressure is 2.0 – 5.0 bar). This bike supports a maximum weight of 100 kg (weight of the user + bike + luggage carried), the bicycle consist of a single-speed transmission system with 5-speed shifter for ease of use. The total mass of the instrumented bicycle including the sensors and a laptop is 28 kg (the bicycle mass is 15.3 kg). The location of the instrumentation on the bicycle is detailed in the schematic in Fig.3.1, and described bellow.

Figure 3.1. Schematic of the instrumented bicycle, more details about the different sensors following the correspondent numbers below.

1. **SG-LINK-200-OEM + Hall Effect Sensor** from Alliantech was used to count the number of rotations per minute (RPM) for the front wheel in order to calculate its angular velocity, the sensor was fixed on the front fork and connected to 9V battery, and a magnet was attached to one of the spokes, each time the magnet passes the sensor it counts one rotation. The sampling rate was set to 250 Hz (adjustable up to 1024 Hz), the data was logged remotely using WSDA 200 USB, Fig. 3.2 shows the sensor and the related parts.

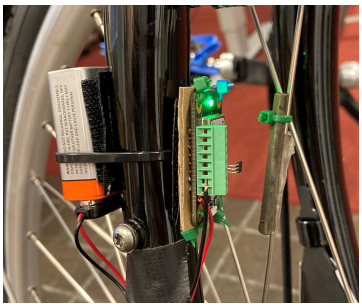

Figure 3.2. SG-LINK-200-OEM + Hall-effect sensor.

Figure 3.3. G-link-200 Triaxial accelorometer.

2. **G-link-200 Triaxial accelorometer** from AlianTeck is a wireless 3-axis accelerometer with ±2 to ±40 g measurement range, low noise waveform on all axes with 25 µg/$\sqrt{Hz}$ or 80 µg/$\sqrt{Hz}$, the sampling rate is up to 4096 Hz, it was set to 500 Hz in this experiment. The sensor connects wirelessly to WSDA 200 USB to log the data. It was fixed on the front basket over the front wheel (see Fig. 3.3) and used to measure the accelerations of the front part of the bicycle.

3. **Global Positioning System (GPS):** Edge 130 plus device from Garmin (shown in Fig. 3.4) that includes: GPS, GLONASS and GALILEO systems to detect position in real time; barometric altimeter; accelorometer and Internal memory to save data from other Garmin devices such as: Vector 3, speed and cadence sensors. The device was fixed on the handlebar in order to control it easily.

Figure 3.4. Edge 130 plus device with embedded GPS.

Figure 3.5. The potentiometer connected to Arduino micro-controller.

4. **P25 wire-wound potentiometer** from RS Pro, was connected with specially designed cogs using 3D printer and attached to the handlebar to measure the steering angle (see Fig. 3.5). The potentiometer offers resistance up to 25 Ω with a temperature coefficient of ±50ppm/°C, it includes a shaft of 6 mm diameter and provides 285° rotation (mechanical angle), with rotational life up to 100,000 revolutions. The potintiometer is connected to Arduino micro-controller which allows to log the data using serial portal connection on a laptop. The sampling rate is 100 Hz.

5. **IMU unit+ WLAN "Shell" 4.0 Data Logger:** from Avisaro, was used as a data logger with 6 DOF IMU unit (3 axis acceleration / 3 axis gyro), Build-in GPS Satellite Receiver and a slot for USB memory where the date are logged. The logger was fixed on the rear seat to measure the accelerations of the rear part of the bicycle and the rotations of the bicycle, the IMU sampling rate was set to 100 Hz, the measurement range for the accelerometer and gyrometer were set to $\pm$ 2g and 250 DPS respectively. The GPS receiver is installed inside the data logger avoiding the need for an external antenna, it has a position accuracy of 2.5 m in circular error probability (CEP) and sampling rate of 1 Hz.

Figure 3.6. The data logger, IMU and GPS.

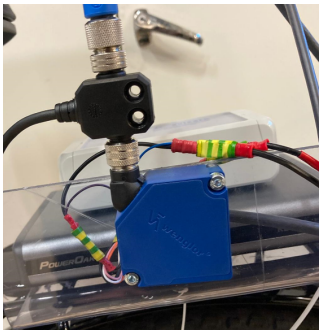

Figure 3.7. The laser scanner.

6. **OY1P303P0189 laser scanner** , from Wenglor, was used for the continuous measuring of the distance between the top of the rear seat and the road surface. The laser was fixed at the same level of the data logger and around 10 cm from the center of the rear wheel. The effective working range of the laser beam is 50-3050 mm, the measuring rate 1-500 Hz, the reproducibility is 1 mm maximum. The data are logged using RS-232 interface connected through a serial portal to a computer. The sampling rate is 30 Hz.

7. **K2 powerbank** ,from PowerOak, was used as a battery to provide power to the laser scanner and the data logger. It has a capacity of 185Wh / 50000 mAh with 6 output ports, one 20V/5A, one 12V/2.5A, two 5V/2.1A and two 5V/1A with Max power of 80W. The dimensions of the battery 20,6 x 13,5 x 3,3 cm and it weights 1,26kg.

8. **Speed sensor 2**, from Garmin, is a wireless sensor that gives longitudinal velocity and distance at all times with no magnets or other exposed parts, it was fixed on the hub of the rear wheel. The sensor self-calibrates with Edge 130 plus using Bluetooth, the wheel circumference was set to 2.15 m in the settings of Edge 130 plus for more accurate measurement of the speed.

Figure 3.8. Garmin speed sensor fixed on the rear wheel hub.

Figure 3.9. Power meter pedal+cadence sensor.

9. **Vector 3 power meter pedals** from Garmin provides dual-sensing on both pedals, each pedal weights of 316 g, it bears a maximum rider weight of 105 kg with measurement accuracy of +/- 1.0%.

10. **Cadence sensor 2** from Garmin, was fastened to the left-side crank arm to measure pedal strokes per minute, it self-calibrates with Edge 130 plus using Bluetooth.

11. **WSDA 200 USB** from AlianTeck, it is a data acquisition gateway that collects synchronized data from scalable networks of wireless sensors such as G-link-200 and SG-link-200, it has a timestamp of ±50 µS in LXRS+ and LXRS-enabled modes, wireless range up to 2 km (400 m typical).

12. **Pro-Glasses 2 Mobile Eye-Tracker** from Tobii was used to record the gaze of the participant in the experiment environment, data is captured at 50 or 100Hz. The glasses are connected to a recording unit where the data are saved on SD card. The tracker consists of gyroscope and accelerometer, 4 eye cameras, a scene camera with resolution of 1920 x 1080 pixels at 25 fps and field of view 90° 16:9 and visual angle of 82° horizontal and 52° vertical, a microphone to record the ambient sounds and protective lenses as shown in Fig.3.10.

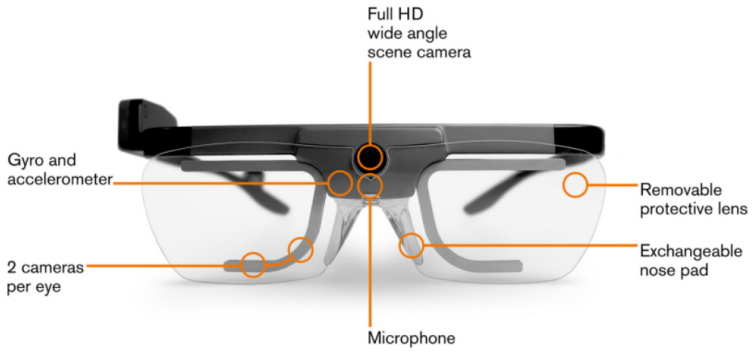

Figure 3.10. Tobii Pro glasses 2.

3.3 Experimental Procedure

3.3.1 Participants

22 cyclists participated in this experiment riding the instrumented bicycle on pre-determined route, they were recruited by sending emails to the mailing lists of The Research Institute of Sweden (RISE) [108] and The Royal Institute of Technology in Stockholm (KTH) [109] and posting on social media groups in the city of Stockholm. 13 of them were males and 9 were females, aged 11-65 years (M= 36.5 years, SD=12.85 years). 5 of the participants conducted the experiments twice in two different weather conditions.

All participants were asked to sign a standard consent form including a brief details about the experiment, the data collected and the following analysis. As one of the participants was under 18, her father signed the consent form and he accompanied her to the lab and stayed until she completed the experiment. All participants were obliged to wear a helmet. Wearing a reflective vest was optional. In the inclusion criteria we tried to achieve the balance between males and females, however, more males volunteered, having an experience cycling on snowy surface was mandatory.

Initially, we asked the participant to wear the mobile eye-tracker in order to calibrate it by looking at a fix point on the wall (see Fig. 3.11). After the calibration finished , the participant was asked to look into random points around the lab to check that his gaze

matches the cursor on the live video displayed on a connected tablet.

Figure 3.11. One of the participants during the eye-tracker calibration, he appears holding the storage unit, which is connected to the eye-tracker and to the tablet used during the calibration process.

After the calibration process finished, the cyclist was asked to ride the bicycle for around 3.5 km. The experiment route begins and ends at Integrated Transport Research Lab (ITRL), Stockholm. The first session consisted of 20 cyclists, the temperature was -3 to -11 degrees, the road surface was a mix between snow-sludge and ice along the experiment route; the second session consisted of 6 cyclists, the temperature was 3 to 9 degrees, the surface was wet at some places and dry at others with snow-sludge at some places like intersection. It was cloudy for both sessions. The experiment's itinerary is shown in Fig. 3.12. The road consists of three zones: zone 1 has a length of 750 m and consists of a mixed traffic street with 30 km/h speed limit, where the participant cycles on the carriage way along side cars and other vehicles; zone 2 consists mainly of an on-street separate cycling lane without physical barrier with 1.7 m width and 630 m length and a shared bicycle-bus lane with 370 m length; zone 3 consists of shared pedestrians-cyclists path that goes between tress and parking lots with a width of 5 m and length of 1 km (see Fig. 3.13). The participant follows the predetermined route using GPS map displayed on a mobile mounted on the handlebar. During the test, each participant passed through eleven traffic lights, four of them intersected major roads (main crossings), whereas the

rest intersected secondary roads.

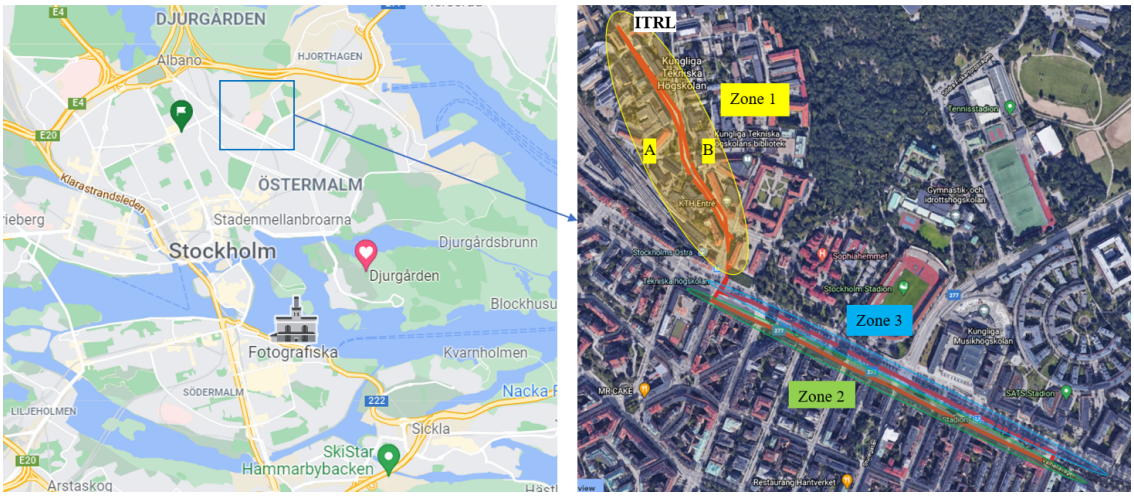

Figure 3.12. The predetermined route of the experiment.

Figure 3.13. The zones of the experiment showing the difference of the geometric design between them in both dry and snowy surface conditions (Google Maps).

After the cycling task finished, the participant completed a questionnaire related to personal general information such as: Age, Gender, weight, cycling experience, and their evaluation of the experiment route regarding safety and comfort. The date was collected from the eye-tracker and the sensors preparing for analysis.

3.4 Signal Processing

After the experimentation, the signals from all sensors were collected and classified preparing for analysis, the total number of the output signals is 17 divided as follows: 7 from the data logger (6 from IMU and 1 from GPS), 4 from Aliantech sensors (G-link-200 and SG-link-200), 1 from the laser scanner, 1 form the potentiometer, and 4 from Garmin system. The output signals of the sensors were treated through multiple phases, as follows:

- Data synchronization: different acquisition systems were used as the sensors were not purchased from the same supplier, therefore, the synchronization of the output signals is essential to calibrate the measurements. The output signals started at different times, which generates a time lag that delicate the comparison between them. In order to remedy this and eliminate the lag effect, start point synchronization has been implemented by shifting the signal to be consistent with the last one to start.

- Signal processing: to better exploit the measurements from the different sensors, a filtering process is necessary to remove the noise and extract the useful signal to be analyzed later. In order to apply filters, we should know the frequency to estimate the power spectral density (PSD) of signal using welch's estimate method to adjust the cut-off frequency. The PSD for most of the signals shows that their energy is concentrated on the frequencies between 0.3 and 30 Hz, hence, a double filtering is necessary: a high pass filtering to remove the low frequencies caused by the low sensitivity of the sensor in order to calibrate it, and a low pass filtering to remove the high frequencies correspond to the noise. Different cutoff frequencies were chosen depends on the frequency of the output signal and the existence of noise: for the IMU output signals a low pass filter at a cutoff frequency of 20 Hz and a high pass filter at a cutoff frequency 0.6 HZ were applied except for yaw rate output a low pass filter of 10 Hz was applied; for the SG-link-200 output signals

a low pass filter at a cutoff frequency of 30 Hz and a high pass filter at a cutoff frequency 0.3 HZ were applied; for the laser scanner output signal a high pass filter at a cutoff frequency 0.6 HZ were applied; and for the potentiometer output signal a low pass filter of 10 Hz was applied.

Fig. 3.14 show the filtration applied on the lateral acceleration of the front wheel, the signal was extracted for SG-link-200. We can notice the noise removal from the original signal and the shape improvement, this become more clear when zooming at 639-644 s.

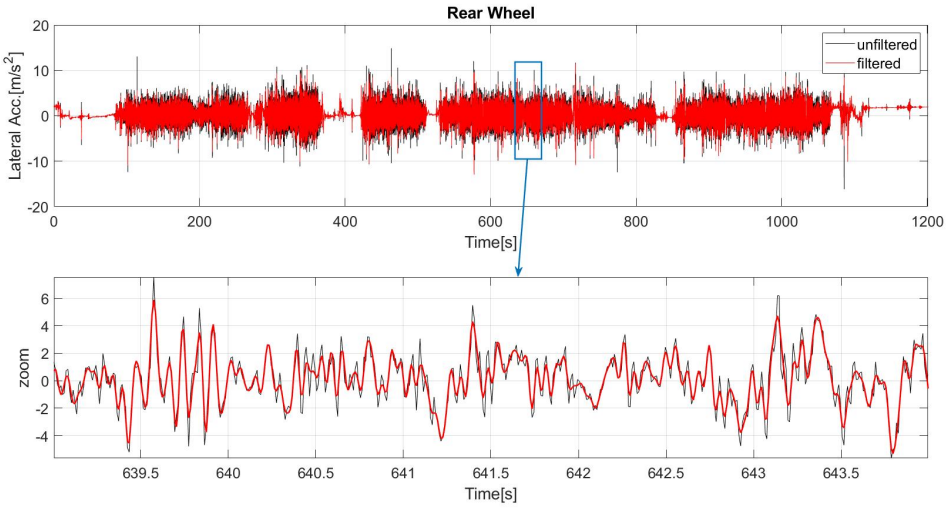

Figure 3.14. Comparison between 'Unfiltered' and 'Filtered' signal of the lateral acceleration measured using the IMU unit.

3.4.1 Trajectory and position

The trajectory of one of the participants is shown in Fig. 3.15. The participant followed exactly the predetermined route, even though the lateral position is inaccurate according to the variation in GPS signal strength. Fig. 3.16 shows the altitude above sea level for the experimental route, we can notice that in zone 1A and zone 2 the route is mostly downhill, while in zone 3 and zone 1B it is mostly uphill.

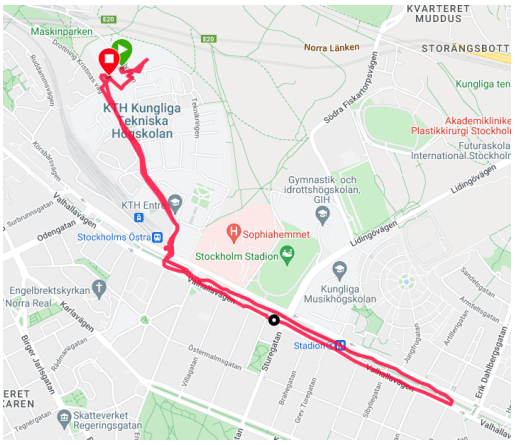

Figure 3.15. The experiment trajectory for a participant extracted.

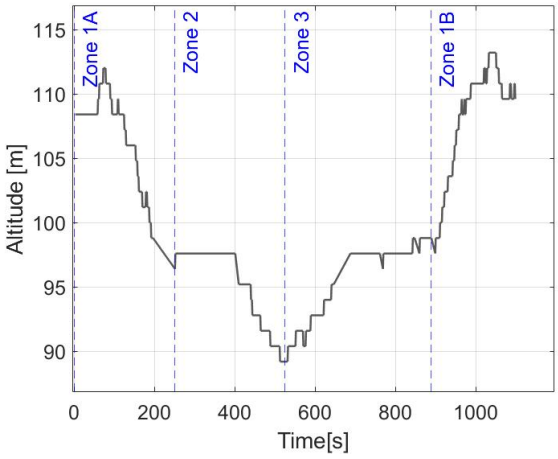

Figure 3.16. Elevation extracted from the GPS device fixed on the rear wheel.

Fig. 3.17 and 3.18 show the longitudinal and lateral positions for one of the participants, that were extracted from east and north coordinates of the GPS. The change of the position is clear at the beginning of zone 3 (525 s) where the cyclist had to make U-turn. The GPS signal from 20 s to 120 s seems to be weak which affected the accuracy of the position measurement.

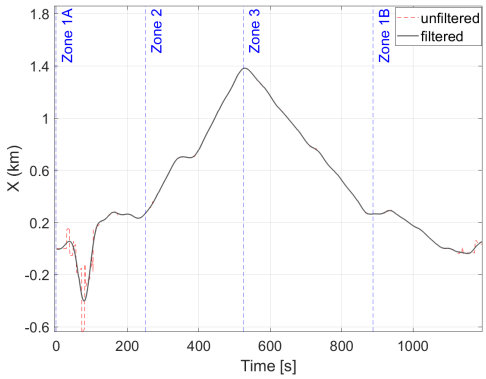

Figure 3.17. Longitudinal position extracted from the GPS device.

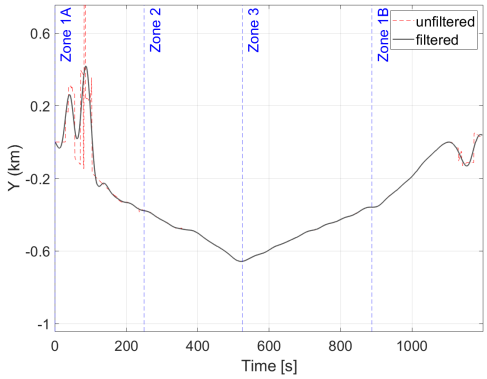

Figure 3.18. Lateral position extracted from the GPS device.

3.4.2 Longitudinal acceleration, velocity and displacement

Fig. 3.19 and 3.20 show the longitudinal acceleration (with zoom between 859-860 s), velocity and displacement for the front and rear wheel respectively. The velocity was

calculated by integration and the displacement by double integration of the acceleration. We can notice the effect of filtering in noise removal and calibration of the signal.

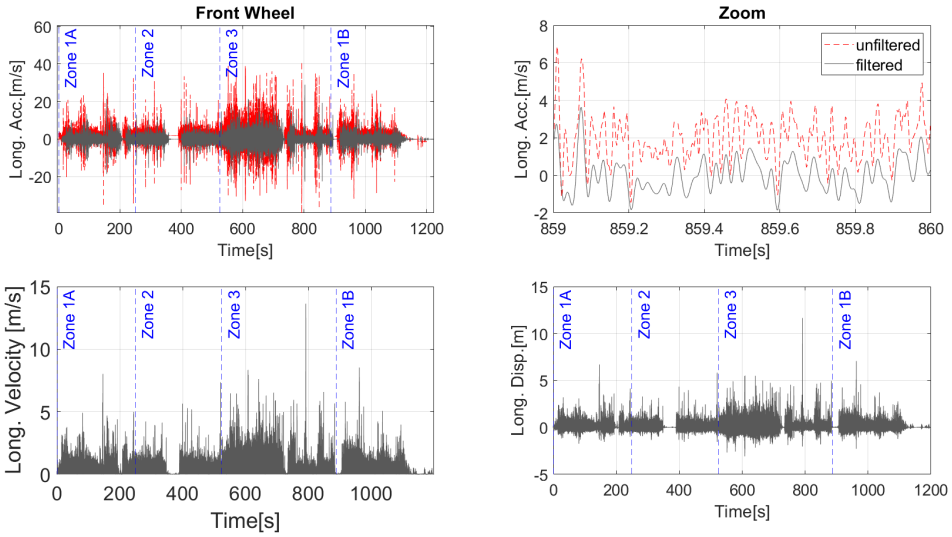

Figure 3.19. Longitudinal acceleration, velocity and displacement extracted from SG-Link-200 which was fixed on the front basket of the bicycle.

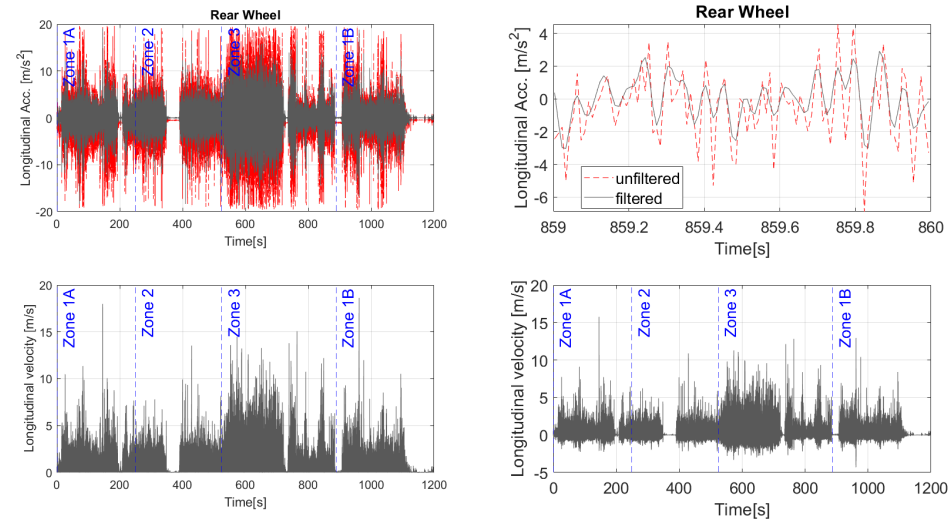

Figure 3.20. Longitudinal acceleration, velocity and displacement extracted from IMU which was fixed on the rear seat of the bicycle.

Fig. 3.21 compares between the speed profiles calculated using different signals. Despite of that all profiles show the same behavior, we can notice that the speed extracted from the IMU unit and SG-link-200 are still very noisy even after the filtration; whereas

the speed coming from G-link-200 has time delay, some perturbations due to the fixation method of the sensor as it consists of two parts,on of them is the hall effect sensor, which is sensitive and it is possible that it moved during the experiment affecting the accuracy of the collected data. As a results, the speed extracted from Garmin speed sensor was chosen to be the most accurate as it is well filtered and has no perturbations.

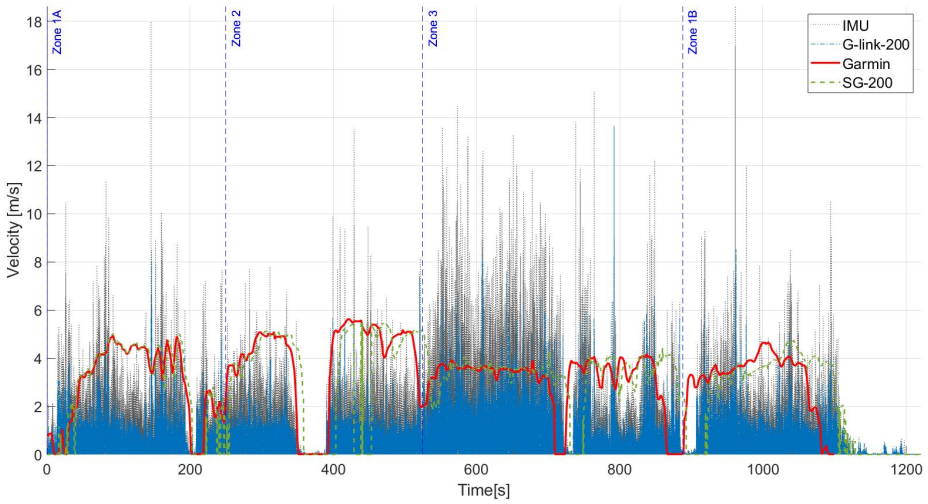

Figure 3.21. Comparison between velocities calculated using different sensors.

3.4.3 Lateral acceleration, velocity and displacement

Fig. 3.22 and 3.23 show the lateral acceleration (with zoom between 859-860 s), velocity and displacement for the front and rear wheel respectively. The velocity was calculated by integration and the displacement by double integration of the acceleration. We can notice the effect of low pass filtering in noise removal and high pass filtering in calibration of the signal.

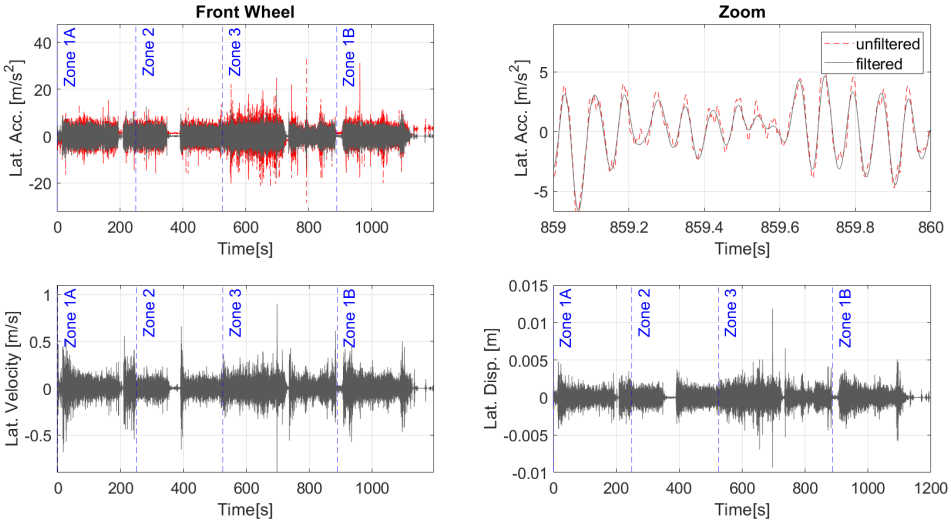

Figure 3.22. Lateral acceleration, velocity and displacement extracted from G-link-200 which was fixed on the front basket of the bicycle.

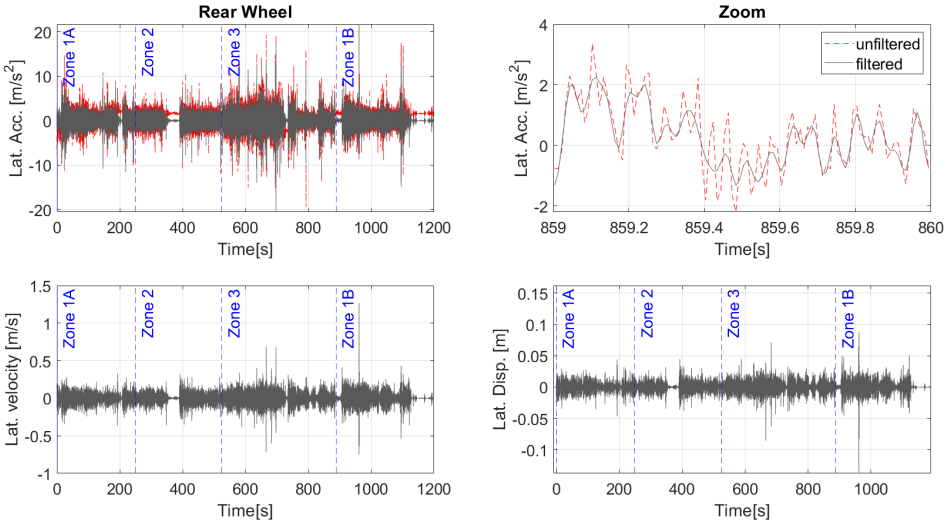

Figure 3.23. Lateral acceleration, velocity and displacement extracted from IMU which was fixed on the rear seat of the bicycle.

3.4.4 Vertical acceleration, velocity and displacement

Fig. 3.24 and 3.25 show the vertical acceleration (with zoom between 859-860 s), velocity and displacement for the front and rear wheel respectively. The velocity was calculated by integration and the displacement by double integration of the acceleration. We can notice the effect of low pass filtering in noise removal and high pass filtering in cali-

bration of the signal. For the rear wheel, the signal shows inaccuracy due to the limitation of the vertical accelerometer tolerance which was set to $\pm$ 2G.

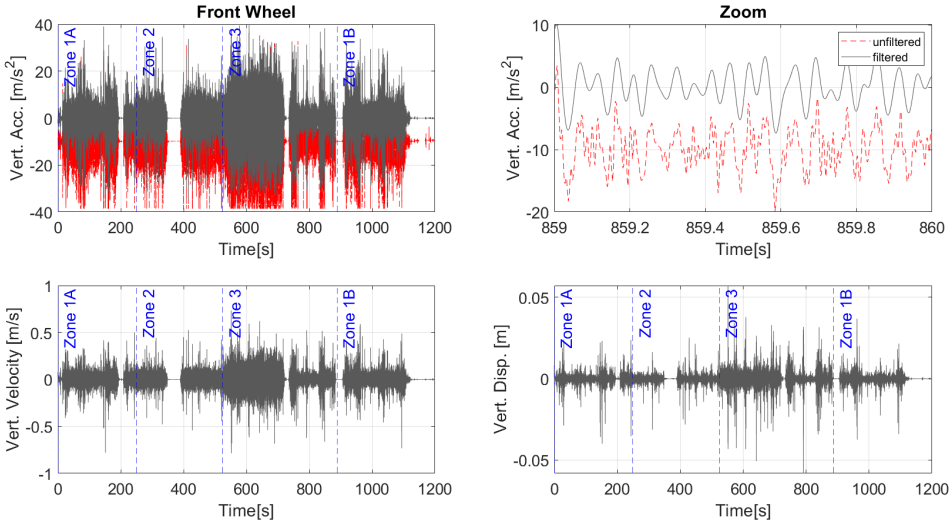

Figure 3.24. Vertical acceleration, velocity and displacement extracted from G-link-200 which was fixed on the front basket of the bicycle.

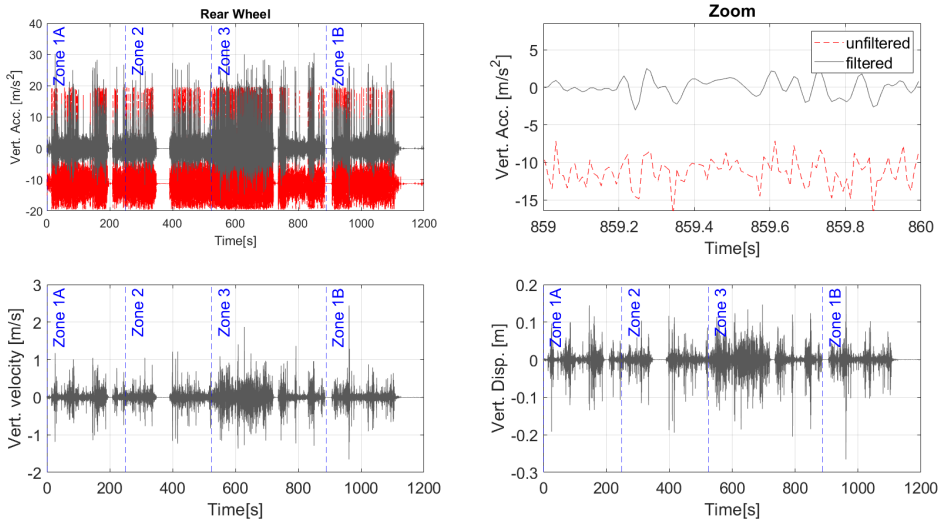

Figure 3.25. Vertical acceleration, velocity and displacement extracted from IMU which was fixed on the rear seat of the bicycle.

Fig. 3.26 shows the output of the laser scanner which is used to calculate the road profile using the inertial method [101, 102] by applying (3.1)

$$u = \iint \ddot{z} - s \tag{3.1}$$

where u is road profile, $\ddot{z}$ is the vertical acceleration output from G-link-200, and s is the distance from the laser scanner and the road surface.

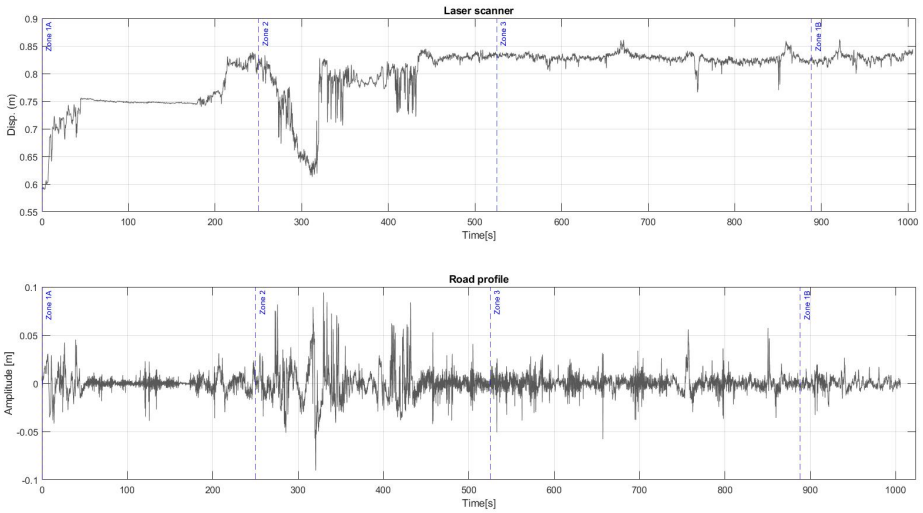

Figure 3.26. The output of the laser scanner and the calculated road profile.

We can notice the perturbations of the laser scanner signal which leads to the increase of the amplitude of the road profile between 240 and 440 s, which mismatch the behavior of the vertical acceleration; this could be explained by the difference of the lateral position between the accelerometer and the laser scanner, which leads to measuring the vertical distance on two different spots; this impact becomes significant since the measurement took place on snowy surface condition; for example, if the wheel roll over a snow puddle, the vertical distance calculated using the accelorometer is to the top of the puddle while the laser scanner measure the distance to the bottom of it.

3.4.5 Rotational outputs

Fig. 3.27 shows the steering angle extracted from the potentiometer attached to the handlebar. The signal was calibrated and a low pass filter was used to remove the noise. The high value of the steering angle at the end (around 84 °) represents the bicycle while stopping. It is noticed that the maximum value of steering occurred when turning left between zone 1A and zone 2, by looking at the trajectory (Fig. 3.15), we notice that the

degree and radius of curvature is low.

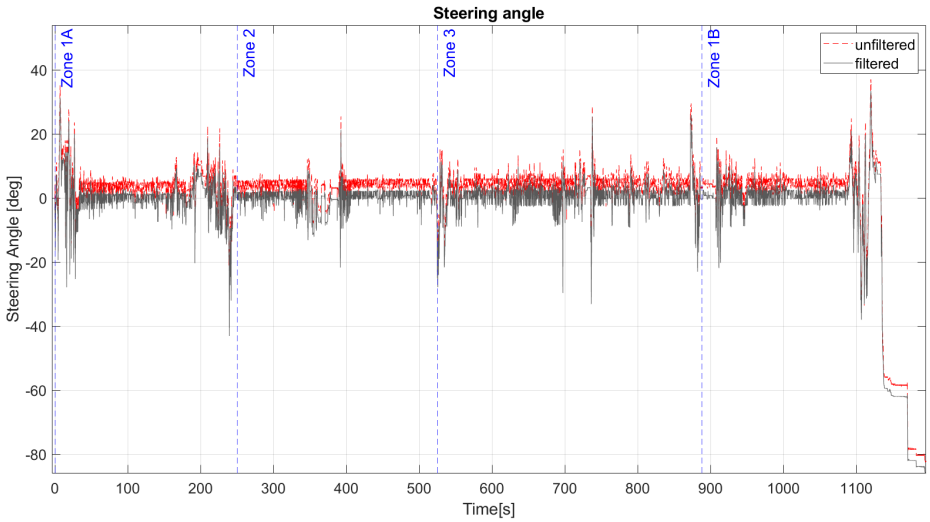

Figure 3.27. Steering angle calculated using the date of the potentiometer, positive value indicates turning right, and negative turning left.

Fig. 3.28 shows the maximum steering angle applied by the participants when turning left between zone 1 and 2 and the correlated lateral acceleration, the angles of curvature at this point in less than 90 ° and accordingly the radius of curvature is very low, it is noticed the increase of the lateral acceleration for all participants when turning left, however, this increase in disproportional due to the different steering behavior of cyclists and the use if the body posture to turn, the increase of the lateral acceleration may lead to rollover. It is noticed that some participants did not follow the cycling path in order to increase the radius of curvature and reduce the steering angle, for example, at steering angle of 23 ° the participant left the cycling lane which led to dramatic increase of in lateral acceleration (18 m/s^2).

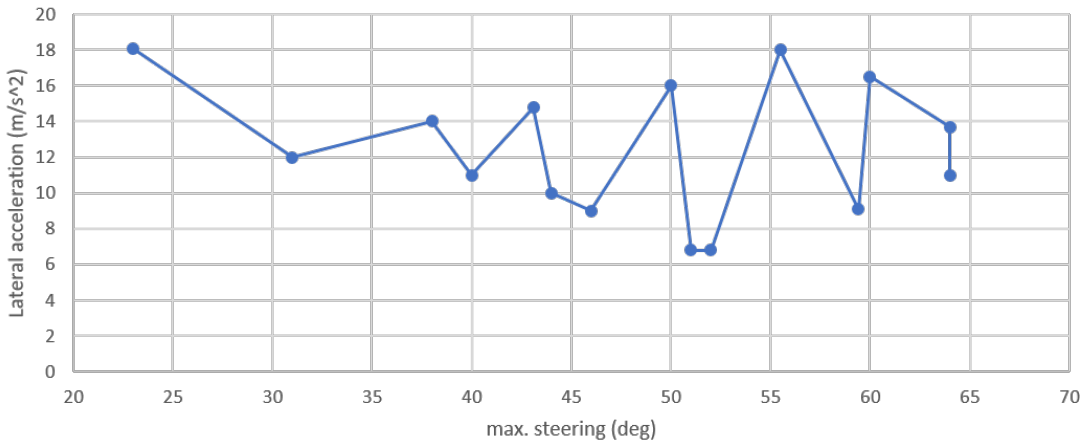

Figure 3.28. The maximum steering angle applied by the participants when turning left between zone 1 and 2 and the correlated lateral acceleration.

Fig. 3.29 shows pitch rate and angle which was calculated by integrating pitch rate over time.

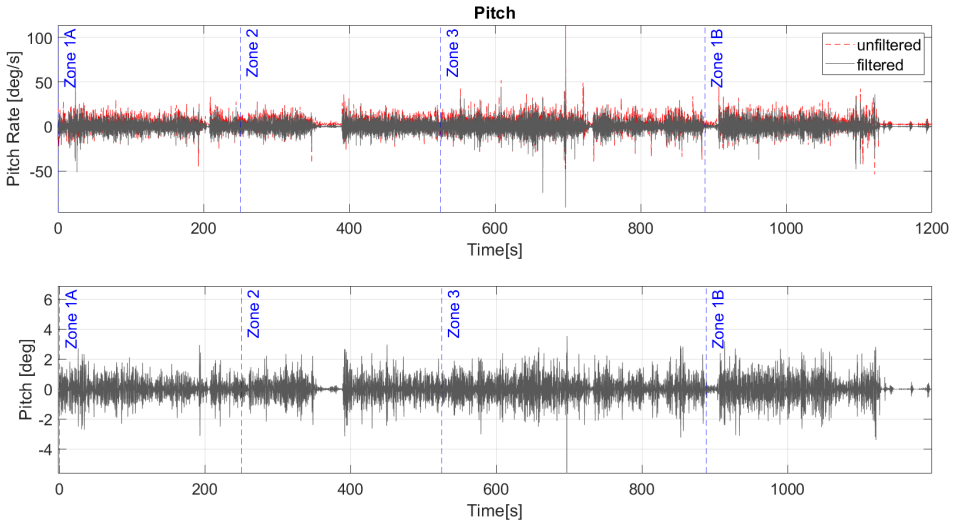

Figure 3.29. Pitch rate and angle extracted from IMU which was fixed on the rear seat of the bicycle.

Fig. 3.30 shows roll rate and angle which was calculated by integrating roll rate over time.

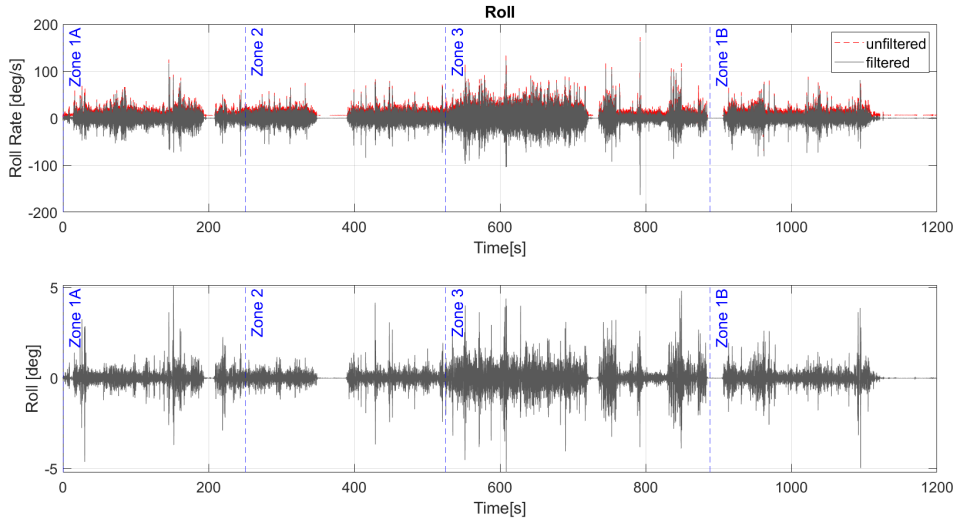

Figure 3.30. Roll rate and angle extracted from IMU which was fixed on the rear seat of the bicycle.

Fig. 3.31 shows yaw rate and angle which was calculated by integrating yaw rate over time.

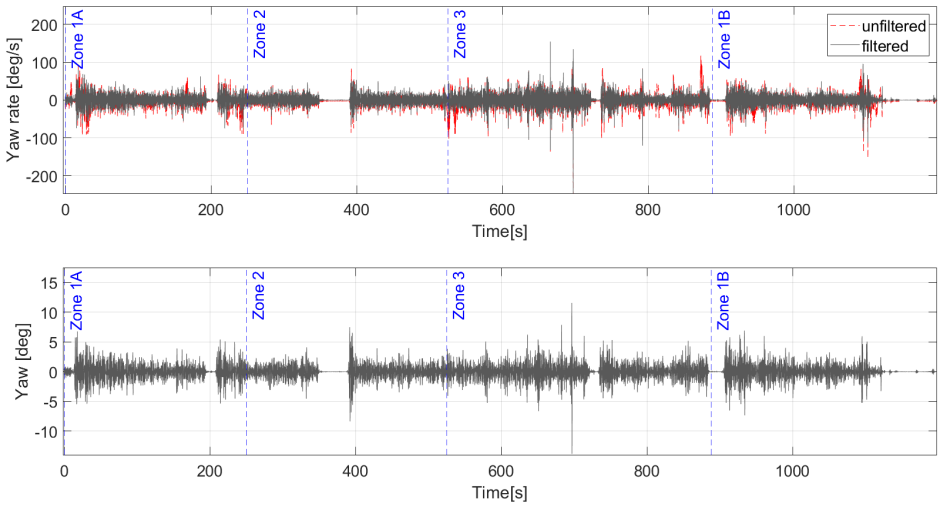

Figure 3.31. Yaw rate and angle extracted from IMU which was fixed on the rear seat of the bicycle.

3.4.6 Pedaling power and cadence

Fig. 3.32 shows the pedaling power for one of the cyclists, it is noticed that the maximum power was consumed in zone 1A according to the increases slope. Comparing to the

speed profile, there was a speed decrease in this area.

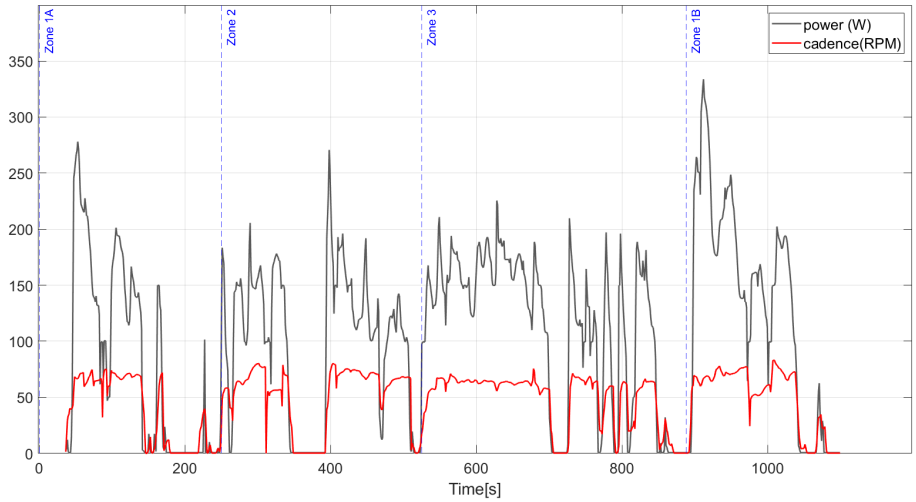

Figure 3.32. Pedaling power and cadence.

Fig. 3.32 shows the pedaling cadence, it is noticed that the cadence is not always proportional to speed. For example, around 400 s the cadence at peak, whereas the peak in speed occurred after 20 s

3.5 Evaluation of Cyclists' Behavior and Interaction with Infrastructure and Other Road-Users

The data from power, speed and cadence sensors were collected for all participants and an in-depth descriptive analysis was performed. Besides, the videos from the eye-tracker was collected and analysed to study the perception-reaction loop and to analyze the behavior of cyclists and their interaction with the different features of road infrastructure.

Three values have been quantified within the three zones of the experimental route, thanks to the use of Garmin system, which are: speed; power; and cadence. The speed could be evaluated as average, moving, or maximum. However, for this analysis, the average normalized speed for all participant was chosen to better reflects speed behavior as the stopping time differs between each participant. The normalized speed was calculated by eliminating the values when the cyclist was stationary (zero values).

Fig.3.33 shows the average normalized speed for all participants for the complete experimental route, for each zone separately and for male and female participants in both snowy and dry surface conditions. Comparing between cycling on snowy and dry surface condition, it is noticed that the speed decreases by 15% from 15.73 km/h to 12.45 km.h for the complete route; the average speed when cycling on dry surface matched the universal average cycling speed, which is 16 km/h [110]. This reduction of speed could be explained by the cyclists' cautiousness to avoid slipping and other weather-related risks.

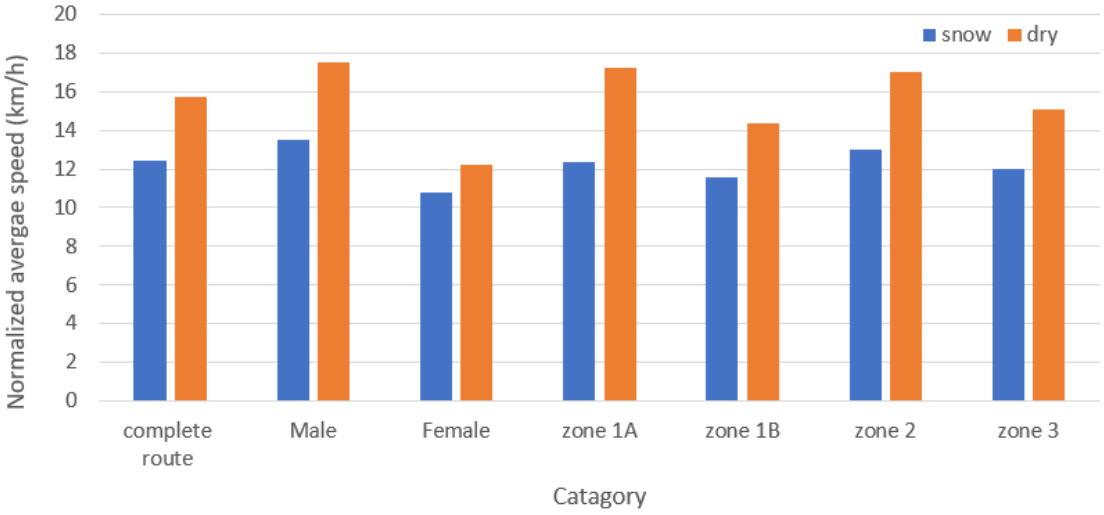

Figure 3.33. The mean normalized speed using Garmin speed sensor, the data categorized according to gender and different zones of the experimental route.

The highest average speed was recorded in zone 2 with 13 km/h on snow and 17 km/h on dry surface conditions, this could be explained by the existence of separate cycling lane on a flat-straight street. A study showed that cycling on a separate infrastructure caused a speed increase [111]. In zone 3, where the geometry is similar to zone 1 but surface and traffic conditions are different, the average speed decreased to 12 km/h on snowy and 15 km/h on dry surface condition; this could be due to the existence of pedestrians walking alongside cyclists. On the other hand, the effect of slopes on cycling speed appears when comparing between zone 1A (snow: 12.4 km/h, dry: 17.2 km/h) where the slopes are mostly downhill, and zone 1B (snow: 11.6 km/h, dry: 14.4 km/h) where the

slopes are mostly uphill. The average maximum speed for all participants was recorded in zone 2 with 20.2 km/h on snowy and 24.4 km/h on dry surface, whereas the maximum individual speed is 26.2 km/h on snowy and 29.9 km/h on dry surface. Moreover, in zone three, the speeds should be around 10 km/h, as suggested by the legislation for the cycle-pedestrian road [112]; however, this condition is not respected particularly in the case of the dry condition.

Fig.3.34 shows the distribution of the average normalized speed for each participant according to age and gender, it is noticed that the maximum speed was around 17.5 km/h for a 46 years old male participant, while the minimum speed of 7.2 km/h was recorded for 58 years old female participant.

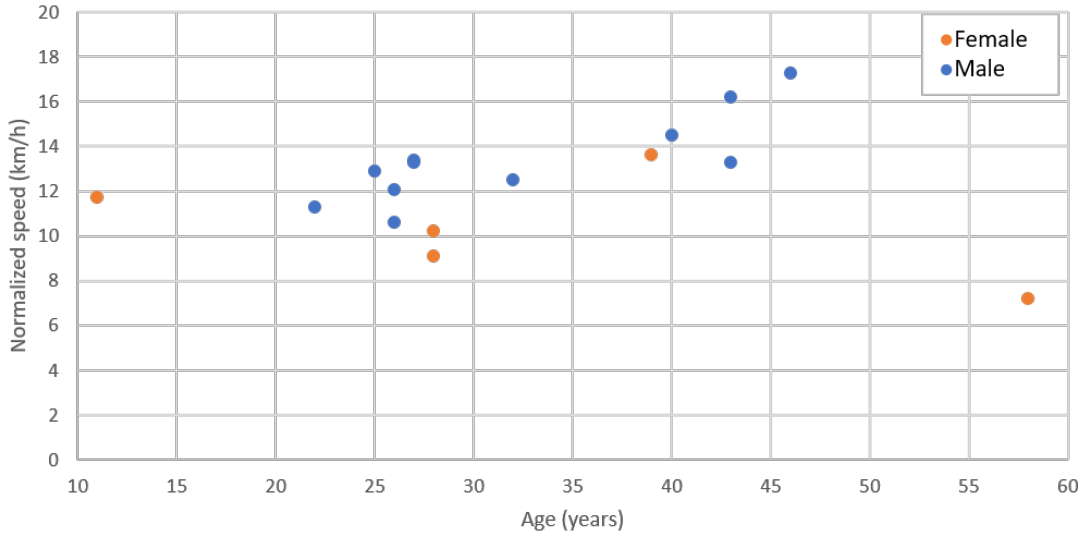

Figure 3.34. Average normalized speed distribution over age.

The evaluation of power consumption (Fig.3.35) shows a difference between cycling on dry or snowy surface conditions; compering the data for each zone, it can be seen that the average normalized power for zone 1b is the highest in both dry and snowy condition; this is explained by the uphill slope in the beginning of the zone, on contrary, the power consumed in zone 1A is the lowest since the slope was mostly downhill. In some cases, the consumed power does not reflect the corespondent speed, for example, in zone 2 where the highest average and maximum speed were recorded.

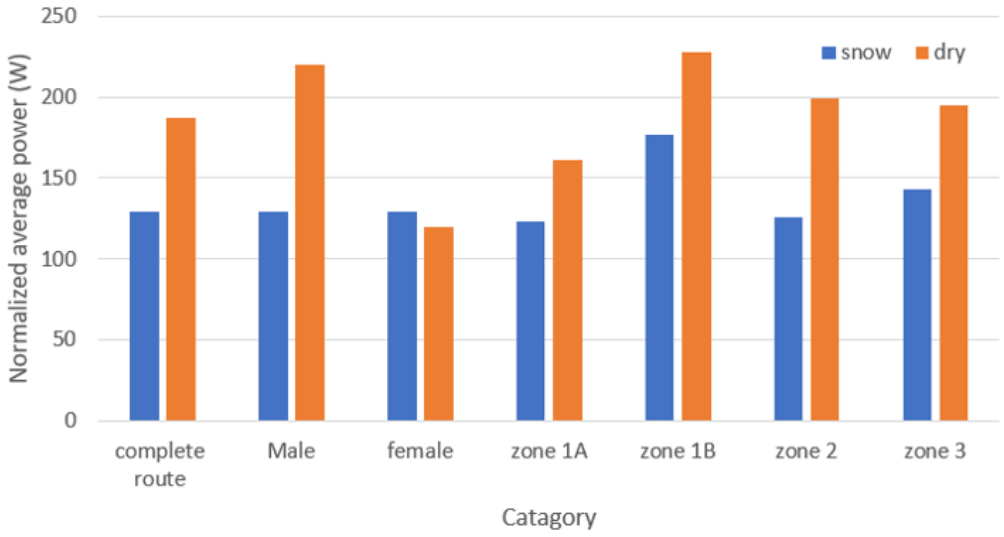

Figure 3.35. The mean normalized power extracted from the pedaling power meter from Garmin.

Fig. 3.36 shows the average cadence in different zones and surfaces conditions. The average cadence for the complete route on snowy surface is 50 RPM, whereas it rises to 60 rpm in dry conditions, as users gain confidence in driving due to increased wheel-road grip. The cadence recorded in zone 2 represents the lowest value, speed, on the other hand, shows an opposite trend, this shows that the increase of speed is not necessary due to the cadence rate. Zone 1B recorded the highest cadence and power and the lowest speed; this could be explained because of the slipperiness between the wheel and the road surface and the negative impact of the uphill slop. The detailed analysis of speed, power and cadence are attached in Appendix C.

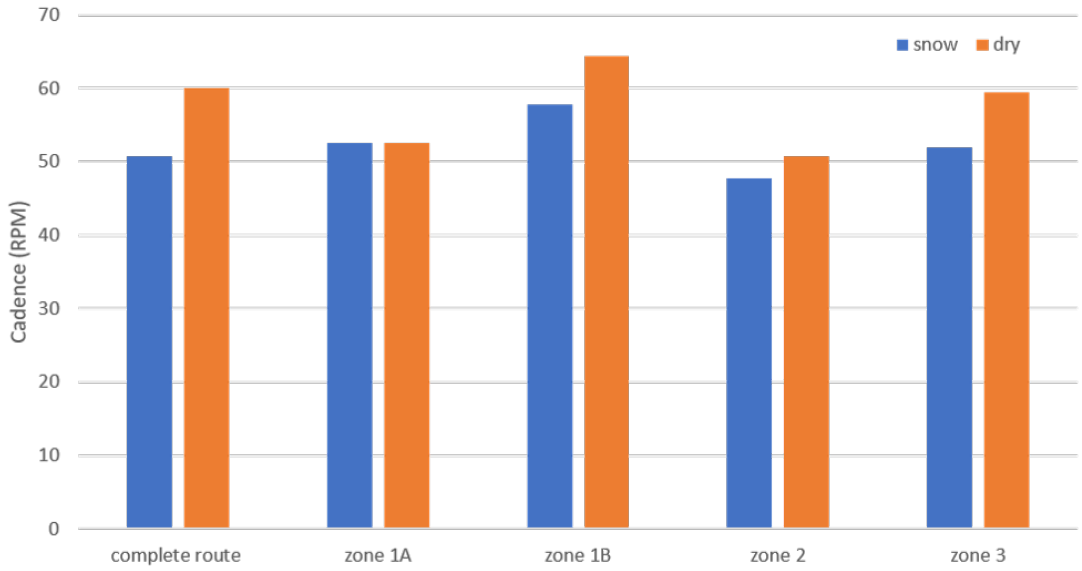

Figure 3.36. Cadence extracted from the cadence sensor of Garmin.

3.5.1 Analysis of perception-reaction loop using eye-tracker videos

19 videos were recorded using the mobile eye-tracker, 16 of them on snowy surface conditions and 3 on dry surface conditions. These videos were analyzed in details in order to study cyclists' behavior and their interaction with different features of the road and with other road users. The results show that when cyclists approach the two-way cycling path in zone 1 and 3. In 33% of the cases they cycle on the middle or left side of the path, opposing cyclists possibly approaching from the opposite side (Fig. 3.37), this could be explained by the lack of vision of the marking and the separating line due to snow accumulation, and in one case due to the existence of pedestrians on the cycling path. In 5% of the cases, the cyclists completely avoided cycling on the for-mentioned path due to lack of attention to the traffic vertical sign and the absence of in-street marking that leads to it.

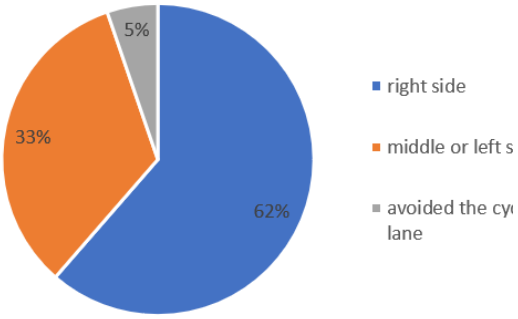

Figure 3.37. The behavior of cyclists when encountering a two-way cycling lane.

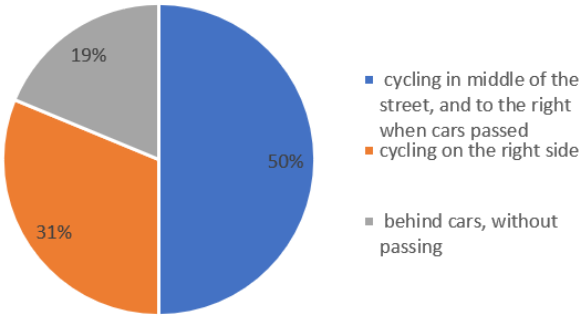

Figure 3.38. The interaction of cyclists with cars in zone 1.

In zone 1, when cycling on street alongside cars, in 50% of the cases, the participants cycled in the middle of the street, but when encountering a car they slide to the right to allow it to pass (Fig. 3.38), this is explained by the accumulation of the snow and the lack of space on the right side because of the snow accumulation. The video analysis showed that in 3 cases there were a risk of collision with parked cars leaving there spots, the cyclist braked heavily and stopped shortly before the car. In zone 2, there were 3 risked collision, because of the heavy traffic and cars stopping on the cycling lane.

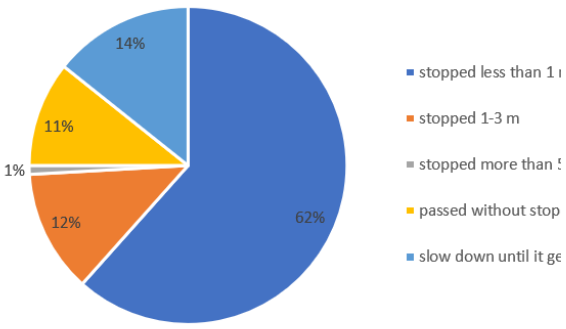

Figure 3.39. The reaction of cyclists when they encounter red traffic light.

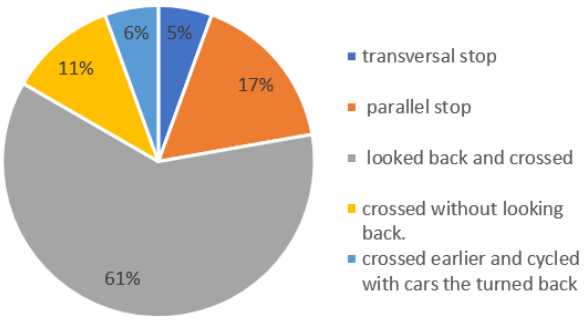

Figure 3.40. U-turn crossing behavior between zone 2 and 3.

When encountering a red traffic light, the results shows that in 25% of the cases, the cyclists did not stop (Fig. 3.39), in 11% they did not even slow down when passing. In case of stopping, the majority (62%) stopped at 1-3 m from the traffic light. When the

cyclists needed to make a U-turn between zone 2 and 3, on a crosswalk with the absence of traffic signal, the results shows that in 11 cases (61%) the participants looked back to check the traffic then turned left and crossed the street (Fig. 3.40), whereas in 11.1% of the cases they crossed with looking back to check the traffic, it seems that they depend on their hearing to the noise caused by cars to check if the road is safe, depending on hearing only is considered risky as there might be silent electric cars approaching.

Studying the interaction of cyclists with pedestrians crossing the street (Fig. 3.41), the results shows that in only 4% of the cases the cyclists stopped when realizing the pedestrians were waiting to cross. In 44% of the cases the cyclists continued cycling in front of pedestrians after they started crossing the street, whereas in the rest of cases (50%) the cyclists slowed down allowing pedestrians to cross, then accelerate again. In zone 1, there was a risk of collision with pedestrians in 7 cases, mainly because the cyclist did not stop. In zone 2 there was collision risk with one pedestrian for the same reason. In others cases, the videos show that, on traffic lights, some cyclists crossed the street within pedestrians which caused discomfort for both sides.

In zone 3, where the cycling path is shared with pedestrians, 28% of the cyclists passed the pedestrians from left, 67% were switching between passing from right or left, and in 5% they passed always from the right side.

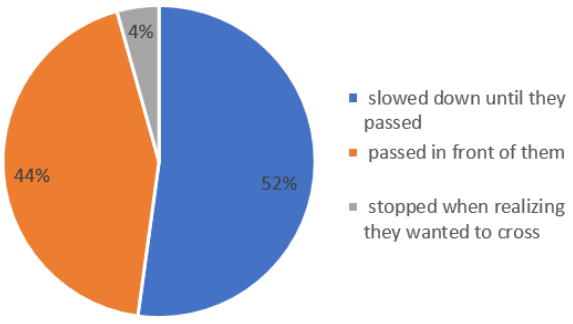

Figure 3.41. The reaction of cyclists to pedestrians crossing the street.

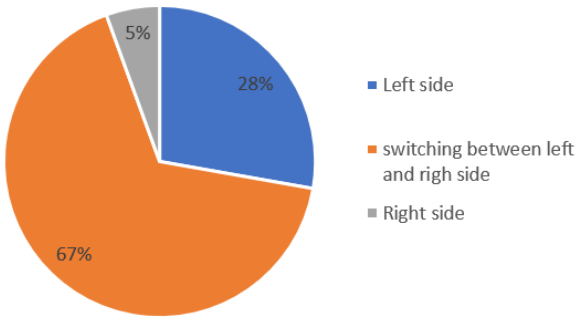

Figure 3.42. The interaction of cyclists with pedestrians in the traffic-free area.

When interacting with buses in zone 2, in 43% of the cases, cyclists passed the bus

while giving attention to their left checking for passing cars, whereas in 43% of the cases, they stayed behind the bus, and in 14% of the cases they passed the bus from the right side when they got enough space from empty parking spots. In zone 3, when the cyclists crossed the streets going through the cycle-pedestrians zone, in 28% of the cases they did not give attention to the crossing traffic and contained cycling normally, whereas in the rest of the cases they checked for incoming traffic before crossing.

3.6 Subjective Evaluation of Cycling Safety and Comfort

After the end of the experiment, the participants filled a questionnaire in regards of their cycling experience and their evaluation of cycling safety and comfort during the experiment, they were handled a map showing the different zones of the experiment in order to help them to answer the questionnaire properly; Table 3.1 summarizes the general data collected by the participants and some of their responses about the risks facing them when cycling in cold weather and snowy surface condition.

It is noticed that the cyclists who were using winter tires before the experiment mentioned that they feel higher grip specially on ice patches. On the other hand, the cyclists who did not use them before the experiment mentioned they felt a better grip, and more stable (7 out of 11 agreed on that). However, some participant consumed more effort comparing to regular tires. One participant said: 'The winter tires were better than regular ones on ice an hard packed snow, but no difference on looser snow. They gave more friction on dry road than regular tires so the effort of pedaling was harder and I sweated more than with normal tires. Another cyclist mentioned: 'The GPS was rather confusing than it was leading me the way.' A different cyclist said he would rather not to cycle on a bus lane since he can no hear the bus sound, another participant agreed that it is harder to cycle on a bus lane.

6 participants experienced negative impact due to the wind, not only related to the effort increasing, but also the discomfort felt when the cold wind blows on their faces and eyes.

Table 3.1 Descriptive characteristics of the study group (means ± SD or N %)

Characteristic	Male	Female	Total
N	14 (64%)	8 (36%)	22
Age (yrs)	37.9 (±13.4)	32.4 (±14.1)	35.9 (±13.3)
Wight (kg)	78.8 (±9.0)	62.5 (±12.5)	72.9 (±12.6)
Cycling experience (yrs)	30.9 (±15.9)	26 (±15.8)	29.1 (±15.3)
Cycling frequency (trips/week)	4.9 (±2.3)	3.1 (±2.2)	4.2 (±2.3)
Cycling distance (km/week)	43.9 (±30.5)	34.4 (±25.5)	40.5 (±27.9)
Cycling on snowy/icy surface	10 (71%)	7 (87%)	17 (77%)
Usage of winter tires	7 (50%)	3 (37.5%)	10 (45.4%)
familiarity with the experiment route	8 (57%)	6 (75%)	14 (64%)
foot slippery when stopping	3 (21%)	3 (37.5%)	6 (27%)
feeling less safe when cycling in cold weather	7 (50%)	2 (25%)	9 (41%)
the comfort of eye-tracker (positive)	8 (57%)	3 (37.5%)	11 (50%)
increasing effort because of the wind	5 (35.7%)	1 (12.5%)	6 (27.3%)

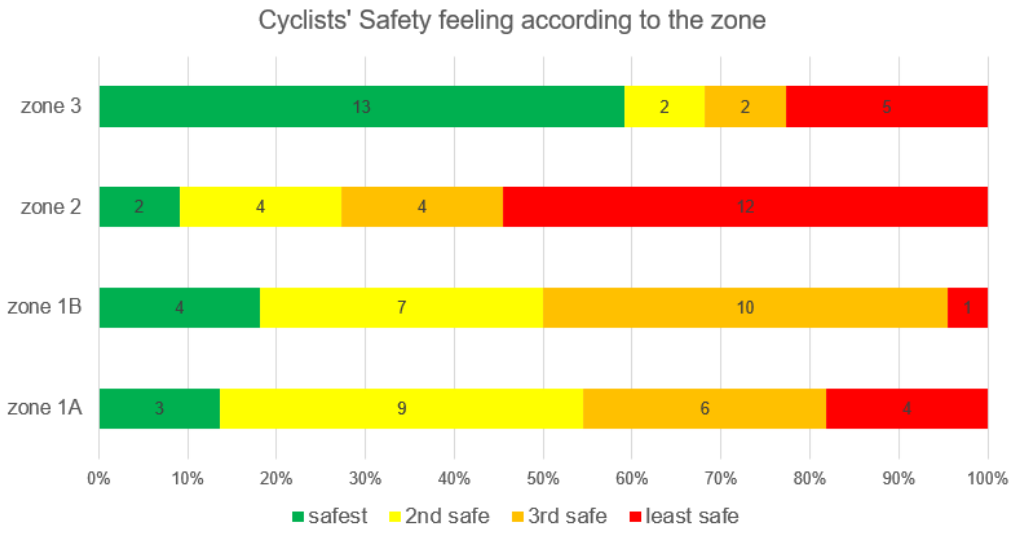

Figure 3.43. The evaluation of the participants of the safety for the different zone of the experiment route, the numbers on the bars represents the number of the participants who voted for the mentioned zone.

Fig. (3.43) shows the response of all the participants about their evaluation of each zone along the experiment route; it is noticed that 13 participants (59%) chose the 3rd

zone as safest. They explained their choice by the absence of passing vehicles, the wide separation to the carriage way, the road was almost flat and the snowy surface was hard and covered with gravel which reduce slippery. Even though most participants chose this zone as the safest, 5 of them (23%) ranked it as the least safe due to the existence of pedestrians, lack of traffic lights at some intersections and surface condition.

Better safety outcomes are associated with a greater prevalence of bike facilities – particularly protected and separated bike facilities [113].

The presence and connectivity of cycling paths and facilities were found to be positively associated with both commuting cycling and general cycling. However, the effects of land-use mix, availability of cycling paths to non-residential destinations, and terrain slope on cycling behaviors remained weak [114].

12 participants (55%) chose zone 2 to be the least safe, this is mainly because it stances on the carriage way without a physical barrier with the passing traffic; the constraint to cycle on the carriage way as the cycling lane was covered by snow and ice (as seen in the recorded videos; the snow was evacuated from the carriage way and accumulated on the cycling lane); and sharing the lane with buses which were not loud enough to be detected, one of the participants commented 'The bike lane was very icy and I had the feeling I could fall quite unexpectedly, and cars overtake me at a quite high speed.'

Zone 1 (A+B) was ranked the safest 7 times (32%) and the second safe 16 times (73%), this significance is explained by better surface condition (less snow and ice) and low and slow traffic. On contrary, the participants who chose it as the least safe explained that by the steep slopes towards the end of the zone and the absence of separate cycling lane.

3.7 Cycling Comfort

As shown in Fig. 3.44, 17 participants (77%) chose zone 1B as the most power demanding among the three zones; they said mainly because it is uphill street with steep slopes, 3 of them mentioned it was because it locates towards the end of the experiment route

where they got exhausted. On contrary, the 3 who chose zone 1A said they consumed more power because it was downhill. 20 participants said that cycling on snow-sludge is the hardest, whereas 2 said it is harder to cycle on ice.

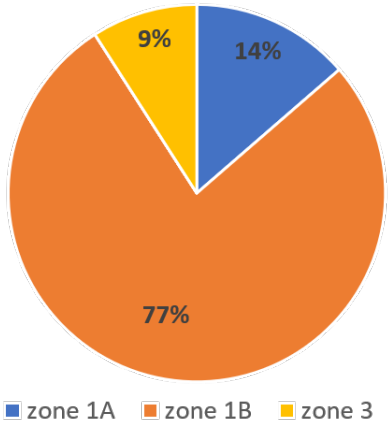

Figure 3.44. The response of the participants about where they consumed more power comparing between zones.

Fig. 3.45 shows the evaluation of the participant of comfort when cycling on different surfaces and different traffic sections; it is noticed that 9 of them (50%) chose zone 2 as the most comfortable and 9 (41%) as second comfortable. The reasons behind that according to them are: the scariness of snow-sludge, the smooth and flat surface and the separate cycling lane. Zone 3 was chosen to be the least comfortable by 9 participant due to the unevenness of the surface caused by small stones spread on top to reduce slipping, the accumulation of snow-sludge mixed with dirt coming from the unpaved surface and the existence of pedestrians. 8 (36%) chose zone 1B to be the least comfortable due to the steep slopes and the snow accumulation.

Answering the question: how cycling in cold weather condition is different than warmer one, the answers are summarized as follows: Cycling in Cold weather is better since the bicycle lanes are not so crowded; Less visibility, less grip, more clothes, a bit slippery and tougher, concentrate much more on the conditions of the surface and eventual fog on glasses, after a while the body becomes cold and cyclists react slower to the traffic around; it is more energy demanding; difficult to breath in cold air; mainly the

ice/snow that is just unpredictable which draws a lot of attention; surface is unpredictable and slippery, If the clothes are sufficient the road surface and the combination of strong winds create a sense of danger; I have to use very bulky gloves and quite heavy shoes. Also you have to have thicker hats on limiting your hearing a bit and sometimes you have to use a balaclava to protect your face, limiting your vision. The use of ski goggles to protect their eyes as well, cold wind can be irritating and the small stones on the road make riding the bicycle less comfortable and bumpy.

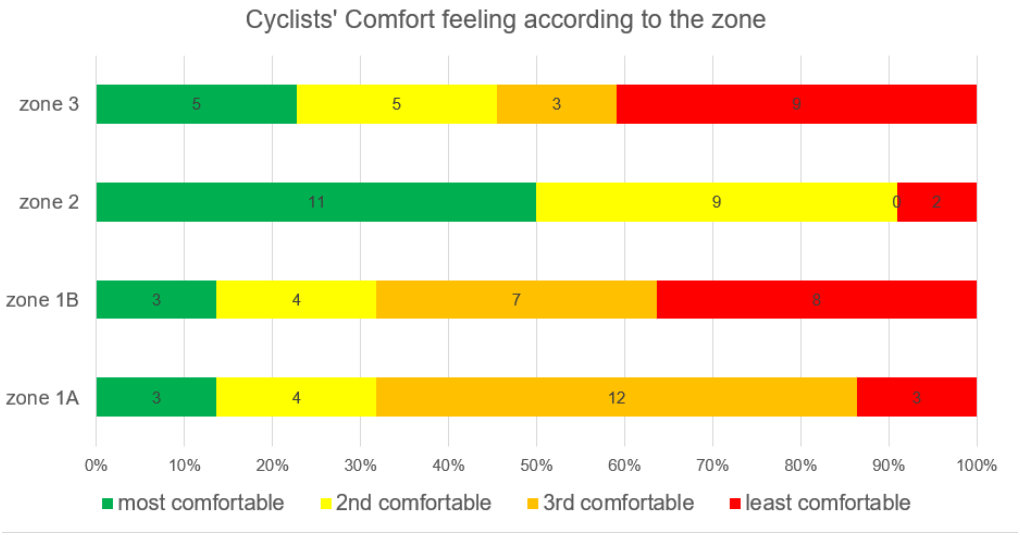

Figure 3.45. The response of the participants about where they felt more comfortable comparing between zones.

The analysis of the questionnaire shows that all participants agreed that they increase their effort, reduce their velocity to avoid slipping and experience steering difficulty when cycling on snow-sludge and ice, some of them justified this by using the winter tires which could be caught in snow sludge; one of the participants describes the feeling: 'I don't like it. It feels like the most accident prone surface as you get stuck in dips and grooves left by previous bikers, walkers and prams. Also it feels very unreliable because sometimes it is hard and sometimes it is soft and you have to be on high alert just to stay upright on the bike, even if you are a regular biker and ride every day. Answering the question if cycling in cold weather conditions is less safe, 9 participants responded positively claiming this mainly to the surface condition; beside the discomfort due to

wearing special clothes and thick gloves which limits the body movements, and impaired visibility. 6 participants experienced foot-slip upon stopping especially for the red lights (see table 3.1), 3 of them anticipated this to happen and slowed down before stopping. The tire/road friction depends on the following factors: road surface characteristics (e.g. texture, bitumen, aggregates properties); tire characteristics (e.g. size, width, tread depth, rubber); contact conditions (e.g. wheel speed, slip ratio, normal load, tire pressure); presence of contaminants at the interface (e.g. water, snow, ice, dust). Road surface texture is provided by fine and coarse aggregates and the compaction mode. It is composed by asperities of different sizes separated into two scales: the macrotexture and the microtexture. Macrotexture is defined as surface irregularities whose dimensions range between 0.1 and 20mm vertically, and between 0.5 and 50mm horizontally (ISO 13473-1 1997). Microtexture is defined as surface irregularities whose dimensions range between 0.001 and 0.5mm vertically, and below 0.5mm horizontally (ISO 13473-1 1997). [115]

3.8 Evaluation of infrastructure related risks and associated cyclist' behavior

After the analysis of the different outputs of the sensors, the eye-tracker videos and the post-experiment questionnaire, the effects of road surface characteristics and geometric design on the behavior of cyclists and their interaction with other road users were studied. Table 3.2 shows the different risks, caused by the mis-geometric design or lack of maintenance of the road surface, and the associated behavior of cyclists and the type of accident related to these risks.

1. The decreased low adhesion, due to the icy/snowy surface condition, may lead to sliding of the bicycle wheels or to foot slipping when the cyclist stops due to the decrease of friction force, this goes inline with the simulation results that show the increase of longitudinal force calculated using (2.32) when the road surface has high road adhesion, and a decrease in the friction force when it has low road adhesion as in our case, the analysis of the videos and the questionnaire show that 6 participants experienced foot slippery when stopping and all of them experienced

Table 3.2 The evaluation of risks related to the interaction between cyclists and road infrastructure.

no.	Infrastructure parameter drawback	Cause	Associeted behavior	Type of accident			
				lane departure	collision	rollover	sliding/slipping
1	low road adhesion	accumulation of snow and ice	speeding, foot slipping when standing	X			X
2	unevenness of road profile	damage of road or mis-design of the pavement	increase of vertical acceleration which affects stability and comfort	X		X	
3	increase in conflict points at interesections	poor geometric design	crossing in front or between pedestrains without slowing	X	X		
4	poor road marking and signs	lack of maintenace	not following cycling path	X			
5	low radius of curvature	poor geometric design	speeding on sharp curves which increase of steering angle and	X			
6	absence of physical barrier between cycling	limited space	cycling near other vehicles		X		
7	walking and cycling shared path	mis-use of the space	passing pedestrian from right		X		
8	bus/cycle shared lane	limited space	passing buses without attention		X		
9	high slopes	ignoring cycling needs in design	speeding downhill, consume more power uphill		X	X	X
			Cyclist misbehavior (irrelated to infrastructure)				
10			non-using winter tires				X
11			cyling in narrow spaces		X		
12			lack of attention crossing the street		X		
13			breaking red light		X		

wheel slippery because of the ice and snow accumulation. In order to reduce the impact of low road adhesion, the cyclists need to increase attention, reduce their speed, using winter tires for their bicycles and wearing appropriate winter shoes to improve the contact when stepping on slippery surface.

2. Analysing the road profile, it is noticed that the unevenness of the road, caused by the mis-implementation or damage of the road surface such as cracks and potholes, caused an increase in the vertical acceleration, this matches the simulation results obtained applying (2.25), which shows the increase of vertical acceleration depending on the amplitude of the road profile, this increase of the vertical acceleration -beside affecting cycling comfort- leads to an increase in the lateral acceleration and roll rate, the lateral instability of the bicycle may subsequently leads rollover or lane departure. In order to avoid the impact of the unevenness of the road, it is noticed that cyclists tend to avoid the defects in road surface (lane departure), or reduce their speed, however, in some cases the cyclist continued cycling at the same speed, when as they did not notice the defect or had limited time to react. The recommended behavior could be keeping attention when avoiding these defects or reducing speed if they are unavoidable.

3. The increase of conflict points with other road users (pedestrian and vehicles) on intersection increases the probability of collision with them, in order to avoid this it is recommended to add more space between crossing lines of cyclists and pedestrians to reduce the conflict.

4. The lack of vertical and horizontal traffic signs and marking misdirect cyclists away from cycling lane, the videos analysis beside the questionnaire show that some cyclist failed to follow the bicycle lane in zone 1 as they did not detect it because they are unfamiliar with the experimental route, this increased the conflict with vehicles as the cyclist are forced to cycle on-street which could lead to collision with other vehicles , this could be solved by increase the number of traffic signs and add directional arrows on bicycle path.

5. The low radius of curvature, due to inappropriate design because of the limited space, lead to an increase of lateral acceleration and roll rate as noticed when analyzing IMU signals. Comparing this to the simulation results show a compatible

response, for example, we can see the impact of steering angle (Fig. 2.27) on roll angle and rate (Fig. 2.33 and 2.34) and lateral force (Fig. 2.30) which was calculated using (2.14). The increase lateral acceleration and roll rate is an indication for rollover risk, however, some cyclists did not follow the cycling lane in order to increase their turning radius and maintain their speed, this lane departure may lead to collision with other vehicles passing by. To solve this issue, the radius of curvature should be designed to accommodate the cyclists needs, or a physical barrier should be added to force cyclists to follow the cycling path and reduce their speed.

6. The absence of physical barrier between cycling lane and other vehicles may lead to collision as other vehicles may invade cycling space and decrease the feeling of safety as shown from the results of the questionnaire.

7. Sharing cycling path with pedestrian increase the risk to collide with them, reduce their comfort and safety feeling, and reduce the speed and comfort of cyclists themselves as the behavior of pedestrians are unpredictable.

8. Cycling on a shared bus-bicycle lane negatively affect the safety feeling of cyclists specially with electric buses, because they are less predictable as they are silent, the conflict increases when the bus stop and passing decision becomes harder as the passing distance increases, loss of attention may lead to collision with other passing vehicles, in order to reduce this risk it is recommended to add a separate passage for cyclists behind the bus stop to avoid conflict with both pedestrians and stopping bus, and to allow smooth passing for cyclists.

9. The increase of longitudinal slopes leads to increase in speed downhill, or a decrease in speed and an increase in the consumed power uphill as shown in Fig. 3.33 and 3.35. The geometric design of slopes should take into consideration the physical abilities of cyclists to reduce risks facing them.

   On the other side, some cyclists behavior depends mainly on their awareness and

abiding by the law and irrelevant to the infrastructure design, during the analysis of the videos the following points are observed:

10. Breaking red traffic light by cyclists without keeping attention may lead to collision, especially on intersections with reduced sight distance, the inappropriate sight due to the building blocking the view makes it very difficult to detect vehicles joining the road from the right.

11. Cycling in narrow spaces between cars and other obstacles in the road, it was noticed that some cyclists were cycling very close to cars especially in the parking lots, and they had to heavily break to avoid collision with cars leaving the parking zone. In order to avoid this it is recommended to construct cycling paths away from parking lots or add physical barriers between cycling path and on-street parked cars.

12. Lack of attention when crossing the street: it was noticed in zone 3 when cyclists cross multiple streets that they do not look around when crossing, and seems they only depend on their hearing, even though hearing is very important to detect passing vehicle, looking around still necessary especially with the emerge of elect-silent vehicles, The awareness of the cyclists about the importance and increasing the communication with him though horizontal sign may lead to fix his crossing behavior.

The combination of infrastructure parameters drawback and the associated cyclist's behavior, which are listed in Table 3.2, were used to calculate Cycling Risk Indicator (RI) by applying (3.2):

$$RI = \frac{\sum B.S}{n} \tag{3.2}$$

Where B represents the mis-behave of the cyclists when interacting with the infrastructure design or independent from it, S is the severity of the possible accident that may

occur because of the mis-design of the infrastructure and n is the number of parameters under investigation. The calculation of the safety indicator for all participants is attached in Appendix D The risk indicator (RI) ranges between 0 and 10 (0 the safest and 10 the riskiest); the cyclist's behavior is considered 'Risky' if the cycling risk indicator (RI) is above 5, whereas it is considered 'Safe' if RI is equal or less than 5.

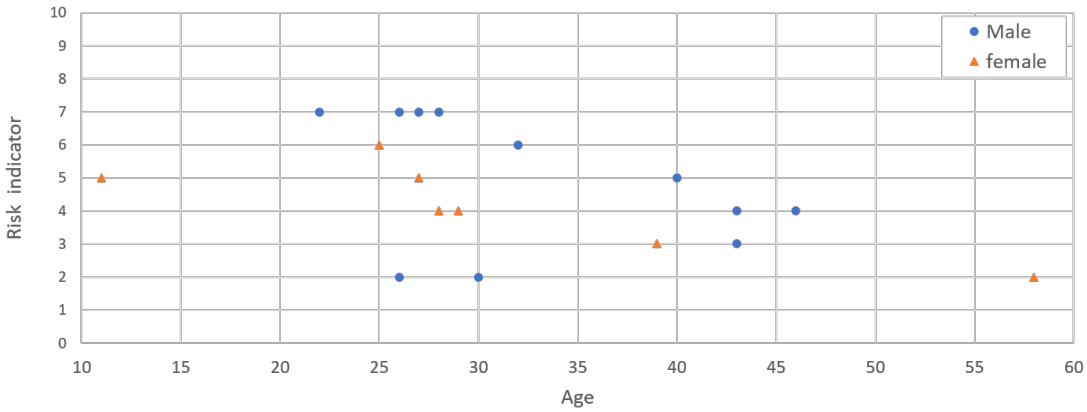

Figure 3.46. The cycling risk indicator for the cyclist participated in Stockholm experiment.

The analysis of the cyclists safety profiles (Fig. 3.46) shows that 30% of the participants have risky behavior, their ages ranges between 22 and 32 years, 45% of males and 17% of females have risky behavior.

3.9 Conclusion

This chapter presents the bicycle instrumentation and the subsequent experimentation conducted in Stockholm city. The instrumented bicycle was equipped with sensors that could measure the bicycle's kinematical and dynamical properties, while taking into account all six degrees of freedom (longitudinal, lateral, vertical, Yaw, Pitch and Roll). The inputs of the system such as steering angel and pedaling cadence were measured and logged. We observed their impact on speed, power, acceleration and other outputs of the system. The effect of the evenness of the road surface could be observed on the vertical and lateral acceleration, this impact could affect the stability of the bicycle and

may lead to lose of control specially in slippery weather conditions. The experimentation results for all participants, the subsequent questionnaire, and the eye-tracker videos were analyzed in order to study the behavior of the cyclists and evaluate cycling safety on the experimental route. The results revealed some of the risks facing cyclist, particularly in snowy weather conditions; the accumulation of the snow forced the cyclists in many cases to leave their cycling path putting them in risk of collision. The analysis also shows the reckless behavior of cyclists put them or other road users in danger; some examples of this behavior are: passing red traffic light, passing pedestrians from right side, crossing streets without paying enough attention. The self-evaluation of cycling safety shows that the participants felt safer in zone 2, where there is a separate cycling lane, even though the absence of any physical barrier. A direct link was found between the road surface characteristics and the geometric design of the infrastructure and the cyclist's behavior, the reaction of the cyclist to the drawback of the infrastructure design was evaluated in order to calculate cycling risk indicator for each cyclist and classify the behavior as risky or safe. Different measure are recommended to improve the behavior of cyclist when interacting with the infrastructure and other road users, these measures include:

1. Removing the accumulated snow from the cycling lane will improve the road adhesion and reduce the risk of sliding or slipping.

2. Installing a physical barrier between the cycling lane and the carriage way, which reduce the conflict and the risk of collision with other vehicle and improve the feeling of safety when cycling which could encourage people to cycle more.

3. Separate between cycling and pedestrian paths, which may improve the comfort and reduce the risk of collision with pedestrians.

4. Improve the communication between the road designer and cyclists through vertical and horizontal sign, in order to give the right directions for cyclists and advice them to slow down and keep attention at critical points.

CHAPTER 4. BEHAVIORAL VALIDITY OF THE BICYCLE SIMULATOR AND COMPARISON TO A REAL-LIFE EXPERIMENT IN STOCKHOLM

4.1 Introduction

Simulator studies are valid as far as they provide results that could be generalized to real-world situations and lack the side-effect symptoms affecting subjects participating in simulations. Therefore, the outputs of simulation and on-road experimentation should be analysed and compared to find the similarities and differences between the two situations. In order to to achieve similar outputs between simulation and on-road experiments, the inputs of the simulation should be as close as possible to reality, in 4 different levels: the physical feeling of cycling; the enviromental sensory ques, such as wind and traffic sounds; the road surface inputs, such as the unevenness of road profile and road adhesion; the virtual environment and the angle of view associated with it. These inputs have direct impact on the subject behaviour and the perception-reaction loop.

This chapter aims to compare between riding a bicycle simulator and on-road cycling in order to validate the simulator from physical, subjective and, more importantly, behavioral aspects. The chapter is structured as follows: the second part is devoted to explain the experimental procedure; the third part shows the outputs of the 6 DoF model and compare them to the output signals of the instrumented bicycle; the forth part is dedicated to the analysis of the videos and the behavior of cyclists and their interaction with the road infrastructure and other road users; the fifth part shows the analysis of the questionnaire answered by the participants regarding simulator sickness, NASA task load index and their evaluation of cycling safety and comfort comparing to the on-road experiment; and finally the conclusion.

4.2 Experimental Procedure

I order to create similar situation to the Stockholm on-road experiment using the instrumented bicycle, the same experimental scenario was reproduced on PICS-L bicycle simulator in Paris. The 3D model of the experimental route was created using Roadrunner software [116, 117] (a screenshot of Roadrunner interface while creating the 3D model of the route in Stockholm is attached in Appendix E), and then converted to a virtual environment using a local software called Archisim [118], the scene on the virtual environment from point of view of the cyclist is shown in Fig. 4.1. Besides, medium to heavy traffic was generated depending on the zone to simulate the traffic in real situations. In addition to the components of the bicycle simulator shown in Fig. 2.1, the power meter pedals, the cadence and speed sensors, which were fixed on the instrumented bicycle, were fixed on the bicycle simulator to collect more comparable data.

Figure 4.1. The scene in the virtual environment between zone 1 and 2.

4.2.1 Participants

31 cyclists, 19 males and 12 females, aged 11-65 years (M= 36.5 years, SD=12.85 years), participated in this experiment, they were recruited randomly from the campus of Gustave Eiffel University and in collaboration with local cycling groups around Paris. None of the participants participated in the on-road experiment in Stockholm.

All participants were asked to sign a standard consent form including a brief details about the experiment, the data collected and the following analysis. 5 participants were under 18, the acceptance of their parents was required, and they were accompanied by

their school mentors until they completed the experiment. In the inclusion criteria we tried to achieve the balance between males and females and include all age groups.

4.2.2 Experiment route and Scenario

The experiment took place in a simulated urban environment of Stockholm reproducing the on-road experiment that took place in the same city (see chapter 3. The total cycling distance was 1.8 km, which represents half the distance of the on-road experiment, it was unattainable to create the whole route on the simulator due to technical limitations. The road consists of three zones: zone 1 has a length of 400 m and consists of a mixed traffic street with 30 km/h speed limit; zone 2 consists of an on-street cycling lane that has a width of with 1.7 m and a length of 500 m; zone 3 consists of shared pedestrians-cyclists way that goes between tress and parking lots with a width of 5 m and length of 500 m. The experiment's itinerary is shown in Fig. 4.2. The participants had to follow the experimental route through on-street painted signs showing the directions. In zone 1, a light traffic was generated; whereas in zone 2, moderate to heavy traffic were generated in the same and opposite directions of the cyclist; and in zone 3, two pedestrians moving in the sames direction of the bicycle were generated, as well as multiple stationary pedestrians on the same and opposite way of the bicycle, some of them blocked the way of the bicycle to study cyclists' passing behavior. The participants were asked to ride the simulator for around 5 minutes to familiarize themselves with it (the virtual environment of Vanves was used for the familiarization phase). After the familiarization phase, we asked them to perform the cycling task consisting of riding the bicycle for a promenade in Stockholm city following the directional arrows painted on their way lane until they reached the stop sign. During the test, each participant passed through six traffic lights, two of them intersected major roads (main crossings), whereas the rest intersected secondary roads.

At the end of the experiment, the participants answered three questionnaires: The first one to collect general information about the participants and their cycling experience in real life and using the simulator; the second one was the Simulator Sickness Question-

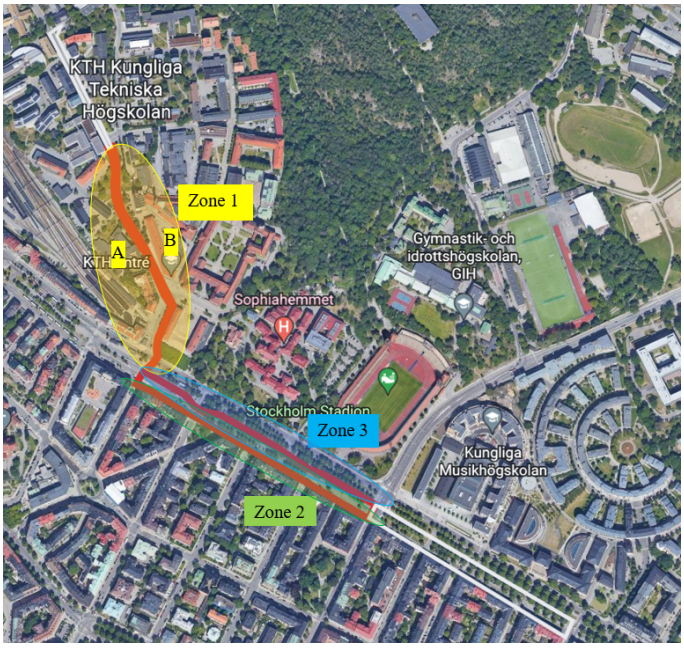

Figure 4.2. The planned cycling route on Stockholm virtual environment, the red line represents the route on the simulator, and the white line represent the extra part of the on-road experiment.

naire (SSQ) [99]: with 16 questions to evaluate the occurrence of different symptoms during the experiment using a four-level scale (None, Slight, Moderate and Severe); and the third one was the NASA Task Load Index (TLX) [98], to evaluate the overall work-load of the cycling task and the importance of each of the 6 work-load-factors under investigation. The questionnaires were available both in English and French, as some participants only speak French.

4.3 Comparison between the bicycle simulator and the instrumented bicycle output signals

For the sake of comparison, the output signals of two participants were chosen considering that they have similar profile; a female who has 39 years old was selected from the on-road experiment and a female who has 40 years old was selected from the simulator experiment. The data from both participants were analysed and compared as following:

4.3.1 Trajectory and position

The trajectory from the simulator experiment and the trajectory from the on-road experiment are shown in Fig. 4.3, the participant on the simulator followed exactly the predetermined route. It is noticed that the simulator trajectory shows more accuracy comparing to the on-road experiment (Fig. 3.15), as it does not depend on the strength of the GPS signal.

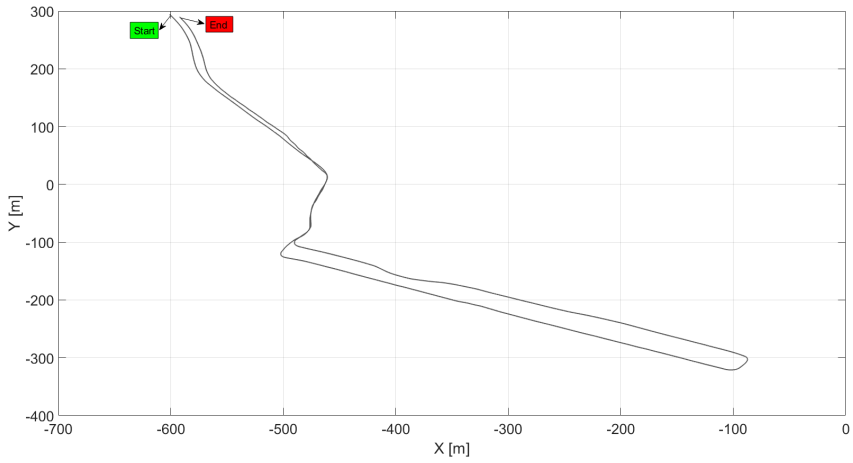

Figure 4.3. The experiment trajectory for one of the participants on the simulator.

Fig. 4.4 and 4.5 show the longitudinal and lateral positions for one of the participant. The positions calculated on the simulator shows more accuracy comparing to the on-road experiment, as they do not rely on the strength of the GPS signal. It is noticed that, even-though the distance on the simulator is shorter than the on-road experiment, the position changes in the same manner; this becomes clearer at the beginning of zones 2,3 and 1B in both experiments.

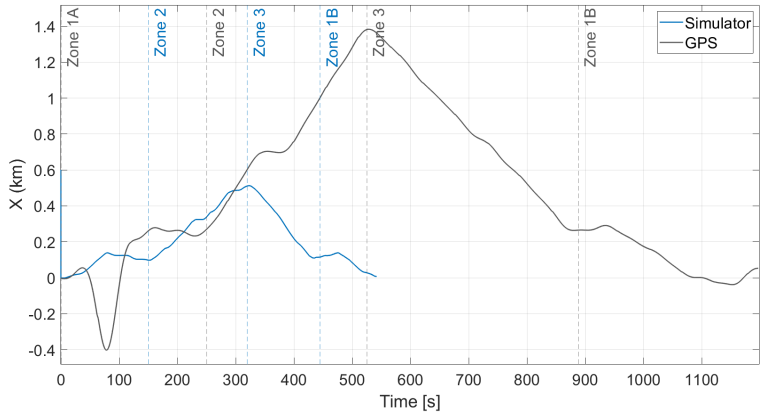

Figure 4.4. Comparison between the longitudinal position of the bicycle simulator and the instrumented bicycle.

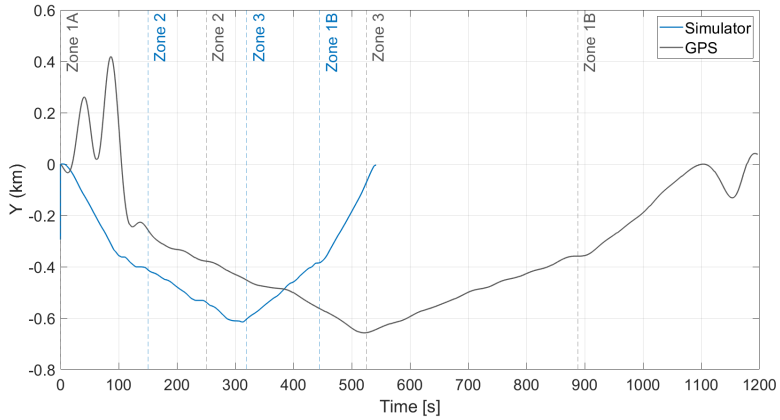

Figure 4.5. Comparison between the lateral position of the bicycle simulator and the instrumented bicycle.

4.3.2 Longitudinal acceleration and velocity

Fig. 4.6 shows the longitudinal acceleration for the front and rear wheel of the instrumented bicycle and the longitudinal acceleration of the bicycle simulator calculated using (2.19) (with zoom between 160-180 s). We can notice that the longitudinal acceleration has bigger absolute value in the on-road experiment compared to the simulation. The road adhesion input is shown in Fig. 2.31.

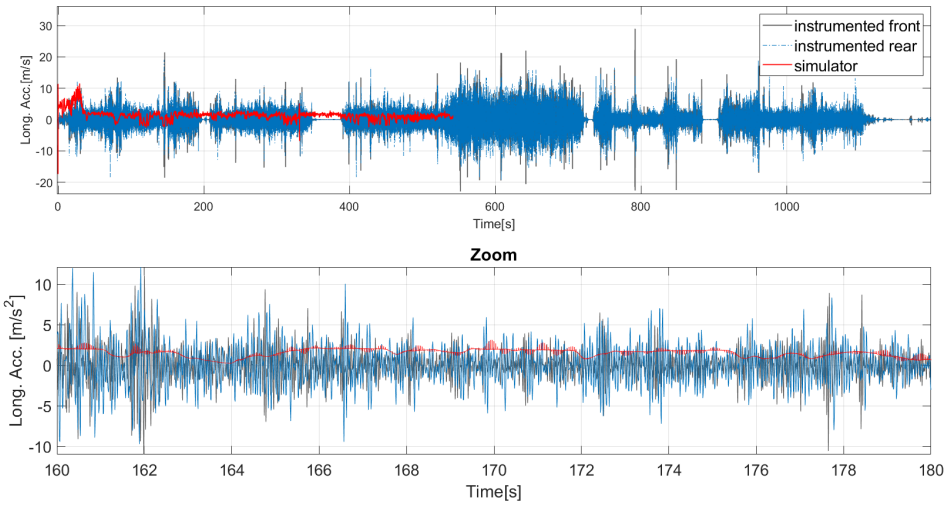

Figure 4.6. Comparison between the longitudinal acceleration extracted from the instrumented bicycle and the calculated acceleration of the simulator.

Fig. 4.7 compares between the speed profiles of the instrumented bicycle (extracted from Garmin speed sensor) and the bicycle simulator (extracted from both the incremental encoder attached to the rear wheel and Garmin speed sensor), the zoom shows the common area of zone 2. The speed behavior for both systems seems to be akin, for example, the maximum speed for both participants is almost identical, even-though they were reached in different zone of the experiment. We can also notice that the speed profile coming from the speed sensor, which is installed on the rear wheel of the simulator, matches the one calculated using the incremental encoder.

4.3.3 Lateral acceleration, velocity and displacement

Fig. 4.8 shows the lateral acceleration for the front and rear wheel of the instrumented bicycle and the longitudinal acceleration of the bicycle simulator calculated using (2.15) (with zoom between 160-180 s).

4.3.4 Vertical acceleration

Fig. 4.9 shows the road profile calculated using the instrumented bicycle and the part of it used as an input for the simulator (starting from 590 s to the end); this part was chosen

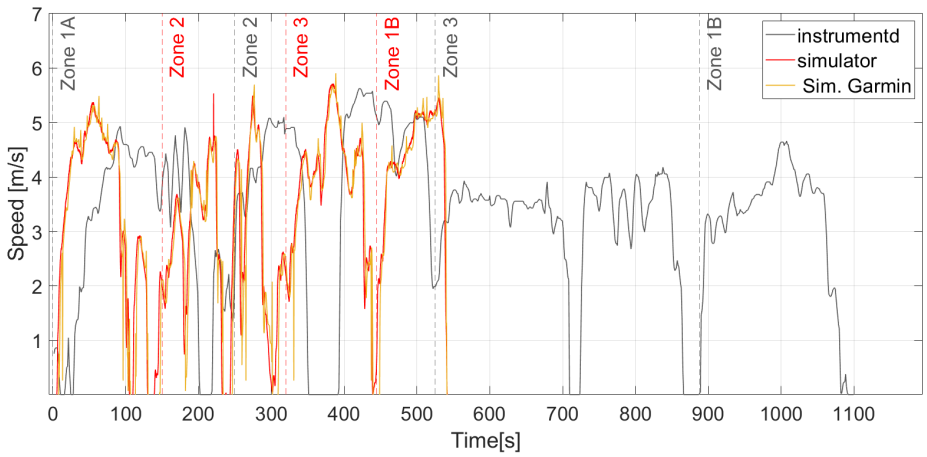

Figure 4.7. Comparison between the speed profiles of the instrumented bicycle and the bicycle simulator. The zoom shows the common area of zone 2 in both experiments.

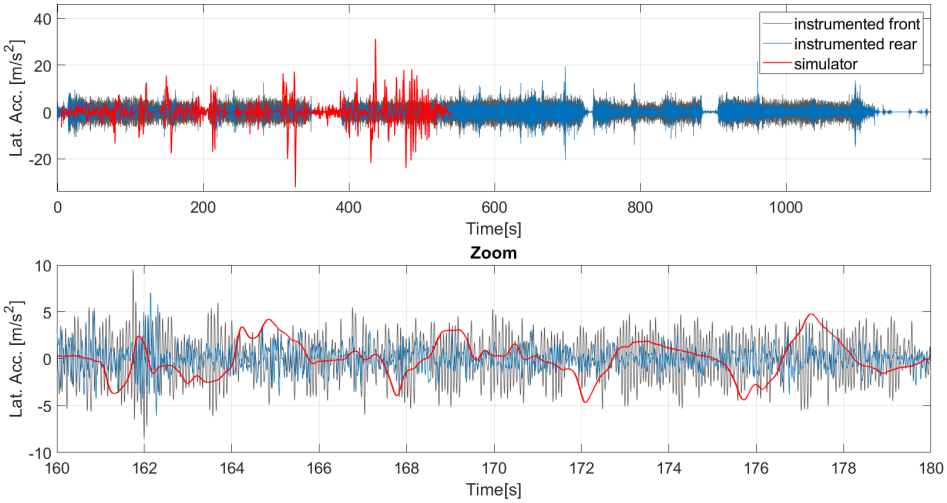

Figure 4.8. Comparison between the lateral acceleration extracted from the instrumented bicycle and the calculated acceleration of the simulator.

as it has less noise than the firs part. This road profile was used to calculate the vertical acceleration for the bicycle simulator.

Fig. 4.10 and 4.11 compare the vertical acceleration from both systems for the front and rear wheel respectively (with zoom between 170-180 s) .

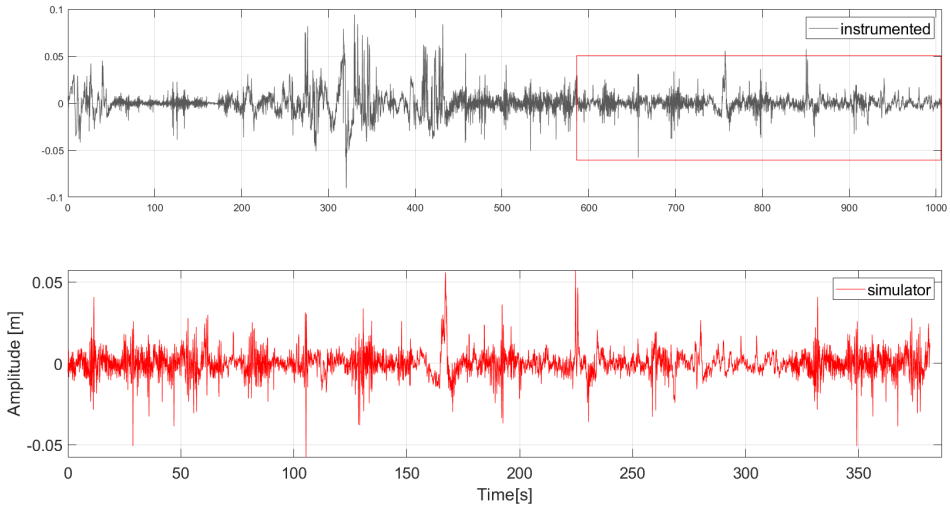

Figure 4.9. Calculated road profile, the red part represents the input of the bicycle simulator.

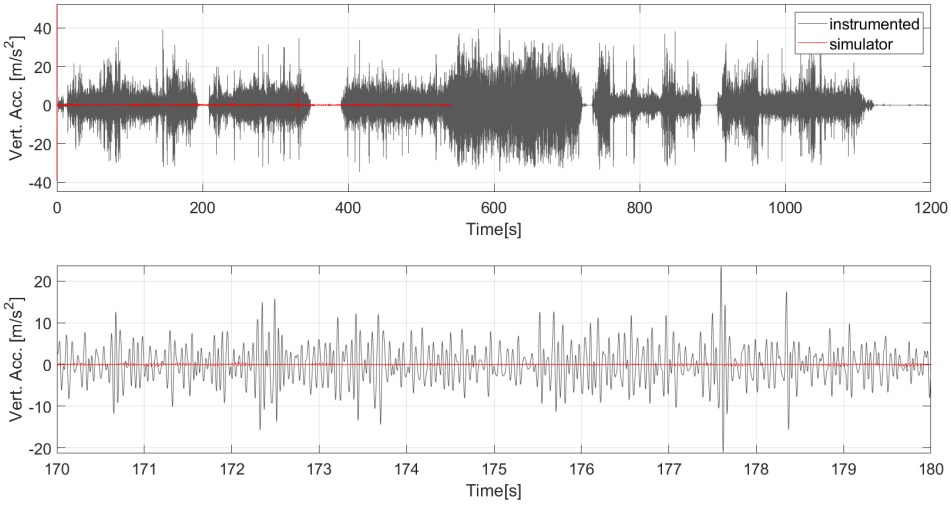

Figure 4.10. Comparison between the vertical acceleration extracted from the instrumented bicycle and the calculated acceleration of the simulator.

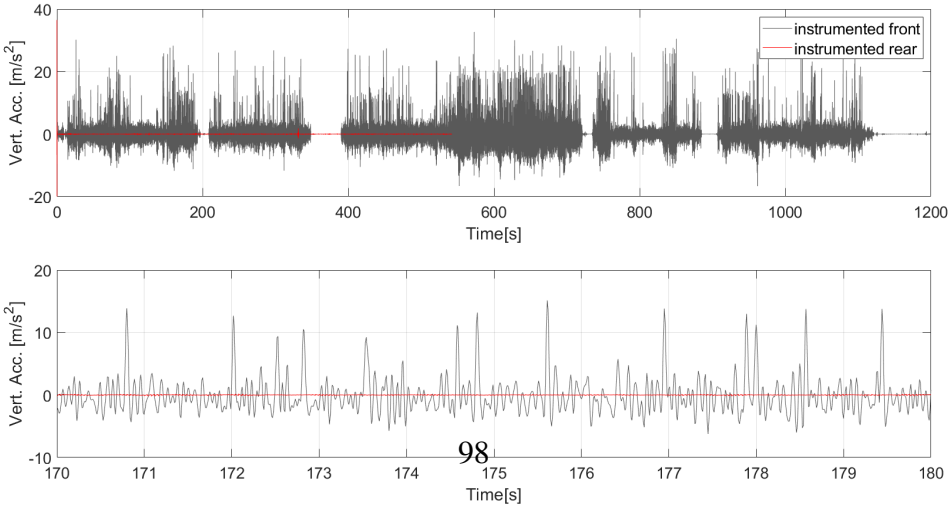

Figure 4.11. Comparison between the vertical acceleration extracted from the instrumented bicycle and the calculated acceleration of the simulator.

4.3.5 Rotational outputs

Fig. 4.12 compares the steering angle for both systems. Zooming of the beginning of zone 2 for both systems, it is noticed that the maximum value of steering for both systems are identical, when turning left between zone 1A and zone 2. On contrary, when cycling straight, the steering angle when cycling on-road varies more than when riding the simulator- both direction and value.

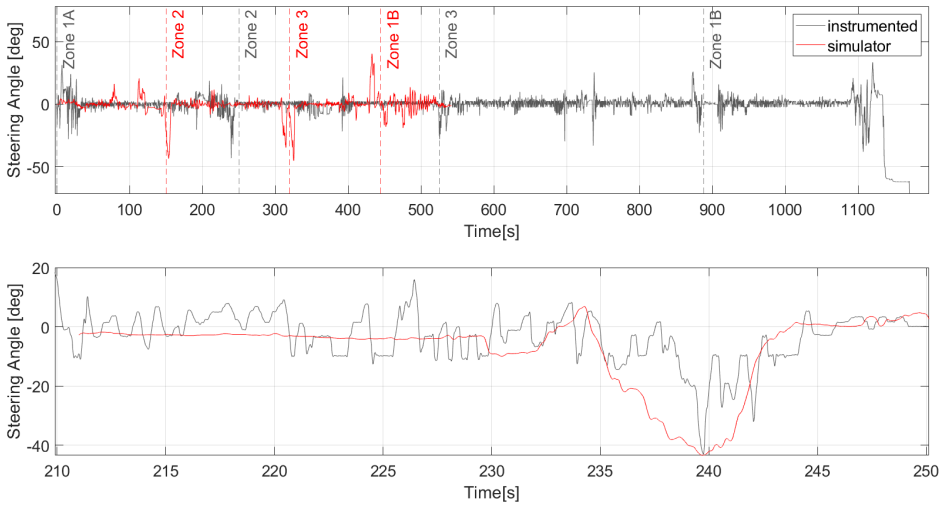

Figure 4.12. Comparison between the steering angles of the instrumented bicycle and the bicycle simulator.

Fig. 4.13 shows pitch rate for both systems. It is noticed that the value of pitch rate for the simulator, which was calculated by integration pitch acceleration in (2.31), is lower than the instrumented bicycle, this could be explained by the assumption of riding the simulator on flat surface.

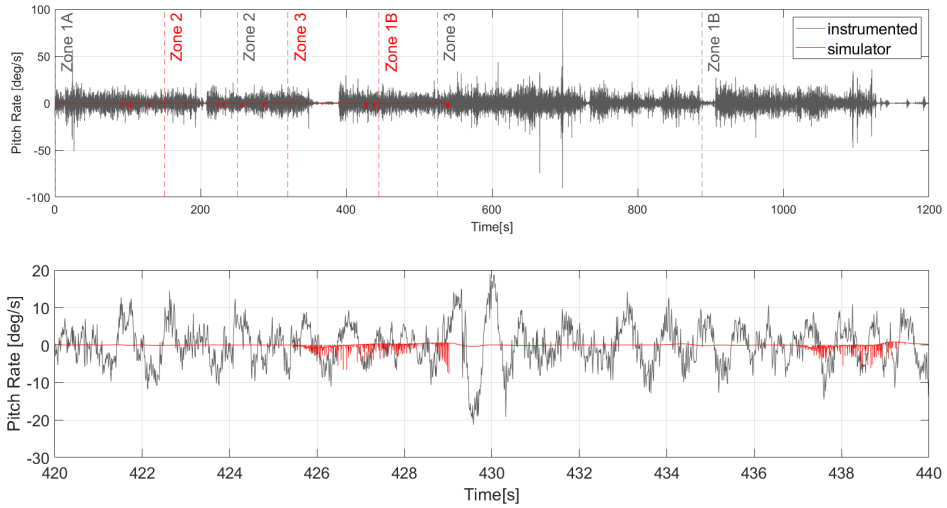

Figure 4.13. Comparison between pitch rates of the instrumented bicycle and the bicycle simulator.

Fig. 4.14 shows roll rate for both systems. It is noticed that the value of roll rate for the simulator, which was calculated by integration roll acceleration in (2.22), is lower than the instrumented bicycle.

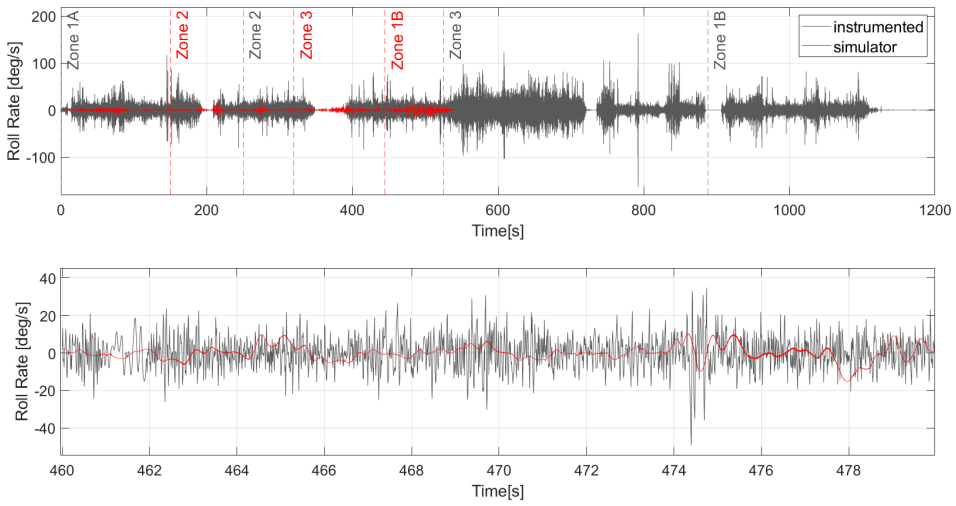

Figure 4.14. Comparison between roll rates of the instrumented bicycle and the bicycle simulator.

Fig. 4.15 shows yaw rate for both systems. It is noticed that the value of yaw rate for the simulator, which was calculated by integration pitch acceleration in (2.37), is lower than the instrumented bicycle.

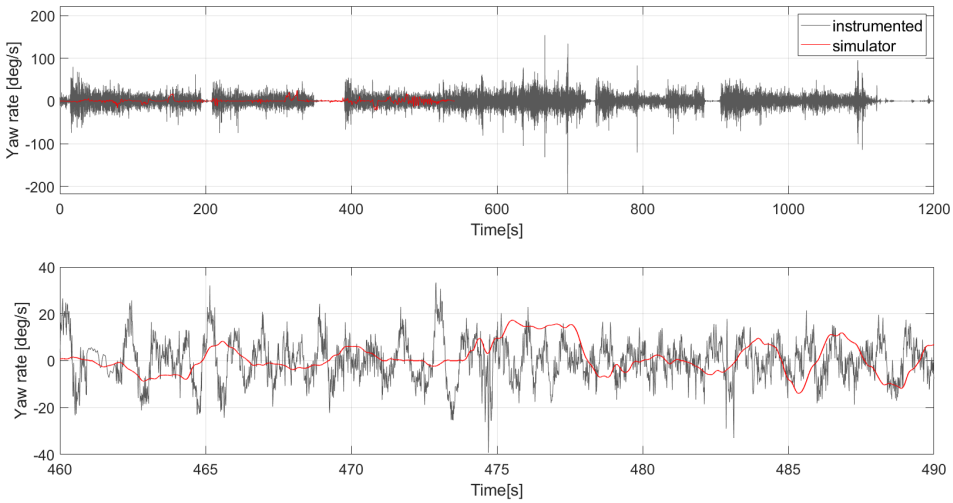

Figure 4.15. Comparison between yaw rates of the instrumented bicycle and the bicycle simulator.

4.3.6 Pedaling power and cadence

Fig. 4.16 shows the pedaling power consumed in both systems, it is noticed that both system have similar pattern, for example, the power increases when accelerating and decreasing when braking despite the fact that the power consumed on the bicycle simulator is less than the instrumented bicycle.

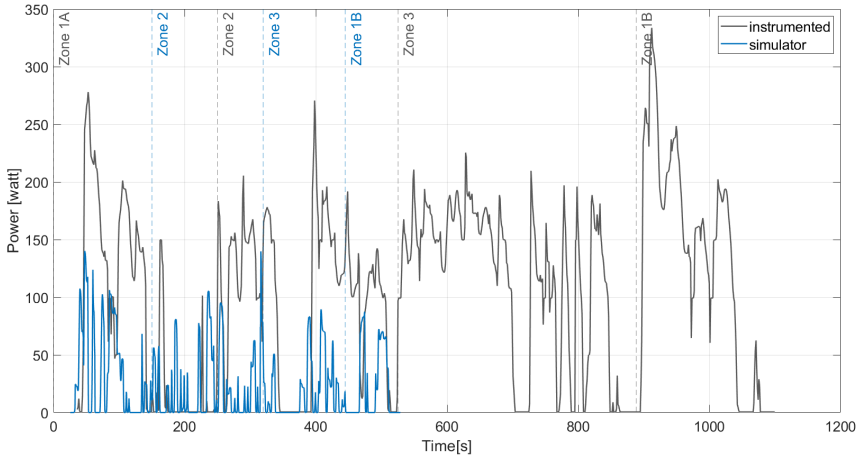

Figure 4.16. The power consumed during the cycling task for both the instrumented bicycle and the bicycle simulator extracted from the power meter pedals.

Fig. 4.17 shows the pedaling cadence for both systems, it is noticed that both sys-

tem have similar pattern, for example, the cadence rate increases when accelerating and decreasing when braking.

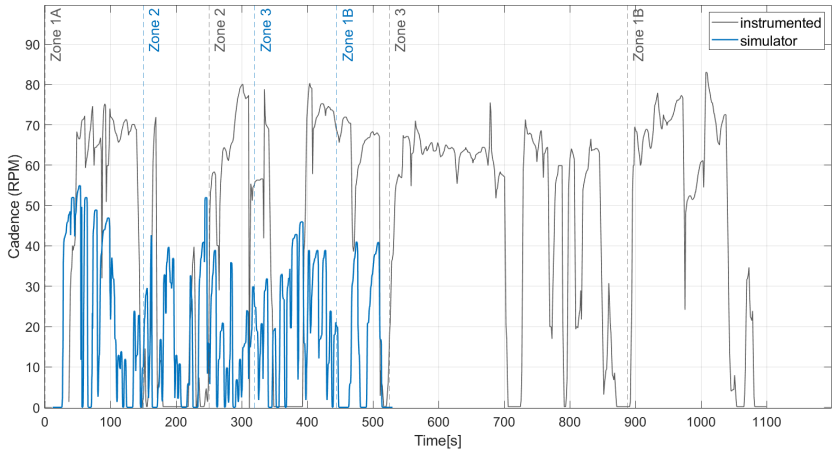

Figure 4.17. The cycling cadence during the cycling task for both the instrumented bicycle and the bicycle simulator extracted from cadence sensor fixed on the pedal crank.

In order to validate the physical aspects of the bicycle simulator, a comparative study between the on-road experiment and the simulation output signals is necessary to assess the degree of similarity between them, the comparative results are illustrated in Appendix F, and summarized as following:

- There is a high correlation between the speed signal on the simulator and the on-road experiment, the correlation coefficient is 83%, their averages are approximately the same.
- A high correlation is also observed with respect to the lateral (80%) and longitudinal (83%) front accelerations, it is noticed that the front part correlation percentage is better than the rear one, this could be explained by the difference of the sensors fixation, their sensitivity to noise, and the sampling frequency.
- Concerning the roll and yaw rates acquired , the correlation remains significant, being 76% for roll, and 86% for yaw. However, the mean difference in amplitude for roll is -8.5011 $^{\circ}/s$, and for yaw is -2.2814 $^{\circ}/s$.

- The minimum correlation values are observed on the data linked to the Z axis, namely the front and rear vertical acceleration, the lack of correlation in this case is due to the fact that the vertical model of the simulator was developed without taking into account the road slopes beside the noisy signal of the sensors .
- The steering angle is part of the highly correlated data with a rate of 80%, and a negligible average difference in amplitude, of -2.1372 degrees.
- The power is an uncorrelated data (negative correlation coefficient), with a very significant average difference in amplitude, equal to 30 watts, this result is explained by the fact that the cyclist on the simulator bicycle faces lower resistance conditions (lack of wind resistance and stationary and flat platform).

4.4 Evaluation of cyclists' behavior and interaction with infrastructure and other road users on the simulator

After the end of the experiment, the data for all participants were collected and an in-depth descriptive analysis was performed in order to compare it with the equivalent data from the on-road experiment. Besides, the videos from the camera installed behind the simulator were collected and analyzed in order to compare them with the eye-tracker videos collected during the on-road experiment in Stockholm; to study the differences and similarities between cyclists' behavior and their interaction with the different features of road infrastructure and other road users in both systems.

4.4.1 Cycling behavior in terms of speed, power and cadence

Fig.4.18 compares between the cycling speed on the bicycle simulator and on-road in both dry and snowy surface. The results show that the average moving velocity for all participants on snowy surface is 12.45 km/h, 15.73 km/h on dry surface, whereas on the bicycle simulator it is in-between with 14.34 km/h (10% lower than cycling on dry surface and 15% faster than cycling on snowy surface). This phenomena is also correct

for zones 1A and 3, whereas in zone 2 the normalized speed on the simulator is less than cycling on dry or snowy surface. In zone 1B the normalized speed is higher than cycling on both dry and snowy conditions, this could be explained by the absence of the uphill slopes that exists on reality. The average maximum speed recorded is 20.2 km/h on snowy surface, 24.4 on dry surface and 22.9 km/h on the simulator.

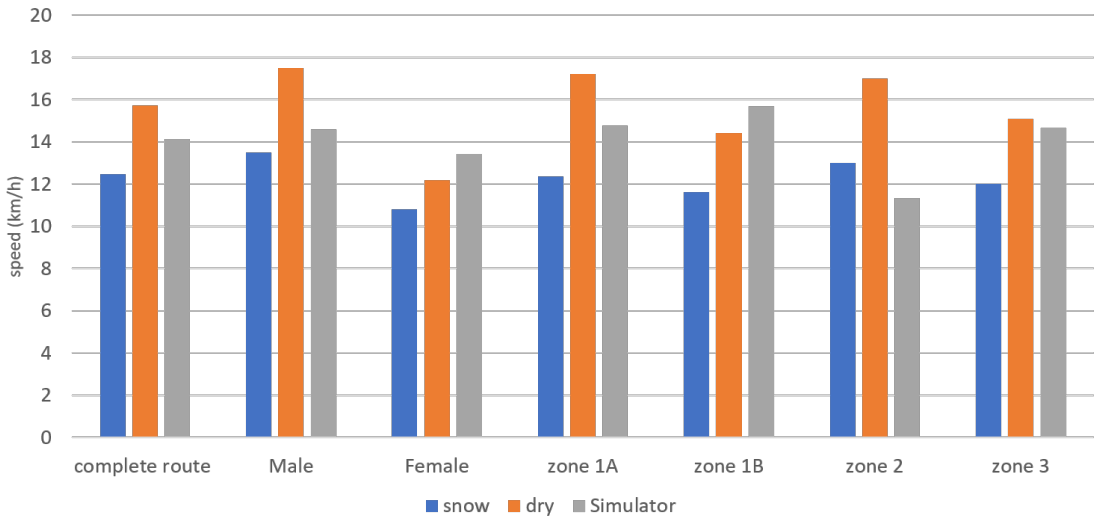

Figure 4.18. The mean normalized speed using Garmin speed sensor, the data categorized according to gender and different zones of the experimental route.

Fig.4.19 shows the distribution of the average normalized speed for each participant according to age and gender, it is noticed that the maximum speed average on the simulator (19 km/h) is higher than the on-road experiment (17.5 km/h); similarly, the minimum speed average on the simulator (9.5 km/h) is higher than the on-road experiment (7.2 km/h) which was recorded for 58 years old female participant.

(Fig.4.20) shows the difference in power consumption when cycling on dry, snowy surface conditions, and when riding the simulator. The results show that the average power consumed on the simulator is lower by 52% comparing to snowy and by 52% when comparing to dry surface conditions. The average normalized power is 121 W on snowy surface, 187 W on dry surface and 63 W on the bicycle simulator; this could be explained by the absence of some factors from the simulator that may lead to the increase of power consumption, such as: uphill slops, wind and obstacles on the road surface.

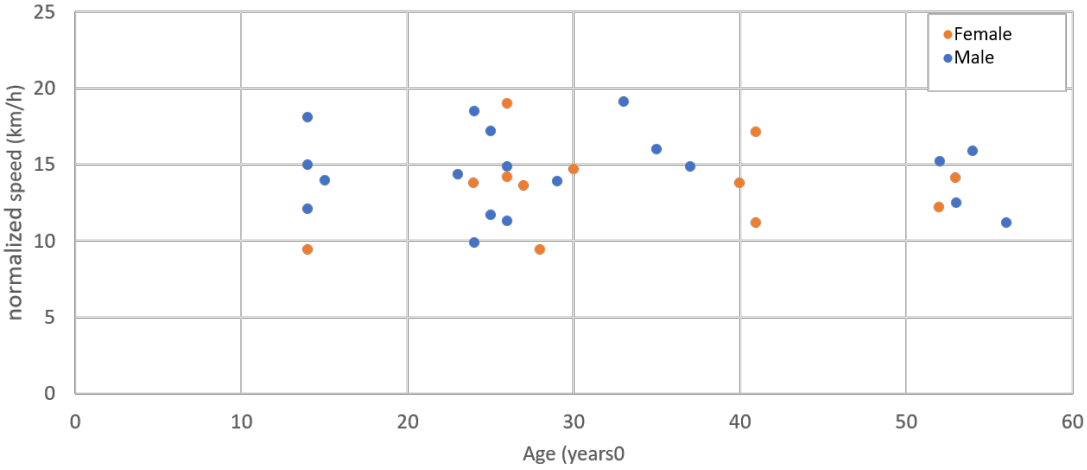

Figure 4.19. Average normalized speed distribution over age for the test group on the bicycle simulator.

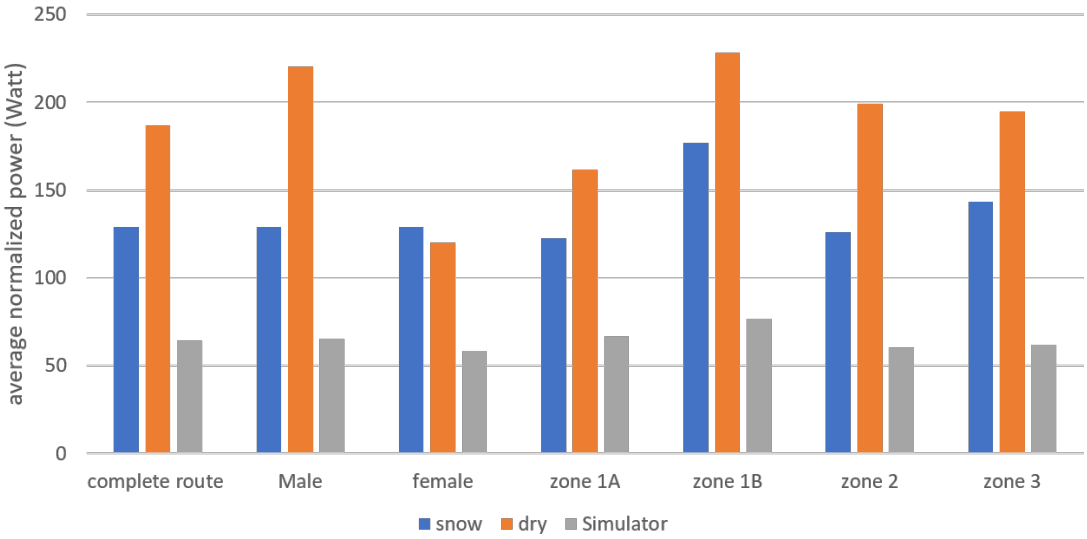

Figure 4.20. The mean normalized power extracted from the pedaling power meter from Garmin.

Fig. 4.21 shows that the average cadence rate on the simulator is lower than the cadence cycling on road for both dry and snowy surface conditions. This is applicable for all zones. The average cadence on the simulator (38 RPM) is 37% less than the cadence on dry surface (60 RPM), and 24% less than the cadence on snowy surface (50 RPM).

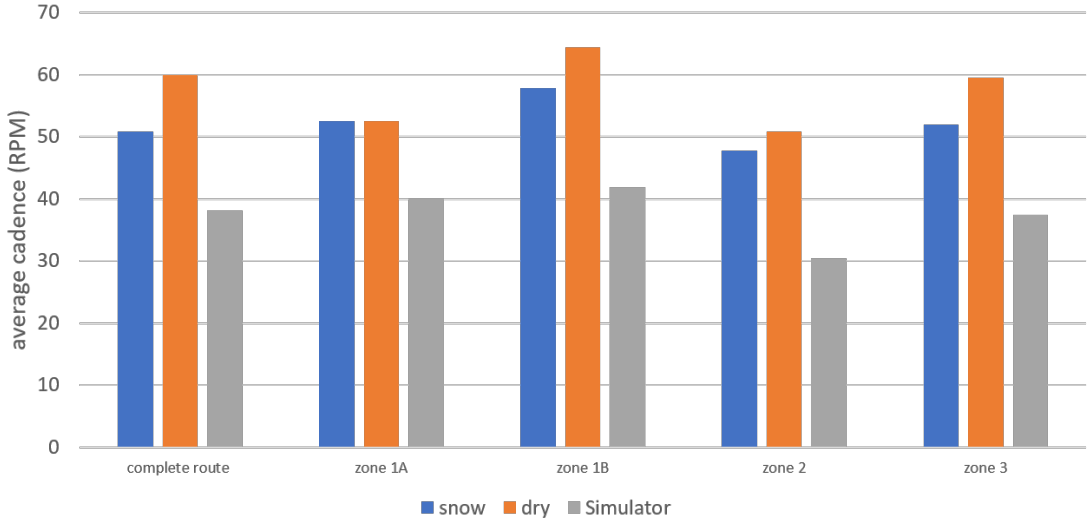

Figure 4.21. Cadence extracted from the cadence sensor of Garmin.

The detailed analysis of speed, power and cadence of both the simulator and the on-road experiments are attached in Appendix C.

4.4.2 Analysis of perception-reaction loop

31 videos were recorded using a camera installed behind the bicycle simulator. These videos were later analyzed in details in order to compare the cyclists' behavior on the simulator with the on-road experiment (see Fig. 4.22). The results shown in Fig. 4.23 reflect nearly the same behavior when cyclists approach the two-way cycling path in zone 1 and 3, 32% of the cases on the simulator and 33% on-road, the participants cycled on the middle or left side of the path, opposing cyclists possibly approaching from the opposite side, in 4% of the cases on the simulator and 5% on-road, the cyclists completely avoided cycling on the for-mentioned path due to lack of attention to the traffic signs.

Fig. 4.24 compares between the behavior of passing other cyclists in the on-road and the simulator experiments, the results show that in 41% of the cases on the simulator and 14% the participants chose to pass from the right side, the high percentage on the simulator could be explained by the space available due to the absence of parking cars, while in the on-road experiment the parking space was almost full most of the time.

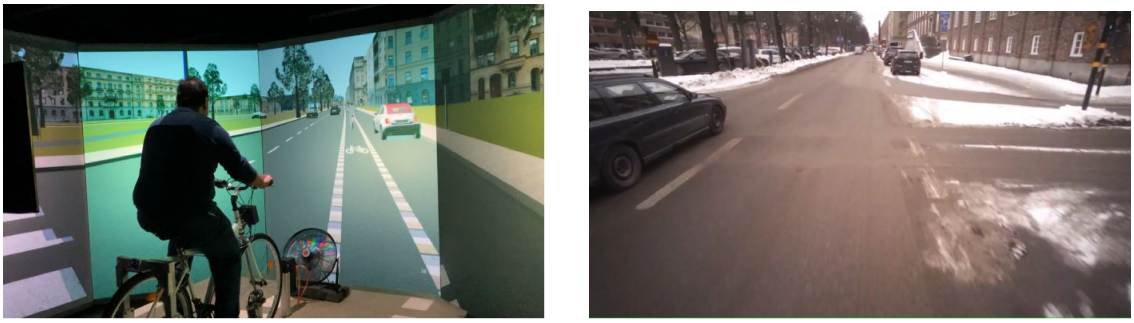

Figure 4.22. A scene from zone 2 of the experimental route in both the simulator and Stockholm.

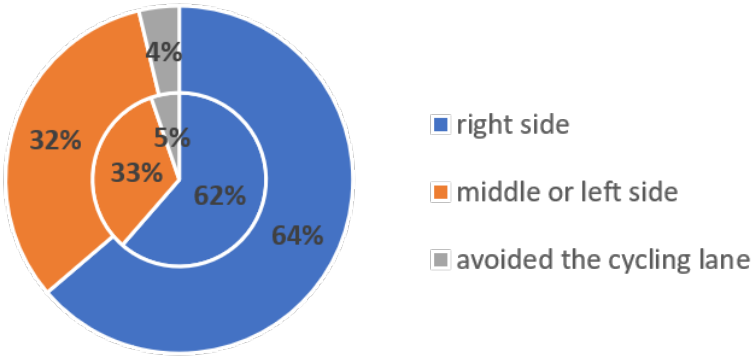

Figure 4.23. Comparison between the behavior of cyclists when encountering a two-way cycling path; the inner results represent the on-road experiment and the outer represents the simulation.

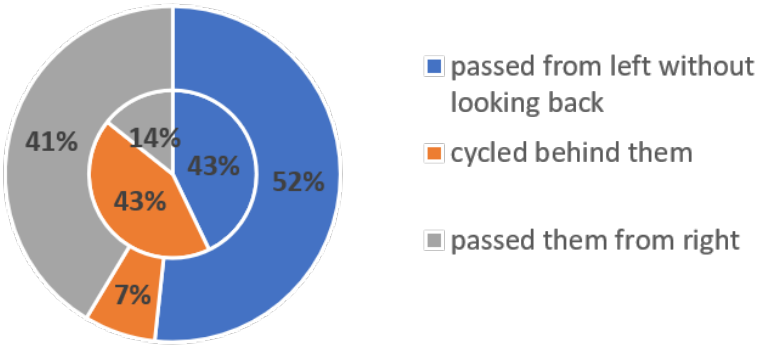

Figure 4.24. Comparison between the behaviour of passing another cyclists in zone 2; the inner results represent the on-road experiment and the outer represents the simulation.

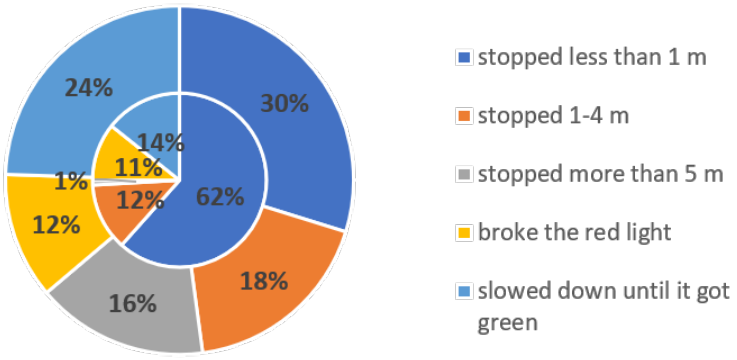

Figure 4.25. The reaction of cyclists when they encounter red traffic light; the inner results represent the on-road experiment and the outer represents the simulation.

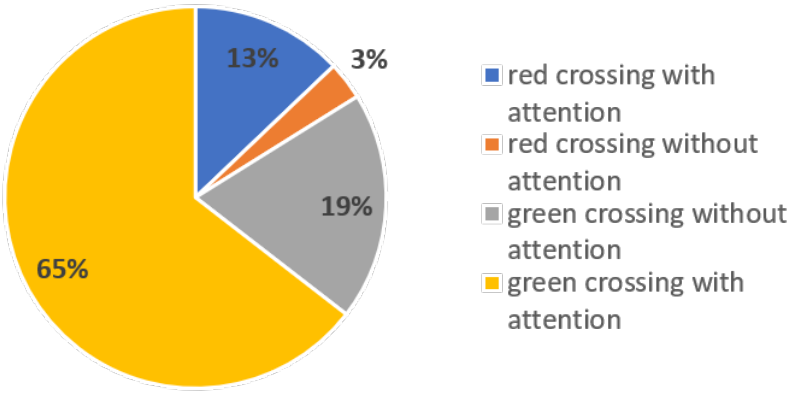

Figure 4.26. U-turn crossing behavior between zone 2 and 3; the inner results represent the on-road experiment and the outer represents the simulation.

When encountering a red traffic light, the results in Fig. 4.25 show that in 12% of the cases on the simulator and 25% on the instrumented bicycle the participants broke the red traffic light. When the cyclists needed to make a U-turn between zone 2 and 3, with the existence of traffic signal, the results in Fig. 4.26 show that (65%) the participants crossed the street while the traffic light was green for the vehicle-this means it is red for users crossing the street, which is considered a wrong behavior, even though they checked for passing vehicles before crossing; only 16% of them crossed when the traffic right was red for the vehicles.

Studying the interaction of cyclists with road-users crossing the street, the results in Fig. 4.27 show in 10% of the cases on the simulator and 4% on-road the cyclists stopped when realizing the pedestrians were waiting to cross ,in one case, on the simulator, the participant collided with the wheelchair user that was crossing the street.

In zone 3, where the cycling path is shared with pedestrians, 7% of the cyclists on the simulator and 28% on-road passed the pedestrians from left (Fig. 4.28), 14% and 67% of them were switching between passing from right or left, and in 79% and 5% they passed always from the right side. The high percentage for passing from the right side on the simulator could be explained by the empty space to the right and the absence of snow there.

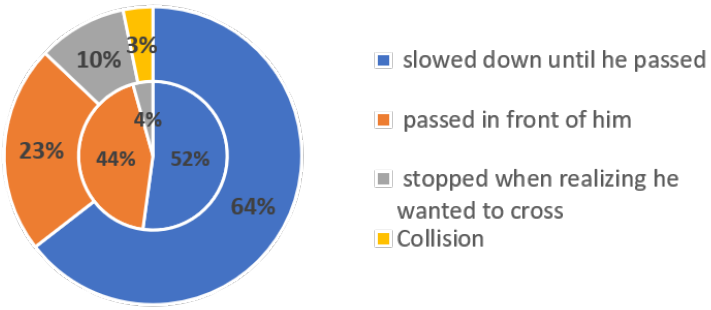

Figure 4.27. The reaction of cyclists to a wheelchair crossing the street in zone 2 on the simulator; the inner results represent the on-road experiment and the outer represents the simulation.

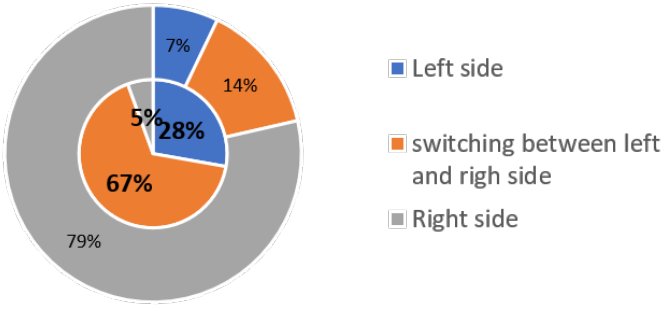

Figure 4.28. The interaction of cyclists with pedestrians in the traffic-free area in zone 3; the inner results represent the on-road experiment and the outer represents the simulation.

Table 4.1 Descriptive characteristics of the study group (means ± SD or N %)

Descriptive charactaristic of the study group, means ± SD or N %)			
Characteristic	Male	Female	Total
N	19 (61%)	12 (39%)	31
Age (yrs)	33.8 (±12.8)	28 (±13)	31.6 (±13.1)
Wight (kg)	77.3 (±13.7)	59.6 (±12.2)	70.5 (±15.6)
Cycling experience (yrs)	17.6 (±13.7)	18.1 (±15.3)	17.8 (±14.1)
Cycling frequency (trips/week)	1.6 (±2.6)	1.4(±2.3)	1.5 (±2.4)
Cyling distance (km/week)	20.6 (±40.2)	12.5 (±28.6)	17.6 (±35.9)
Waering lenses/glasses	13 (68%)	5 (41.6%)	18 (58%)
Previous usage of bicycle simulator	2 (10.5%)	3 (25%)	5 (16%)
Motion sickness	7 (36.8%)	5 (41.6%)	12 (38.7%)
Realism of the simulator	6.4 (±2.1)	6.5 (±1.6)	6.45 (±1.9)

4.5 comparison between The Subjective Evaluation of Cycling Safety and Comfort

After the end of the experiment, the participants filled a questionnaire about personal general information, their cycling experience and their evaluation of cycling safety and comfort during the experiment. They were handled a map showing the different zones of the experiment in order to help them to answer the questionnaire properly; Table 4.1 summarizes the general data collected by the participants and some of there responses about the risks facing them while cycling.

The results show that 5 of the participants had participated in a previous experiment using the same bicycle simulator. 12 of them declared sensitivity to motion sickness. On evaluating the realism of the simulator (compared to riding a real bicycle) the participants rating ranges between 3 and 10 on scale of 10 (mean=6.45, SD=1.9). Answering a question about the most realistic aspects of the simulator, they mentioned: the physical effort of cycling, the design of the virtual environment and traffic, the vibrations and the feeling of wind. However, some of the participants mentioned other aspects that need

improving, such as: the effect of the body posture when turning, the sound effects and the braking (the simulator takes more distance to stop than in reality).

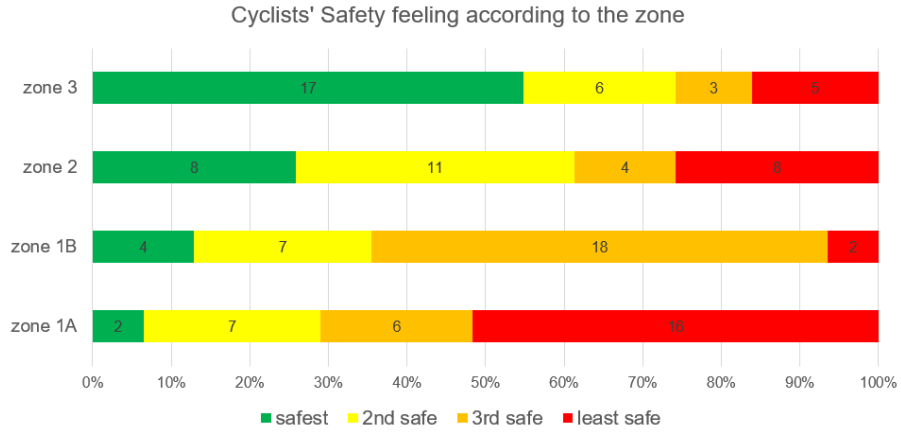

Figure 4.29. The participants' safety evaluation for the different zones of the experiment route.

Fig. (4.29) shows the response of all the participants about their safety evaluation of each zone along the experiment route on the simulator; it is noticed that 17 participants (55%) chose the 3rd zone as safest compared to 13 participants (59%) for the on-road experiment, they explained their choice by the absence of passing vehicles,and the separation from the carriage way. On contrary, 16% ranked the same zone as the least safe compared to (23%) in the on-road experiment, they explained this by the existence of pedestrians and their unexpected behavior. 16 participants (52%) chose zone 1A as the least safe due to the absence of separate cycling lane and cycling alongside traffic, whereas 12 participants (55%) chose zone 2 as the least safe in the on-road experiment, this is mainly because its existence on the carriage way without a physical barrier with the passing traffic.

Fig. 4.30 compares between the feeling of power consumption on the simulator and on the road experiment, 13 participant (42%) felt no-difference in power consumption between the different zones, this could be explained by the absence of slopes that exists in reality. 22% felt that they consumed more power in zone 3, because they were faster in this zone and they did not stop for long time. In the on-road experiment, 17 participants (77%) chose zone 1B as the most power demanding.

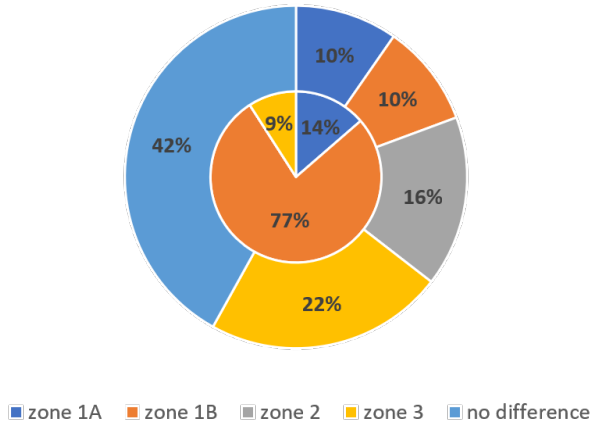

Figure 4.30. The power consumption evaluation between zones.

Fig. 4.31 summarizes the results of NASA TLX questionnaire for the 31 participants, we can notice that the simulation has moderate load index, which can be explained by the effort required to ride the bicycle and the need for concentration to navigate through the traffic and interacting with other road-users.

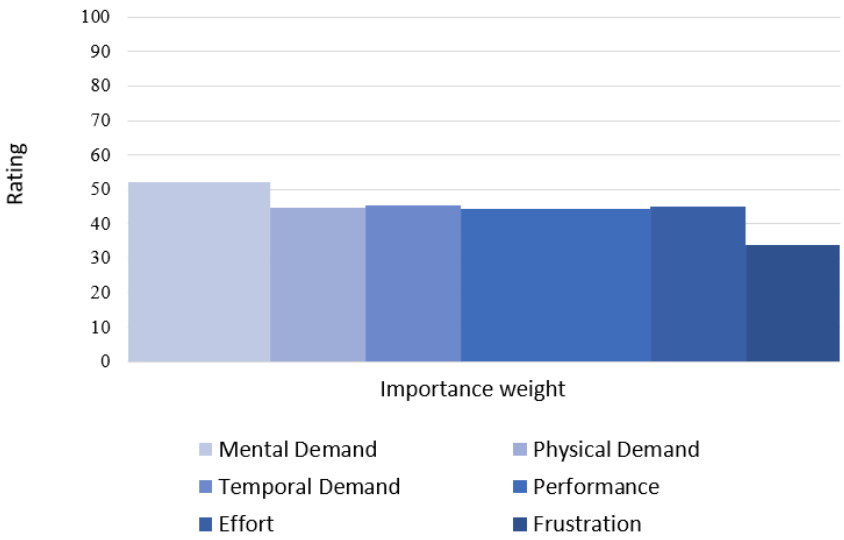

Figure 4.31. Weighted ratings of Nasa Task Load (TLX), the width of each column represents the importance weight of each factor.

The analysis of the simulator sickness questionnaire listed in Table 2.5 shows that the average total severity for all participants is 36.4. By comparing this result to the possible scores listed in Table 4.2, we see that the total severity of the simulator is slight (less

than 78.5). The results show that 4 participants (13 %) reported no symptoms from their exposure to the simulator, 23 participants (74%) reported slight symptoms (less than 78.5) and 4 participants (13%) reported medium symptoms of simulator sickness, and no-one reported severe symptoms.

Table 4.2 Mean scores observed in each item of the simulator sickness questionnaire during the experiment.

	Nausea	Oculomotor	Disorientation	Total Severity
mean	30.2	25.0	45.5	36.4
SD	27.7	24.9	51.9	34.3
min	0.0	0.0	0.0	0.0
max	95.4	106.1	222.7	149.6

4.6 Conclusion

In this chapter, the experimental data of both the instrumented bicycle and the bicycle simulator was studied and analyzed. The results revealed the similarities and differences between both experiments; for example, the comparison between speed profiles of all participants shows that the virtual velocity of the bicycle simulator is 10% lower than cycling in real conditions when the surface is dry/wet; this difference increases to 15% faster than cycling on snowy/icy surface. The results also show that the average power consumed on the simulator is lower by 52% comparing to snowy/icy and by 52% when comparing to dry/wet surface conditions. The subjective evaluation of safety for different traffic zones shows quite similar results: 59% of cyclists in reality chose zone 3, while in simulation 55% of them chose the same zone. The comparison between the 6 DoF in both experiments shows that the following outputs are highly correlated: Lateral and longitudinal accelerations, roll, pitch and yaw rates, on contrary it is noticed that the

vertical acceleration is uncorrelated, this could be explained by the high noise affecting the sensor and the absence of the slopes on the simulator.

The comparison between the cyclists' behavior and interaction with the infrastructure and other road users shows a significant correlation between both, for example, following the cycling lane, pedestrian passing behavior and the reaction to road users crossing the street, however, it is noticed that some behaviours are different, for example, the lane departure in zone 2, in the on-road experiment, most of the cyclists left the cycling lane due to the accumulation in snow, whereas on the simulator all followed the cycling lane, this is explained by the absence of the snow on the virtual reality.

These results leads to the behavioral validity of the following aspects of the bicycle simulator: Speeding behavior, interaction with pedestrians, interaction with traffic lights, cyclists passing behavior, crossing behavior and following the directional signs, however, some aspects could not be compared due to the limitation on the bicycle simulator, particularly in simulating snow, and bus passing behavior.

CHAPTER 5. THE SPECIAL NEEDS OF ELDERLY AND WHEELCHAIR-USERS AND THEIR INTERACTION WITH OTHER ROAD USERS

5.1 Introduction

Mobility, as well as the observation and comprehension of information about the urban environment, are more difficult for people with physical, mental, or sensory disabilities, wheelchair users, and people with vision impairment. The EU members committed, as a part of the convention on the United Nations Rights of Persons with Disabilities (CRPD), to improve the situation of people with disabilities: socially and economically which includes improving the mobility and accessibility of transportation networks [119]. To accomplish this, the metropolitan road network must be altered to accommodate the particular demands of the disabled and aged. These requirements vary depending on the disability type; for example, wheelchair users require wide sidewalks with plenty of space; smooth, durable, and non-slippery pavement in both dry and wet circumstances; and well-designed ramps.

As a part of the EU commitment, this chapter of the research focuses on studying the mobility needs of people with disabilities, including their perception of the different features of geometric design of the road, the share of the sidewalk with other road users and the detection and interaction with cyclists. In addition, the hypothesis of sharing cycling infrastructure with wheelchair-users is also investigated. The chapter is structured as follows: the second part is devoted to the analysis of a survey about the challenges facing people with disabilities when interacting with cyclists; the third part describes the experimentation conducted using wheelchairs and bicycles in order to compare between their speed and behaviour; and finally the conclusion.

5.2 The perception of cyclists by disabled and elderly

A questionnaire was published on the website of Fundacion ONCE [120] targeting people with disabilities or movement difficulties. The main goals of this survey are: analysing disabled and elderly users' mobility needs in order to include their behaviour in driving systems; analysing the influence of the road surface characteristics and geometric design on safety and behaviour of disabled road users; and studying the interaction between cyclists and disabled and elderly. The questionnaire consisted of questions related to personal general information such as: age, gender and type of disability; the experience and challenges facing them as a road-users; and the interaction with cyclists and road infrastructure.

165 people responded to the questionnaire: 92 (55.8%) of them were males and 73 (44.2%) were females; 3 of them were children (less than 14), 3 youth (15-24), 146 adults (25-64) and 12 seniors (more than 65). 42 (25.5%) of them said that the sidewalk is not shared with bicycles in their cities, whereas, 123 (74.5%) confirmed that the sidewalk is shared with bicycles. Fig. 5.1 shows the different groups of people who responded to the questionnaire.

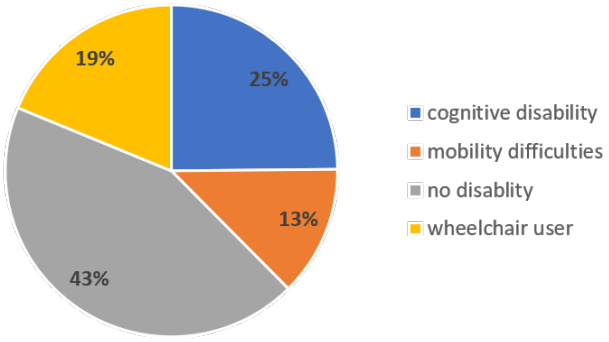

Figure 5.1. The classification of people who responded to the questionnaire.

The analysis of the questionnaire shows that 76.4% of respondents do not feel safe when sharing the sidewalk with cyclists, because of cyclists' speeding and invasion of the limited space of the sidewalk; 77.6% said that cyclists ride their bicycles very fast on

the sidewalk and 61.6% said they have difficulties detecting bicycles circulating in their path including lack of viability and trouble hearing them.

Responding to a question about their reaction to cyclists crossing their way, 83% said they choose to stop until the cyclist passes, 7.3% said they continue their way hoping the cyclist stops, 4.2% said it depends on the condition and the passing priority and the rest did not give a clear answer. In regards to their opinion about the right time for the cyclists to stop, 90% responded that they should stop when realizing there is a person with a special need intending to cross, whereas 10% responded that they should stop when the person with special need starts crossing.

40.6% of the respondents said they experienced risky situations interacting with cyclists, in 20 cases (12%) an accident occurred leading to falling and causing bruises, one respondent suffering from visual impairment wrote: ”Despite having a bike path, they go on the sidewalk and they often complain that I don’t move away. Once they confronted me, they tried to attack me and my guide dog”. About the most appropriate place for cycling, 79.9% of the respondents suggested it should be on a separate cycling lane on street level, whereas 10.4% said the cycling lane should be on sidewalk level, the rest were neutral.

5.3 Interaction between wheelchair-users and cyclists

32 wheelchair-users responded to the questionnaire, including 17 male, between 5 and 64 years old, and 15 females, between 11 and 63 years old, the group included 2 children (less than 14) and 30 adults (25-64). 22 of them use manual wheelchairs and 10 use electric wheelchairs. The results of the questionnaire show that 24 respondents (75%) feels unsafe when sharing the sidewalk with cyclists, and only 25% feel safe. The respondents mentioned that they face some difficulties while driving on sidewalks including: high curbs with the absence of ramps, insufficient width, poor condition asphalt, steep ramps, conflict with pedestrians, architectural barriers, tree roots, unevenness of the road surface, lack of signals, and other obstacles like garbage bins, traffic signs, bushes and

advertisement banners, besides the low awareness of other road users and misbehavior like speeding and stopping, 25 (78%) said that the sidewalk is not well shared with other road users. A wheelchair user commented: ”the small wheels of the wheelchair get stuck sometimes, I use the cycling lanes when there is few bicycles but the wheelchair is wider then the bicycle. If the sidewalk is crowded some people cant see you, and possibly crash you, when the sidewalk is narrow, I use the street despite that it is dangerous.”

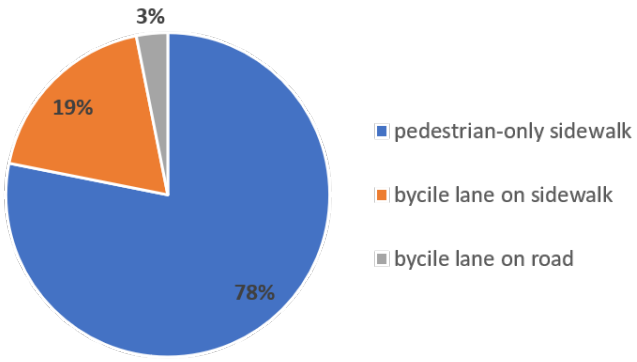

Figure 5.2. The response of the wheelchair-users about the most appropriate lane to drive the wheelchair.

About the detection of cyclists using the sidewalk, 15 respondents (47%) said they have difficulty to detect bicycles, especially when they come from behind, it becomes hard to hear them.

In regards to their estimation of the wheelchair speed, manual wheelchair-users estimated their average speed between 1 and 6 km/h (the average for all is 4.36 km/h), whereas, the electric wheelchair-users estimated their average speed between 4 and 10 km/h (the average for all is 6.43 km/h), and their maximum speed between 10 and 15km/h.

Fig. 5.2 shows the choice of the wheelchair-users regarding the most appropriate lane to drive their wheelchair, the results show that 78% of them prefer to drive their wheelchair on pedestrians-only sidewalk without sharing it with cyclists, they justify this choice by safety feeling as there is no other speeding cyclists, 19% chose a separate cycling lane on the same level of the sidewalk, they justified their choice as the pavement

is more homogeneous, better ramps when joining the street at intersections, and there is no direct interference with vehicles as they drive on different levels.

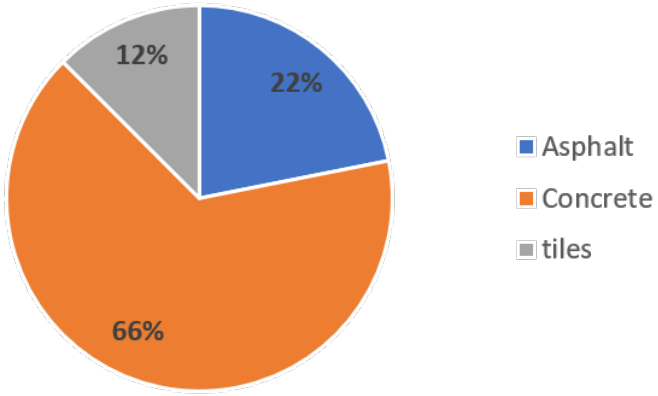

Figure 5.3. The most comfortable surface to move on according to wheelchair-users.

Fig. 5.3 shows the choice of wheelchair-users for the most comfortable surface to drive on. The results show that 66% chose concrete pavement, as it has good grip, smoother surface, fewer joints and less bumps and puddles comparing to asphalt or tiled surfaces. These results correlate with a study by Fundacion ONCE shows that increased ground roughness, such as cobblestone pavement or tiles, cause dizziness and back pain for wheelchair-users when moving on them for a long time [121].

5.4 Case study: the use of wheelchair-users of cycling infrastructure

Comparing to other road users, wheelchair-users need more space, evener and flatter surface, lowered footpaths and barrier-free ways [121]. The universal dimensions of the wheelchair are 1.35*1.35 m [122]. The goals of this case study are: analysing the wheelchair-users' behaviour when using a separate cycling lane on the sidewalk level; analysing the road characteristics and their influence on safety and behaviour of road users; and studying the interaction between cyclists and wheelchair-users. Expected results will help to improve the infrastructure in terms of accessibility, safety and comfort of road users.

5.4.1 Experimental Procedure

Two cyclists (males age 24 and 47 years old) and 5 wheelchair-users (4 males and one female) participated in the experiment. One of them repeated the experiment twice, in Alcala and Madrid. Their age range between 33 and 50 years old. 4 of them mentioned that they use the electric wheelchair all the time, 2 said they use it only for shopping or going for a walk. They have been using the wheelchair between 8 and 28 years on daily basis. Their weekly travel distance ranges between 15 and 40 km (mean=29 km, SD=10.8). Three of them estimated their average speed to be 10 km/h, one 4 km/h and one 7 km/h. The average maximum speed for all wheelchairs is 18.25 km/h; one wheelchair has a maximum speed of 30 km/h. Two of the participants said that they normally drive their wheelchair on the sidewalk, whereas three of them drive on cycling lane when there is enough space.

The experiment took place in two locations: the first one in Alcala where two experimental sessions were conducted on a two-way two-lane cycling path that has a length of 2.8 km, and the second one in Madrid with 2.83 km length, the route started at Plaza de Frencisco Morano and ended at Fundacion ONCE headquarter. 4 experimental sessions were conducted, the route was divided into two zones: zone 1 composed of a two-way two-lane cycling path separated by a physical barrier from other traffic, and has 2 km length (until point C on Fig. 5.4), and zone 2 composed of a sidewalk where the wheelchair dives alongside pedestrians for around 0.8 km. The detailed instructions concerning the experiment procedure were provided verbally during the test by the responsible people. The participants have to follow the predetermined route using GPS. The participants were provided with Edge 130 plus device from Garmin to record their speed and trajectory, and a sport camera was fixed on a helmet to record the experiment as shown in Fig. 5.5. An interceptor was standing near point C (the end of zone 1) and stopping passing cyclists and scooter users and asking them about their perception of the wheelchairs driving on the cycling infrastructure.

Figure 5.4. Experimental route in Madrid.

After the driving phase, the participants answered a questionnaire related to personal general information and their experience during the experiment and evaluation of the interaction with cyclists.

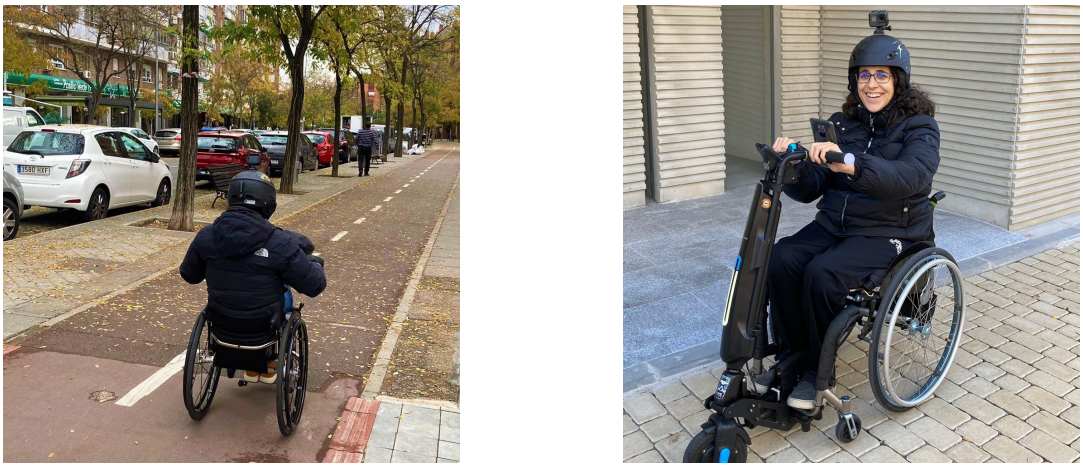

Figure 5.5. Two of participants wearing a helmet with a camera and holding a mobile to follow the experimental route.

5.4.2 Speed analysis of wheelchair and comparison with cyclists

Fig. 5.6 shows the speed profile for a wheelchair and a bicycle on the same experimental route. It is noticed that the cyclist speed is higher than the wheelchair user, even though acceleration and braking behavior match at some points along the route.

Fig. 5.7 shows the average speed, the average moving speed and the maximum speed for all participants including cyclists, we can notice that the average normalized speed for

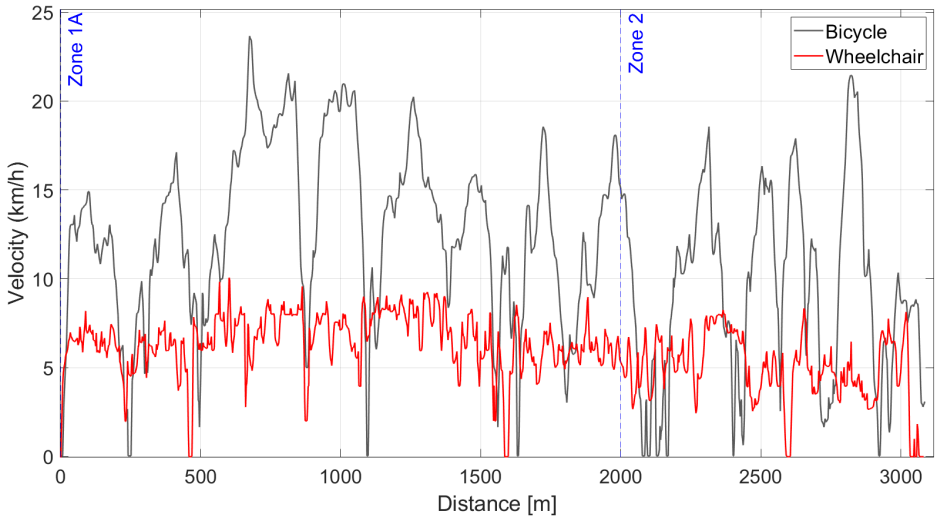

Figure 5.6. Comparison between the speed profiles of a wheelchair and a bicycle.

all wheelchairs (9.64 km/h) is less than for cyclists (13.15 km/h), however, the wheelchair speed is still higher than pedestrians' who have an average walking speed of 4.32 km/h [123].

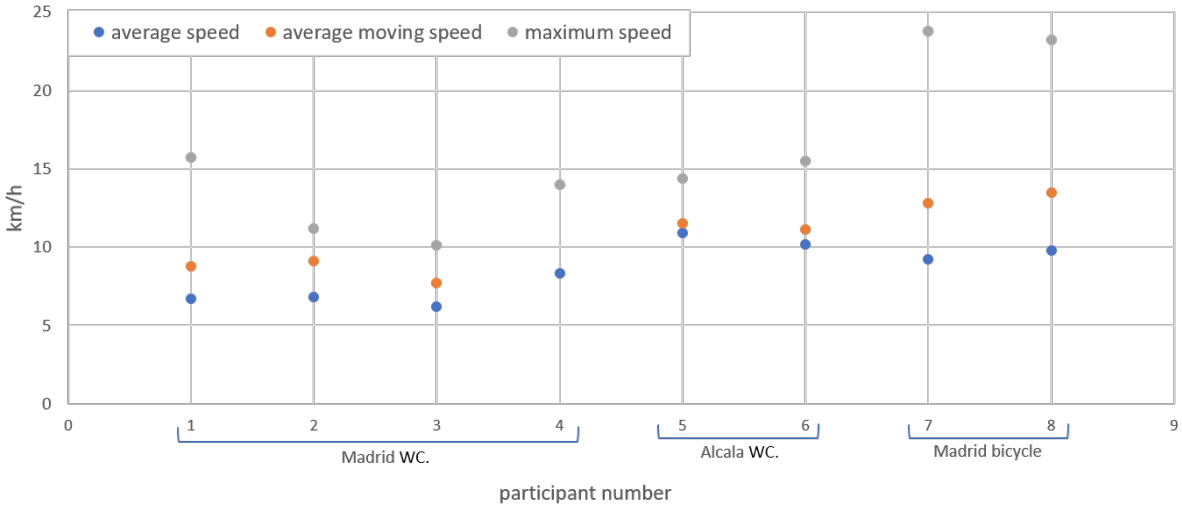

Figure 5.7. The average speed, average moving speed and maximum speed for all cyclists and wheelchair-users who participated in the experiment.

5.4.3 Analysis of the post experiment questionnaire

The analysis of the post experiment questionnaire shows the evaluation of wheelchair-users of the driving experience on cycling lane; 4 of them mentioned that they have a positive experience and general comfort, whereas one rated his experience as negative; all of them agreed it is useful to use the cycling lane, as it is safer, faster and more comfortable with less conflict points. In regards to their safety feeling, 3 participants said it is safer to use cycling lane, whereas 2 said they felt the same driving on cycling lane or on sidewalk. One participant felt unsafe because there were parked cars on the cycling lane and he had to drive beside cars. In regards to the width of the cycling lane, 3 participants thought that the space on cycling lane is not sufficient for their wheelchairs, whereas 2 thought it is sufficient. All of them agreed they drove faster on cycling lane, because the surface is smoother, has less conflict with pedestrians and less obstacles on the way; one participant commented: 'Accessibility on cycling lane is better because the pavement is even and it is respected by all pedestrians so the wheelchair can go faster'.

About the interaction with passing cyclists, 4 participants mentioned that a cyclist passed them during the experiment. In 2 cases the wheelchair-user noticed the cyclist before he started passing him as he rang the bell before passing, whereas in 4 cases the participants noticed the cyclists only when he started passing. When the cyclists used the ring, the wheelchair-users tried to slide right to allow more space for the cyclists.

Regarding their evaluation of road geometric design and surface condition, they all agreed that the pavement condition of cycling lane is better than the sidewalk. They mentioned as difficulties encountered them during the experiment: sharp curves, unevenness of the road, damage of road surface and water channels. these obstacles forced them to slow down and made them feel uncomfortable. One participants recommended: 'I would like to see cycling lanes shared with wheelchairs in all cities, because this allows wheelchair-users to go faster and safer.'

5.4.4 Cyclists' perception of wheelchair and the interaction with infrastructure and other road users

At the end of zone 1 of the experimental route, eight cyclists and one scooter were intercepted to answer some questions about passing the wheelchair-users. All were males between 24 and 47 years. Seven of them (78%) said there is enough space to share the cycling with wheelchairs, where as 2 (22%) said the space is insufficient. Seven of them said they did not use the ring bell when passing, one cyclist explained: 'when I use the ring, people get scared and less predictable, so I prefer to pass them without using it'. Four of them reduced the speed when passing, whereas the rest did not do anything different than passing any other bicycle.

The videos of both: wheelchair-users and cyclists were collected and analyzed. The following points summarizes the behavior of wheelchair-users and cyclists and their interaction with the infrastructure and other road users:

In zone 1:

- The wheelchair-users drove on the right side of the cycling lane for the most of the time, but when they noticed the absence of other users, they drove on the left side or the middle.
- On traffic signals, the pedestrians blocked their way when crossing the street forcing them to slow down or change their trajectory.
- On sharp curves, especially near the intersections where the degree of curvature is around 90, the wheelchair-users depart their lane to the opposite one. On the other side, cyclists left their cycling lane more often on less sharp curves.
- Wheelchairs significantly slowed down when encountering ramps, pavement damage or obstacles, whereas cyclists slightly slowed down and in some cases they did not slow down at all.

- Wheelchair-users passed all pedestrians who were walking in the same direction, in case a pedestrian blocks the way of a wheelchair-user, he slowed down and passed the pedestrian from the left, except in one case where the wheelchair passed from the right as the pedestrian was blocking the way.
- When pedestrians cross in front of the wheelchair, some of them stopped allowing the wheelchair-user to pass, but in other cases the wheelchair slowed down allowing them to pass, in one situation a wheelchair user spoke to crossing pedestrians warning them to keep attention (there was not a cross-line), and he continued his way without slowing down putting them in risk.
- In ALcala, one wheelchair-user, who is familiar with the experimental route, took a short cut and left the cycling lane and rejoined after crossing the street.
- All cyclists passed the wheelchair-users smoothly without even slowing down, in one case, a wheelchair user passed a stopping cyclist on the cycling lane without confusion or speed reduction.

In zone 2:

- The wheelchair-users drove on the right side of the sidewalk, when passing pedestrians, they slowed down and passed them from the left unless a pedestrian was walking on the left side they passed him from right.
- On narrow sidewalks, where there is only space for the wheelchair, the wheelchair-users slowed down and drove behind pedestrians until they got a chance to pass, in some cases the pedestrians noticed and cleared the route for them. One wheelchair user left the sidewalk and drove on on-street cycling lane (without separation with other vehicles) putting himself in conflict with other vehicles.

The analysis of these results shows that there are similar behaviors between cyclists and wheelchair-users when sharing the cycling infrastructure; for example, both road-users expect smooth surfaces and well designed ramps to made their commuting faster

and more comfortable; both are affected by the improper geometric design of the road, which force them to depart the lane on sharp curves and took shortcuts to shorten the travelled distance. It is also noticed that wheelchair-users are more affected by the unevenness of the road profile, which force them to reduce their speed more often than cyclists.

5.5 Conclusion

This chapter presented an original study of the special needs for one of the most vulnerable road users: people with physical disabilities, cognitive disabilities, and elderly. Two methods were used: the first one is distributing an online questionnaire asking about their perception of cyclists and the challenges when interacting with them, and the second one is conducting an on-road case study including electric wheelchair-users and cyclists to compare between the two groups speed and behavior.

The results of the questionnaire show that people with disabilities feel threatened by cyclists who share the sidewalk with them; mainly because they have difficulty detecting them, as bicycles are silent vehicles. The respondents to the questionnaire suggested to make the sidewalk free of cyclists to avoid the conflict and improve safety.

Beside, an authentic case study was presented to check the hypothesis of sharing cycling lanes with electric wheelchair-users. The results show the positive response of the participants and the improvement of speed and safety feeling of wheelchair-users without disturbing other cyclists using the same path. This may lead to allow wheelchair-users to use cycling infrastructure under the condition that the width of the cycling lane should be sufficient to allow cyclists to pass when necessary. However, the number of the wheelchair users are insufficient to validate this conclusion,so it is recommended, for similar studies, to ask more wheelchair-users to participate to obtain more reliable and generalizable results.

CHAPTER 6. CONCLUSION

The thesis presented the improvements conducted on PICS-L bicycle simulator and the instrumentation of a city bicycle providing objective measures to evaluate cycling safety based on cyclist's behavior and the interaction with the road infrastructure and other road-users.

In the second chapter of the thesis, the improvement on PICS-L bicycle simulator is investigated. These improvements included: first, upgrading the vehicle dynamic model of the bicycle to have 6 DoF (longitudinal, lateral, vertical, Yaw, Pitch and Roll). The model's key benefits are its simplicity, compatibility with the bicycle simulator, and ability to be used on a real bicycle; second, simulating the wheel-road contact by installing three actuators to reproduce the vibrations caused by the unevenness of the road profile and replacing the plastic cylinder attached to the rear wheel with an asphalt specimen to better model the road adhesion, these improvements positively affect the immersion of cyclists in virtual reality and improved accelerating and braking behavior; and third, creating new virtual reality that better simulates the road geometric design and traffic conditions. The validity of the developed bicycle dynamic model was then studied experimentally on the immersive bicycle simulator at various speeds and scenarios. The model's inputs were recorded and logged in real time, including steering angle, pedaling, and braking. The effects of these inputs on vertical, lateral, and longitudinal forces, velocities, and displacements were observed. The proposed model gives more accurate estimates when compared to the previous SimTeam model. The compatibility of the lateral position with the trajectory and yaw angle, the noise removal when calculating yaw, pitch, and roll accelerations, the impact of the unevenness of the road profile on the vertical displacement and force, the effect of the steering angle on the side slip angle, lateral displacement, and yaw, and the effect of road adhesion on the longitudinal force all have improved. The bicycle simulator allowed us to put cyclists in a riding set-

ting and properly quantify their effective behavior while regulating the variables at play and eliminating the risks associated with a real-world situation. In the two case studies presented in this chapter, a total number of 46 cyclists participated in the experiments without having any significant side effect; the analysis of The Simulator Sickness Questionnaire (SSQ) shows that the simulator has slight severity. The analysis of The Nasa task Load Index (TLX) shows that cyclists consumed moderate effort during the cycling task, their evaluation of the realism of the simulator was 6.74/10, which is considered acceptable for this kind of low-budget simulator; this leads to the conclusion that the bicycle simulator is a safe tool for experimentation and valid to conduct more studies. The bicycle simulator's validity allows to study cyclists' behavior in dangerous situations and analyze their reactions and interactions with different features of the infrastructure such as, radius of curvature, intersections, lateral and longitudinal slopes.

Chapter 3 details the bicycle instrumentation and subsequent testing that took place in Stockholm. Multiple sensors were installed on the bicycle to measure its kinematic and dynamic features while accounting for all 6 DoF (longitudinal, lateral, vertical, Yaw, Pitch and Roll). The system's inputs were recorded and logged, including steering angle and pedaling cadence. The impact of theses inputs on the bicycle's speed, power, acceleration, and other outputs were analyzed; for example, the unevenness of the road surface has an effect on vertical and lateral acceleration, which can alter the stability of the bicycle and lead to loss of control, especially on a slippery surface conditions. The evaluation of cycling safety in snowy weather and surface conditions was investigated through a case study in the city of Stockholm, the instrumented bicycle was used to conduct an experiment with the aim to evaluate cycling safety and cyclist's behavior in cold weather conditions and on snowy surface. The experimentation results for all participants, the subsequent questionnaire, and the eye-tracker videos were analyzed. The findings indicated some of the dangers that cyclists face, particularly in winter weather; in many cases the accumulation of snow drove riders to leave their bicycle paths, placing them at risk of accident. It was also found that cyclists' risky behavior may put them and

other road users in danger; examples include breaking red lights, passing pedestrians on the right side, and crossing streets without paying enough attention. The analysis of the cyclists' safety feeling shows that the participants felt safer in zone 2 (where there is on-street separate cycling lane) despite the absence of any physical barriers between cycling lane and other vehicles. A direct link was observed between road surface characteristics and infrastructure geometric design and cyclists' behavior. The cyclists reaction to the infrastructure design was assessed in order to calculate the cycling risk indicator (RI) for each cyclist and classify their behavior as risky or safe. Different strategies are advocated to improve cycling behavior while engaging with infrastructure and other road-users, including: removing the accumulated snow from the cycling lanes, add physical barriers between cyclist and other traffic, separate cycling and pedestrian ways, and improves the communication with cyclists through vertical and horizontal traffic signs.

In order to validate the simulation outputs, they should be compared to the output of an on-road experiment. This was studied in chapter 4, where a comparison between the outputs of the on-road experiment in Stockholm and the mimic experiment on the simulator is presented. The experimental route of Stockholm was recreated into a virtual reality and used on the simulator, the results of this case study show that there are similarities and variances between the two experiment regarding the dynamical outputs and the cyclist's behaviour. The experimental data from both the instrumented bicycle and the bicycle simulator were studied and analyzed. The results revealed similarities and differences between the two experiments; for example, a comparison of all participants' speed profiles shows that when the surface is dry/wet, the virtual velocity of the bicycle simulator is 10% lower than cycling in real conditions; this difference increases to 15% faster when cycling on a snowy/icy surface. The results also demonstrate that the simulator's average power consumption is 52 % lower when compared to snowy/icy and 52 % lower when compared to dry/wet surface conditions. The findings of subjective safety assessments for various traffic zones are relatively similar: In reality, 59% of cyclists chose zone 3, while 55% chose the same zone in simulation. The follow-

ing outputs are highly correlated when the 6 DoF in both studies are compared: lateral and longitudinal accelerations, roll and yaw rates; whereas, pitch rate, cadence, power and the vertical acceleration are uncorrelated. The comparison of cyclists' behavior and interactions with infrastructure and other road0users reveals a significant correlation between both, for example, the participants behave the same when following the two-way cycling lane, pedestrian passing behavior, and reacting to road-users crossing the street; however, some behaviors are distinct, for example, the lane departure in zone 2, where most cyclists left the cycling lane in the on-road experiment due to the accumulation of snow, was not replicated in the simulation due to the absence of snow rendering in the virtual reality. These findings support the behavioral validity of the following aspects of the bicycle simulator: speeding, interaction with pedestrians, interaction with traffic lights, cyclists passing behavior, crossing behavior, and following directional signs. However, due to limitations in the bicycle simulator, some aspects could not be validated, particularly snow simulation and bus passing behavior.

A special attention should be given to the most vulnerable road users, as they represent a considerable percentage of any society. Chapter 5 focused on the mobility needs of disabled and elderly specifically when interacting with cyclists. A survey was distributed online including questions about the perception of cyclists in urban environment and the challenges facing people with special needs when interacting with them. The results of the questionnaire show that people with special needs feel unsafe when commuting near bicycles because they are undetectable and relatively fast, beside the reckless behavior of some cyclists. An on-road case study was conducted in Madrid to study the speed behavior of electric wheelchair-users and cyclists and to test the possibility to share cycling infrastructure with wheelchair-users, the results show that wheelchairs average speed is higher than pedestrians' average speed but 15% less than the bicycle, this leads to the conclusion that sharing cycling infrastructure with electric wheelchair-users is beneficial for the later in terms of speed and safety, and, on the other hand, does not negatively impact cyclists; however, the cycling infrastructure should be designed to allow the ac-

commodation of wheelchairs in terms of providing enough space to allow cyclists to pass wheelchairs comfortably and adapt the slops and ramps to facilitate the movement of the wheelchairs.

6.1 Perspectives

The work achieved during this research opened the door for further development and experimentation to study and improve cycling safety, the following points summarize the most important perspectives of this study:

- The dynamic model of the bicycle may be improved so that the simulation better match the on-road experimental outputs:
  - Identify the missing dynamic parameters of the bicycle, such as: stiffness and damping coefficient, through analyzing the outputs of the sensors on the instrumented bicycle, the calculated parameters could be then used as inputs for the bicycle mathematical model for better simulation of the outputs.
  - Include the effect of slopes in calculation of the vertical acceleration, by measuring the slopes of a real road and use it as an input for the vertical model.
  - The slopes were simulated in the virtual environment, but their physical impact on the pedaling effort was missing, this impact could be added or subtracted using the motor attached to the rear wheel.
  - Include the effect of cyclist's tilting on virtual trajectory of the bicycle simulator, this could be achieved by measuring the bicycle roll angle using an gyrometer and use it as an input for the mathematical model.
- The on-road experiment and the simulation were conducted by different groups of cyclists, which made it difficult to compare between their behavior, it would be interested in the future to conduct the simulation and the on-road experiment by the same group of cyclists and compare their behavior in both situation more accurately.

- The recommended safety measures and their impact on cycling behaviour could be investigated using the bicycle simulator. By comparing different scenarios and road geometric design, it would be possible to apply the best design on reality, the following scenarios could be tested:
  - The difference in behavior when drawing horizontal signs and markings on street and the absence of them and depending only on vertical signs.
  - The effect of the physical barrier between cycling lane and other vehicles on the trajectory and safety feeling of cyclists, this could be done by creating two virtual realities for the same route, one by adding physical barrier and one without it and accurately measures the inputs of cyclists and their trajectory and speeding behavior.
  - Testing different geometric design of intersection, to choose the best design to reduce the conflict points between different road users, for example, adding space between cycling and pedestrian crossings and use different styles of channeling at intersections.
- The bicycle simulator could be used to study the interaction with people with disabilities, for example, the detection of blind people using a directional dog or a white cane; this could be done by analyzing cyclists' gaze that could be recorded using an eye-tracker. The simulator could also be used to study the behavior of cyclists when encountering wheelchair-user commuting on cycling infrastructure, and evaluate the impact of the wheelchair on the behavior of cyclists; different geometric designs could tested by changing the lane width and adding horizontal signs to warn the cyclist of the existence of wheelchair-users.

Appendices

APPENDIX A. PARAMETERS OF THE BICYCLE

Appendix A shows the different dynamic and mechanical parameters of the bicycle used in the mathematical model of the simulator.

Parameter	symbol	unit	value
Wheelbase	w	m	1.101
Mass of bicycle + rider	m	kg	85
Center of gravity (bicycle+rider)	COG	m	x= 0.291 , z=-1.09
Distace from COG to the center of rear wheel	lr	m	0.293
Distace from COG to the center of front wheel	lf	m	0.808
the horezental distance between Gf and Gr	K	m	0.614
the frontal surface for the bike and the cyclist body	S	m^2	0.4
coefficient of aerodynamic resistance	Cax		0.824
Steer Axis tilt (caster angle)	Lambda or Epsilon	rad	0.367
trail	c	m	0.083
mass of the front part of the bike	mF	kg	23
Vertical tiffness	k	N/m	108000
Damping ratio	B	N.s/m	5448
Moment of inertia around x	IxGf	$kg.m^2$	0.387
Moment of inertia around z	IzGf	$kg.m^3$	0.167
Mass of the rear part of the bike	Mr	kg	62
Moment of inertia around x	IxGR	$kg.m^2$	11.96
Moment of inertia around z	IzGr	$kg.m^2$	3.105
Wheel radius	rF	m	0.35
Front tyre lateral stiffness	Cyf	N/m	490
front wheel moment of inertia around y axis	IFyy	$kg.m^3$	0.144

APPENDIX B. SIMULATOR SICKNESS QUESTIONNAIRE RESULTS

In this appendix B, simulator sickness questionnaire results are presented.

Table B.1 Simulator sickness results for all participants in the second case study.

Participant no.	Nausea	oculomotor	Disorientation	Total severity
1	9.54	22.74	13.92	18.7
2	9.54	22.74	55.68	29.92
3	0	7.58	0	3.74
4	0	0	13.92	3.74
5	0	0	13.92	3.74
6	9.54	15.16	0	11.22
7	19.08	7.58	13.92	14.96
8	19.08	7.58	0	11.22
9	9.54	15.16	0	11.22
10	38.16	30.32	41.76	41.14
11	0	0	0	0
12	0	0	0	0
13	9.54	30.32	27.84	26.18

14	19.08	22.74	0	18.7
15	9.54	7.58	0	7.48
16	19.08	7.58	0	11.22
17	0	0	0	0
18	0	15.16	13.92	11.22
19	0	22.74	0	11.22
20	9.54	37.9	13.92	26.18
21	0	0	0	0
22	0	0	0	0
23	0	7.58	0	3.74
24	9.54	15.16	0	11.22
25	0	0	0	0
26	0	7.58	13.92	7.48
27	9.54	0	0	3.74
28	28.62	15.16	27.84	26.18
29	57.24	37.9	41.76	52.36
30	28.62	37.9	41.76	41.14
31	0	7.58	0	3.74

32	19.08	15.16	0	14.96
33	9.54	30.32	41.76	29.92
34	0	7.58	0	3.74
35	9.54	30.32	41.76	29.92
36	38.16	30.32	27.84	37.4

APPENDIX C. SPEED, POWER AND CADENCE FOR THE ON-ROAD EXPERIMENT AND THE SIMULATION

Appendix C shows the complete analysis of speed, power and cadence for both: the on-road and simulator experiment.

Parameter		complete route			Zone 1A			Zone 1B			Zone 2			Zone 3		
		snow	dry	Simulator	snow	dry	Simulator	snow	dry	Simulator	snow	dry	Simulator	snow	dry	Simulator
Speed (km/h)	mean	9.95	12.1	12.29												
	SD	±2.06	±2.34	±3.21												
Moving speed (km/h)	mean	12.45	15.73	14.14	12.37	17.2	14.76	11.6	14.4	15.67	13	17	11.33	12	15.1	14.65
	SD	±2.52	±3.71	±2.69	±3.3	±3.28	±2.96	±2.9	±3.5	±3.57	±2.76	±4.5	±2.39	±2.7	±4.0	±2.83
Max speed (km/h)	mean	20.21	24.4	22.9												
	SD	±3.650	±5.60	±5.12												
Power (W)	mean	80	131	64.24												
	SD	±44.57	±61.6	±27.64												
Normalized power (W)	mean	121.4	187	64.24	122.8	161.4	66.62	177	228.3	76.67	126	199.1	60.42	143.5	194.8	61.79
	SD	±63.4	±86.8	±27.64	±58	±58.9	±31.07	±65.15	±90.6	±32.45	±53.1	±123.5	±28.73	±52.80	±101.030	±27.83
Max power (W)	mean	326.8	567.7	189.55												
	SD	±166.49	±384.62	±86.03												
Cadence (RPM)	mean	50.8	60	38.16	52.5	52.5	40.04	57.8	64.4	41.93	47.8	50.8	30.42	51.9	59.5	37.4
	SD	±16.66	±19.92	±8.93	±12.4	±12.4	±9.64	±13.75	±17.2	±9.59	±10.8	±21.70	±8.74	±11.1	±20.7	±9.05
Max cadence (RPM)	mean	88.4	99	61.13												
	SD	±30.1	±35.50	±11.92												

APPENDIX D. ROADRUNNER 3D SCENE

Appendix D shows the calculation of the safety indicator for all participants.

no.	gender	Age	unusing winter tires	foot slipping when stepping	cyling in narrow spaces	crossing in front or between pedestrains	lack of attention when crossing	breaking red light	speeding on sharp curves	unfollow cycling lane	passing buses without attention	passing pedestrians from right
1	Male	65	X	X								
2	Female	43	X									
3	Male	42										
4	Male	62		X								
5	Male	43				X	X	X		X		
6	Male	27	X	X	X	X	X	X				X
7	Male	22	X			X	X	X	X	X		X
8	Female	27			X	X	X	X				X
9	Male	26		X		X	X	X		X	X	X
10	Female	25	X			X	X	X		X		X
11	Male	43				X	X	X				
12	Female	58				X	X					
13	Male	26	X									X
14	Female	11			X	X	X				X	X
15	Female	28	X			X	X					X
16	Male	27	X	X		X	X		X	X		X
17	Female	28	X			X	X					X
18	Male	32	X	X		X	X		X	X		
19	Male	46			X	X	X		X			X
20	Male	40	X		X	X	X			X		
21	Female	39	X			X	X					
22	Male	30	X				X					

APPENDIX E. SAFETY INDICATOR FOR ALL PARTICIPANTS

Appendix E shows a screenshot of Roadrunner software interface. We can observe the 3D reproduction of the experiment route of the on-road experiment in Stockholm.

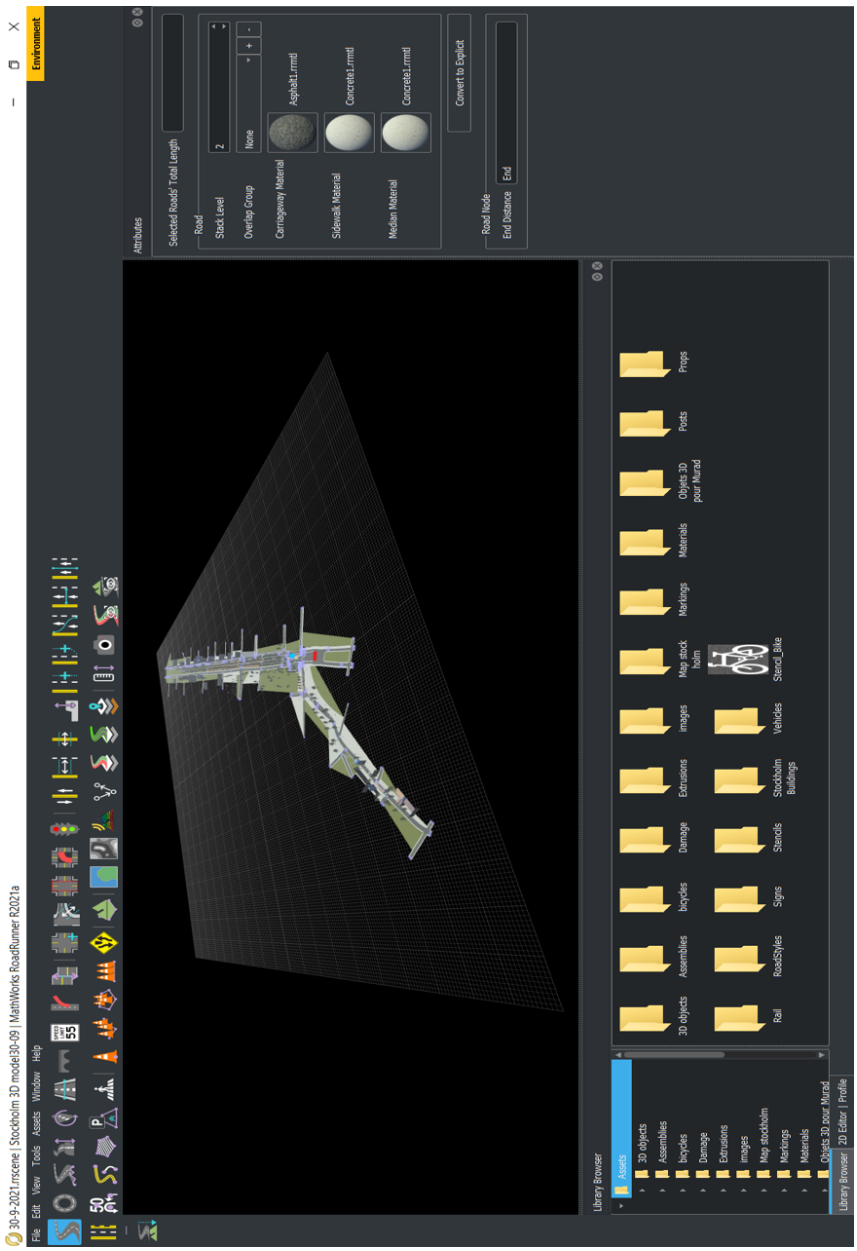

APPENDIX F. COMPARISON BETWEEN THE SIMULATOR AND THE ON-ROAD EXPERIMENTS SIGNALS

Appendix F shows the calculation of cycling risk indicator (RI) for all participants in the on-road experiment in Stockholm.

Signal		Mean	Standard deviation	Difference	Mean squared error	Correlation coefficient
Speed (m/s)	sim	3.364	1.5952	-0.3794	0.1955	0.83
	exp	3.2475	5.4796			
Cadence (RPM)	sim	19.3159	16.725	24.01	584.1516	0.4252
	exp	46.535	28.2807			
Power (watt)	sim	42.3055	25.9383	30.9297	5278.6	-0.2438
	exp	104.2256	79.713			
Stering angle (degree)	sim	-0.8554	7.2172	-2.1372	6.2444	0.8066
	exp	-5.0346	20.4			
Front long. Acc. (m/s^2)	sim	1.6146	4.3468	3.2707	14.4317	0.6753
	exp	0.5822	1.6778			
Rear long. Acc. (m/s^2)	sim	1.6146	4.3468	-1.0173	1.2547	-0.1841
	exp	-0.00016565	2.0499			
Fron lat. Acc. (m/s^2)	sim	-0.00053025	5.1115	-1.2331	1.8925	0.8304
	exp	8.9193E-05	2.1097			
Rear lat. Acc. (m/s^2)	sim	-0.00053025	5.1115	0.7009	1.9069	0.6
	exp	-3.3455E-06	1.1818			
Front vert. Acc. (m/s^2)	sim	0.0001569	7.9356	-1.8153	3.3298	0.0127
	exp	-0.00030777	5.1134			
Rear vert. Acc. (m/s^2)	sim	-0.00024865	4.7323	-0.06	0.0133	0.014
	exp	0.0000217	2.6382			
Roll rate (deg/s)	sim	-5.9376E-11	4.4289	-8.5011	97.5168	0.76
	exp	1.1649E-05	0.4478			
Yaw rate (deg/s)	sim	0.3984	5.8544	-2.2814	25.3711	0.8614
	exp	8.5842E-06	1.1095			
Pitch rate (deg/s)	sim	-0.0049	4.4289	0.824	18.477	0.4298
	exp	-0.00011058	0.4478			

REFERENCES

[1] Thomas Götschi, Jan Garrard, and Billie Giles-Corti. "Cycling as a part of daily life: a review of health perspectives". In: *Transport Reviews* 36.1 (2016), pp. 45–71.

[2] Elisabeth Raser et al. "European cyclists' travel behavior: differences and similarities between seven European (PASTA) cities". In: *Journal of Transport & Health* 9 (2018), pp. 244–252.

[3] Göran Smith, Jana Sochor, and MariAnne Karlssona. "Mobility as a Service: Implications for future mainstream public transport". In: (2017).

[4] John Pucher et al. "Walking and cycling in the United States, 2001–2009: evidence from the National Household Travel Surveys". In: *American journal of public health* 101.S1 (2011), S310–S317.

[5] Daniel Piatkowski and Melissa Bopp. "Increasing Bicycling for Transportation: A Systematic Review of the Literature". In: *Journal of Urban Planning and Development* 147.2 (2021), p. 04021019.

[6] Ralph Buehler and John Pucher. "Walking and cycling in Western Europe and the United States: trends, policies, and lessons". In: *Tr News* 280 (2012).

[7] John Pucher, Charles Komanoff, and Paul Schimek. "Bicycling renaissance in North America?: Recent trends and alternative policies to promote bicycling". In: *Transportation Research Part A: Policy and Practice* 33.7-8 (1999), pp. 625–654.

[8] Piet Rietveld and Vanessa Daniel. "Determinants of bicycle use: do municipal policies matter?" In: *Transportation Research Part A: Policy and Practice* 38.7 (2004), pp. 531–550.

[9] Birgitta Gatersleben and Katherine M Appleton. "Contemplating cycling to work: Attitudes and perceptions in different stages of change". In: *Transportation Research Part A: Policy and Practice* 41.4 (2007), pp. 302–312.

[10] John Parkin, Mark Wardman, and Matthew Page. "Estimation of the determinants of bicycle mode share for the journey to work using census data". In: *Transportation* 35.1 (2008), pp. 93–109.

[11] Phoebe Spencer et al. "The effect of environmental factors on bicycle commuters in Vermont: influences of a northern climate". In: *Journal of Transport Geography* 31 (2013), pp. 11–17.

[12] ILKKA M Vuori, PEKKA Oja, and OLAVI Paronen. “Physically active commuting to work–testing its potential for exercise promotion.” In: *Medicine and science in sports and exercise* 26.7 (1994), pp. 844–850.

[13] James P Byrnes, David C Miller, and William D Schafer. “Gender differences in risk taking: A meta-analysis.” In: *Psychological bulletin* 125.3 (1999), p. 367.

[14] Sandar Tin Tin, Alistair Woodward, and Shanthi Ameratunga. “Injuries to pedal cyclists on New Zealand roads, 1988-2007”. In: *BMC public health* 10.1 (2010), pp. 1–10.

[15] Nebiyou Y Tilahun, David M Levinson, and Kevin J Krizek. “Trails, lanes, or traffic: Valuing bicycle facilities with an adaptive stated preference survey”. In: *Transportation Research Part A: Policy and Practice* 41.4 (2007), pp. 287–301.

[16] David Ogilvie et al. “An applied ecological framework for evaluating infrastructure to promote walking and cycling: the iConnect study”. In: *American journal of public health* 101.3 (2011), pp. 473–481.

[17] John Pucher and Ralph Buehler. “Safer cycling through improved infrastructure”. In: *American Journal of Public Health* 106.12 (2016), pp. 2089–2091.

[18] Grégory Vandenbulcke et al. “Mapping bicycle use and the risk of accidents for commuters who cycle to work in Belgium”. In: *Transport Policy* 16.2 (2009), pp. 77–87.

[19] Zhibin Li et al. “Physical environments influencing bicyclists’ perception of comfort on separated and on-street bicycle facilities”. In: *Transportation Research Part D: Transport and Environment* 17.3 (2012), pp. 256–261.

[20] Luc Int Panis. “Cycling: health benefits and risks”. In: *Environmental health perspectives* 119.3 (2011), A114–A114.

[21] Lotte Jacobs et al. “Subclinical responses in healthy cyclists briefly exposed to traffic-related air pollution: an intervention study”. In: *Environmental Health* 9.1 (2010), pp. 1–8.

[22] Natalie Mueller et al. “Health impact assessment of cycling network expansions in European cities”. In: *Preventive medicine* 109 (2018), pp. 62–70.

[23] Angela Hull and Craig O’Holleran. “Bicycle infrastructure: can good design encourage cycling?” In: *Urban, Planning and Transport Research* 2.1 (2014), pp. 369–406.

[24] John Pucher, Jennifer Dill, and Susan Handy. “Infrastructure, programs, and policies to increase bicycling: an international review”. In: *Preventive medicine* 50 (2010), S106–S125.

[25] Peter G Furth. “Bicycling infrastructure for mass cycling: a trans-Atlantic comparison”. In: *City cycling* (2012), pp. 105–140.

[26] Giulio Dondi et al. “Effects of flickering seizures on road drivers and passengers”. In: *Procedia-social and behavioral sciences* 53 (2012), pp. 711–720.

[27] Alberto Bucchi, Cesare Sangiorgi, and Valeria Vignali. “Traffic psychology and driver behavior”. In: *Procedia-social and behavioral sciences* 53 (2012), pp. 972–979.

[28] Murad Shoman, Andrea Simone, and Valeria Vignali. “Looking behavior to vertical road signs on rural roads”. In: *MOJ Civil Eng* 4.2 (2018), pp. 75–79.

[29] World Health Organization et al. *Global status report on road safety 2018*. World Health Organization, 2018.

[30] Alexandre Santacreu and Pedro Homem de Gouveia. “Safer City Streets Global Benchmarking for Urban Road Safety”. In: *International Transport Forum Working Document, OECD Publishing, Paris*. 2018.

[31] World Health Organization. *Global status report on road safety 2015*. World Health Organization, 2015.

[32] Mohamed Mouloud Haddak. “Exposure-based road traffic fatality rates by mode of travel in France”. In: *Transportation research procedia* 14 (2016), pp. 2025–2034.

[33] S Reynolds et al. “Reported Road Casualties Great Britain: 2016 Annual Report”. In: *UK Department for Transport, Tech. Rep* (2017).

[34] Rikard Fredriksson, Klara Fredriksson, and Johan Strandroth. “Pre-crash motion and conditions of bicyclist-to-car crashes in Sweden”. In: *International Cycling Safety Conference*. 2014.

[35] “Road safety report, Sweden”. In: *International Transport Forum (ITF)*. OECD, 2020.

[36] John Pucher and Lewis Dijkstra. “Making walking and cycling safer. Lessons from Europe.” In: (2000).

[37] Rune Elvik. “The non-linearity of risk and the promotion of environmentally sustainable transport”. In: *Accident Analysis & Prevention* 41.4 (2009), pp. 849–855.

[38] International Transport Forum. *Cycling Safety Summary and Conclusions*. Organisation for Economic Co-operation and Development OCED, 2018.

[39] Melissa R Hoffman et al. “Bicycle commuter injury prevention: it is time to focus on the environment”. In: *Journal of Trauma and Acute Care Surgery* 69.5 (2010), pp. 1112–1119.

[40] Yasuhiro Matsui, Shoko Oikawa, and Masahito Hitosugi. “Features of fatal injuries in older cyclists in vehicle–bicycle accidents in Japan”. In: *Traffic Injury Prevention* 19.1 (2018), pp. 60–65.

[41] Shoko Oikawa et al. *Traffic accidents involving cyclists identifying causal factors using questionnaire survey, traffic accident data, and real-world observation*. Tech. rep. SAE Technical Paper, 2016.

[42] Observatoire national Interministériel de la sécurité routière. *La sécurité routière en France Bilan de l’accidentalité de l’année 2017*. Observatoire national Interministériel de la sécurité routière, 2017.

[43] Jean-Baptiste Richard, Bertrand Thélot, and François Beck. “Evolution of bicycle helmet use and its determinants in France: 2000–2010”. In: *Accident Analysis & Prevention* 60 (2013), pp. 113–120.

[44] Bas de Geus et al. “A prospective cohort study on minor accidents involving commuter cyclists in Belgium”. In: *Accident Analysis & Prevention* 45 (2012), pp. 683–693.

[45] Joon-Ki Kim et al. “Bicyclist injury severities in bicycle–motor vehicle accidents”. In: *Accident Analysis & Prevention* 39.2 (2007), pp. 238–251.

[46] CC Schoon, MJA Doumen, and D de Bruin. *The circumstances of blind spot crashes and short-and long-term measures: a crash analysis over the years 1997-2007, traffic observations, and surveys among cyclists and lorry drivers. Report and appendices.* Tech. rep. 2008.

[47] Peter L Jacobsen. “Safety in numbers: more walkers and bicyclists, safer walking and bicycling”. In: *Injury prevention* 21.4 (2015), pp. 271–275.

[48] Karl J Astrom, Richard E Klein, and Anders Lennartsson. “Bicycle dynamics and control: adapted bicycles for education and research”. In: *IEEE Control Systems Magazine* 25.4 (2005), pp. 26–47.

[49] J Lowell and HD McKell. “The stability of bicycles”. In: *American Journal of Physics* 50.12 (1982), pp. 1106–1112.

[50] Qichang He, Xiumin Fan, and Dengzhe Ma. “Full bicycle dynamic model for interactive bicycle simulator”. In: *Journal of Computing and Information Science in Engineering* 5.4 (2005), pp. 373–380.

[51] Uwe Kiencke and Lars Nielsen. *Automotive control systems: for engine, driveline, and vehicle*. 2000.

[52] Adam Owczarkowski et al. “Dynamic modeling and simulation of a bicycle stabilized by LQR control”. In: *2016 21st International Conference on Methods and Models in Automation and Robotics (MMAR)* (2016), pp. 907–911.

[53] Lamri Nehaoua. “Conception et réalisation d’une plateforme mécatronique dédiée à la simulation de conduite des véhicules deux-roues motorisés”. In: *2011 19th Mediterranean Conference on Control and Automation (MED)* (2008).

[54] Dong-Soo Kwon et al. “KAIST Interactive Bicycle Racing Simulator” The 2nd Version with Advanced”. In: *IEEE/RSJ International Conference on Intelligent Robots and Systems* (2002).

[55] Dong-Soo Kwon et al. “KAIST interactive bicycle simulator”. In: *Proceedings 2001 ICRA. IEEE International Conference on Robotics and Automation (Cat. No. 01CH37164)*. Vol. 3. IEEE. 2001, pp. 2313–2318.

[56] Ching-Kong Chen et al. “Study of interactive bike simulator in application of virtual reality”. In: *Journal of the Chinese society of mechanical engineers* 28.6 (2007), pp. 633–640.

[57] Pieter Vansteenkiste et al. “Cycling around a curve: the effect of cycling speed on steering and gaze behavior”. In: *PloS one* 9.7 (2014), e102792.

[58] Stéphane Caro and Silvia Bernardi. “The role of various sensory cues in self-speed perception: a bicycle riding simulator preliminary study”. In: *DSC 2015-Driving simulation conference*. 2015.

[59] Sabarish V Babu et al. “An immersive virtual peer for studying social influences on child cyclists’ road-crossing behavior”. In: *IEEE transactions on visualization and computer graphics* 17.1 (2011), pp. 14–25.

[60] Shahjahan Miah et al. “An innovative multi-sensor fusion algorithm to enhance positioning accuracy of an instrumented bicycle”. In: *IEEE Transactions on Intelligent Transportation Systems* 21.3 (2019), pp. 1145–1153.

[61] José L Escalona and Antonio M Recuero. “A bicycle model for education in multibody dynamics and real-time interactive simulation”. In: *Multibody System Dynamics* 27.3 (2012), pp. 383–402.

[62] José L Escalona, Adam Kłodowski, and Sergio Munoz. “Validation of multibody modeling and simulation using an instrumented bicycle: from the computer to the road”. In: *Multibody System Dynamics* 43.4 (2018), pp. 297–319.

[63] Hormoz Etemad et al. “Using an instrumented bicycle to help understand cyclists’ perception of risk”. In: *Road & Transport Research: A Journal of Australian and New Zealand Research and Practice* 25.3 (2016), pp. 75–78.

[64] Marco Dozza, Julia Werneke, and Andre Fernandez. “Piloting the naturalistic methodology on bicycles”. In: *Proceeding ot the st International Cycling Safety Conference, Helmond NL, Nov 7-8 2012*. 2012.

[65] Marco Dozza and Julia Werneke. “Introducing naturalistic cycling data: What factors influence bicyclists’ safety in the real world?” In: *Transportation research part F: traffic psychology and behaviour* 24 (2014), pp. 83–91.

[66] Marco Dozza, Giulio Francesco Bianchi Piccinini, and Julia Werneke. “Using naturalistic data to assess e-cyclist behavior”. In: *Transportation research part F: traffic psychology and behaviour* 41 (2016), pp. 217–226.

[67] Ian Walker. “Drivers overtaking bicyclists: Objective data on the effects of riding position, helmet use, vehicle type and apparent gender”. In: *Accident Analysis & Prevention* 39.2 (2007), pp. 417–425.

[68] Ian Walker, Ian Garrard, and Felicity Jowitt. “The influence of a bicycle commuter’s appearance on drivers’ overtaking proximities: An on-road test of bicyclist stereotypes, high-visibility clothing and safety aids in the United Kingdom”. In: *Accident Analysis & Prevention* 64 (2014), pp. 69–77.

[69] Kai-Hsiang Chuang et al. “The use of a quasi-naturalistic riding method to investigate bicyclists’ behaviors when motorists pass”. In: *Accident Analysis & Prevention* 56 (2013), pp. 32–41.

[70] MF Schuntermann. “The International Classification of Impairments, Disabilities and Handicaps (ICIDH)–results and problems.” In: *International Journal of Rehabilitation research. Internationale Zeitschrift fur Rehabilitationsforschung. Revue Internationale de Recherches de Readaptation* 19.1 (1996), pp. 1–11.

[71] Deborah Marks. “Models of disability”. In: *Disability and rehabilitation* 19.3 (1997), pp. 85–91.

[72] Gloria L Krahn. “WHO world report on disability: a review”. In: *Disability and health journal* 4.3 (2011), pp. 141–142.

[73] Henri-Jacques Stiker. *A history of disability*. University of Michigan Press, 2019.

[74] World Health Organization et al. “World report on hearing”. In: (2021).

[75] World Health Organization et al. “World report on vision”. In: (2019).

[76] World Health Organization and International Spinal Cord Society. *International perspectives on spinal cord injury*. World Health Organization, 2013.

[77] World Health Organization. *World health statistics 2008*. World Health Organization, 2008.

[78] Francois Routhier et al. “Mobility of wheelchair users: a proposed performance assessment framework”. In: *Disability and rehabilitation* 25.1 (2003), pp. 19–34.

[79] Lisa I Iezzoni et al. “Mobility problems and perceptions of disability by self-respondents and proxy respondents”. In: *Medical care* (2000), pp. 1051–1057.

[80] NM De Vries et al. “Effects of physical exercise therapy on mobility, physical functioning, physical activity and quality of life in community-dwelling older adults with impaired mobility, physical disability and/or multi-morbidity: a meta-analysis”. In: *Ageing research reviews* 11.1 (2012), pp. 136–149.

[81] Lotte Enkelaar et al. “A review of balance and gait capacities in relation to falls in persons with intellectual disability”. In: *Research in developmental disabilities* 33.1 (2012), pp. 291–306.

[82] Patricia Ladia Falta. “Barrier Free Design For Disabled Persons-Evaluation Framework For Assessing The Quality Of Accessibility In Public Buildings”. In: *Universite de Montreal, Faculty of Environmental Design, Montreal* (1982).

[83] Mukesh Prasad Agrawal and Atma Ram Gupta. “Smart stick for the blind and visually impaired people”. In: *2018 second international conference on inventive communication and computational technologies (ICICCT)*. IEEE. 2018, pp. 542–545.

[84] Rajani Suryakant Kolhe et al. “Smart Stick for The Blind and Visually Impaired People”. In: (2021).

[85] Helen Hoenig et al. “Activity restriction among wheelchair users”. In: *Journal of the American Geriatrics Society* 51.9 (2003), pp. 1244–1251.

[86] Raquel Velho et al. “The effect of transport accessibility on the social inclusion of wheelchair users: A mixed method analysis”. In: *Social Inclusion* 4.3 (2016), pp. 24–35.

[87] Miriam Ricci, Graham Parkhurst, and Juliet Jain. “Transport policy and social inclusion”. In: *Social Inclusion* 4.3 (2016), pp. 1–6.

[88] Stéphane Caro et al. “Conception d’un simulateur de vélo pour l’étude du comportement des cyclistes”. In: *Journées Transports–Déplacements (JTD) du Réseau Scientifique et Technique*. Lyon, France, June 2013.

[89] Stéphane Caro et al. “Un simulateur de Îlo pour de nouvelles recherches”. In: *Géri Vélo-IFSTTAR*. 2015, 29p.

[90] *SimTeam at Gustave Eiffel University*. `https://cosys.univ-gustave-eiffel.fr/plateformes-materielles/simulateurs-immersifs`.

[91] Manfred Burckhardt. *Fahrwerktechnik: Radschlupf-Regelsysteme: Reifenverhalten, Zeitablaeufe, Messung des Drehzustands der Raeder, Anti-Blockier-System (ABS), Theorie Hydraulikkreislaeufe, Antriebs-Schlupf-Regelung (ASR), Theorie Hydraulikkreislaeufe, elektronische Regeleinheiten, Leistungsgrenzen, ausgefuehrte Anti-Blockier-Systeme und Antriebs-Schlupf-Regelungen*. Vogel, 1993.

[92] SAID Mammar. “Contrôle latérale assisté et automatisé des véhicules: Approche par commandes robustes”. In: *Habilitaion à diriger la recherche, HDR de ltUniversité dtEvry’Val dtEssonne (Septembre 2002).(Cité page 117.)* (2001).

[93] Egbert Bakker, Hans B Pacejka, and Lars Lidner. “A new tire model with an application in vehicle dynamics studies”. In: *SAE transactions* (1989), pp. 101–113.

[94] Hans B Pacejka and Egbert Bakker. “The magic formula tyre model”. In: *Vehicle system dynamics* 21.S1 (1992), pp. 1–18.

[95] Jason K Moore et al. “A method for estimating physical properties of a combined bicycle and rider”. In: *ASME 2009 international design engineering technical conferences and computers and information in engineering conference*. American Society of Mechanical Engineers. 2009, pp. 2011–2020.

[96] Jason K Moore et al. “Accurate measurement of bicycle parameters”. In: *Proceedings, Bicycle and Motorcycle Dynamics 2010 Symposium on the Dynamics and Control of Single Track Vehicles, 20Ű22 October 2010, Delft, The Netherlands*. 2010.

[97] Vera E Bulsink et al. “The effect of tyre and rider properties on the stability of a bicycle”. In: *Advances in mechanical engineering* 7.12 (2015), p. 1687814015622596.

[98] Sandra G Hart. “NASA Task Load Index (TLX). Volume 1.0; Computerized Version”. In: (1986).

[99] Robert S Kennedy et al. “Simulator sickness questionnaire: An enhanced method for quantifying simulator sickness”. In: *The international journal of aviation psychology* 3.3 (1993), pp. 203–220.

[100] Robert C McLane and Walter W Wierwille. “The influence of motion and audio cues on driver performance in an automobile simulator”. In: *Human Factors* 17.5 (1975), pp. 488–501.

[101] Hocine Imine. “Observation d’états d’un véhicule pour l’estimation du profil dans les traces de roulement”. PhD thesis. Versailles-St Quentin en Yvelines, 2003.

[102] Hocine Imine et al. *Sliding mode based analysis and identification of vehicle dynamics*. Vol. 414. Springer Science & Business Media, 2011.

[103] Pierre-Marie Damon. “Estimation pour le développement de systèmes d’aide à la conduite des véhicules à deux-roues motorisés”. PhD thesis. 2018.

[104] Murad Shoman and Hocine Imine. “Modeling and Simulation of Bicycle Dynamics”. In: *TRA 2020, Transportation Research Arena*. TRA. 2020.

[105] Murad Shoman and Hocine Imine. “Bicycle Simulator Improvement and Validation”. In: *IEEE Access* 9 (2021), pp. 55063–55076.

[106] Murad Shoman and Hocine Imine. “Subjective Validity of Bicycle Simulators”. In: *Proceedingd, VEHICULAR 2020 : The Ninth International Conference on Advances in Vehicular Systems, Technologies and Applications, October 2020, Porto, Portugal*. 2020.

[107] Murad Shoman and Hocine Imine. “Bicycle instrumentation and analysis of the output signals”. In: *Journal of Advanced transportation* (2022).

[108] *The research institute of Sweden*. `https://www.ri.se/en/about-rise/about-rise`.

[109] *Royal Institute of Technology in Stockholm*. `https://www.kth.se/en/om`.

[110] Soufiane Boufous, Julie Hatfield, and Raphael Grzebieta. “The impact of environmental factors on cycling speed on shared paths”. In: *Accident Analysis & Prevention* 110 (2018), pp. 171–176.

[111] Ahmed El-Geneidy, Kevin J Krizek, and Michael Iacono. “Predicting bicycle travel speeds along different facilities using GPS data: A proof of concept model”. In: (2007).

[112] Andrew Short, Raphael Grzebieta, and Naomi Arndt. “Estimating bicyclist into pedestrian collision speed”. In: *International journal of crashworthiness* 12.2 (2007), pp. 127–135.

[113] Wesley E Marshall and Nicholas N Ferenchak. “Why cities with high bicycling rates are safer for all road users”. In: *Journal of Transport & Health* 13 (2019), p. 100539.

[114] Yiyang Yang et al. “Towards a cycling-friendly city: An updated review of the associations between built environment and cycling behaviors (2007–2017)”. In: *Journal of Transport & Health* 14 (2019), p. 100613.

[115] Minh-Tan Do and Veronique Cerezo. “Road surface texture and skid resistance”. In: *Surface Topography: Metrology and Properties* 3.4 (2015), p. 043001.

[116] *Roadrunner software from Mathworks*. `https://www.mathworks.com/products/roadrunner.html`.

[117] Songtao He et al. “RoadRunner: improving the precision of road network inference from GPS trajectories”. In: *Proceedings of the 26th ACM SIGSPATIAL International Conference on Advances in Geographic Information Systems*. 2018, pp. 3–12.

[118] Stéphane Espié and Jean Michel Auberlet. “ARCHISIM: A behavioral multi-actors traffic simulation model for the study of a traffic system including ITS aspects”. In: *International Journal of ITS Research* n1 (2007), p7–16.

[119] Rosemary Kayess and Phillip French. “Out of darkness into light? Introducing the Convention on the Rights of Persons with Disabilities”. In: *Human rights law review* 8.1 (2008), pp. 1–34.

[120] *Fundacion ONCE*. `https://www.fundaciononce.es/en/about-us/introduction`.

[121] Fundacion ONCE. *Metro4All Research study Detecting users with disabilities´ needs at Metro network*. Fundacion ONCE, 2021.

[122] Fernando Alonso López et al. “Accesibilidad en los espacios públicos urbanizados”. In: (2010).

[123] Jeannette Montufar et al. “Pedestrians’ normal walking speed and speed when crossing a street”. In: *Transportation research record* 2002.1 (2007), pp. 90–97.